ADSORPTION AND DEGRADATION OF ENVIRONMENTAL CONTAMINANTS EXEMPLIFIED BY ARSENIC, VINYL FLUORIDE AND NITRATE

by

Yu-Han Yu

A dissertation submitted to the Faculty of the University of Delaware in partial fulfillment of the requirements for the degree of Doctor of Philosophy in Civil Engineering

Spring 2016

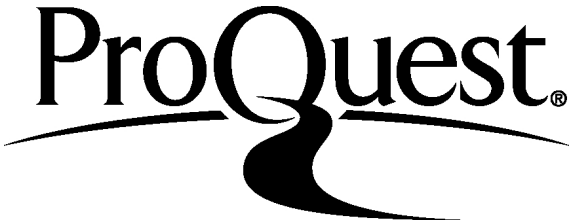

ADSORPTION AND DEGRADATION OF ENVIRONMENTAL CONTAMINANTS EXEMPLIFIED BY ARSENIC, VINYL FLUORIDE AND NITRATE

by

Yu-Han Yu

Approved: _____
Harry W. Shenton III, Ph.D.
Chair of the Department of Civil and Environmental Engineering

Approved: _____
Babatunde A. Ogunnaike, Ph.D.
Dean of the College of Engineering

Approved: _____
Ann L. Ardis, Ph.D.
Senior Vice Provost for Graduate and Professional Education

I certify that I have read this dissertation and that in my opinion it meets the academic and professional standard required by the University as a dissertation for the degree of Doctor of Philosophy.

Signed: _____

Pei C. Chiu, Ph.D.
Professor in charge of dissertation

I certify that I have read this dissertation and that in my opinion it meets the academic and professional standard required by the University as a dissertation for the degree of Doctor of Philosophy.

Signed: _____

Shu-Chi Chang, Ph.D.
Member of dissertation committee

I certify that I have read this dissertation and that in my opinion it meets the academic and professional standard required by the University as a dissertation for the degree of Doctor of Philosophy.

Signed: _____

Chin-Pao Huang, Ph.D.
Member of dissertation committee

I certify that I have read this dissertation and that in my opinion it meets the academic and professional standard required by the University as a dissertation for the degree of Doctor of Philosophy.

Signed: _____

Yung-Hsu Hsieh, Ph.D.
Member of dissertation committee

I certify that I have read this dissertation and that in my opinion it meets the academic and professional standard required by the University as a dissertation for the degree of Doctor of Philosophy.

Signed: _____

Kun-Yi Lin, Ph.D.
Member of dissertation committee

ACKNOWLEDGMENTS

I first would like to acknowledge my advisors, Pei Chun Chiu and Shu-Chi Chang, for their supports throughout the journey for my Ph.D. degrees. I would also like to thank my dissertation committee members, Chin-Pao Huang, Yung-Hsu Hsieh and Kun-Yi Lin for their suggestions on my dissertation. I much appreciate the University of Delaware Department of Civil and Environmental Engineering and the National Chung Hsing University Department of Environmental Engineering for having me in the dual Ph.D. degree program.

I have been fortunate to have great group members in Chiu's and Chang's laboratories. Special thanks to Jovita Saquing and Lauren Lechner for helping me and providing suggestions to my experiments and writing; Rovshan Mahmudov and Michael Davidson for keeping the labs running; and Tsung-Ju yang, Yao-Jen Chang, Li-Lun Huang and Tzu-Wen Chen for their support and encouragement.

Moreover, I would like to thank a lot of friends for bring happiness and fulfilling to my nine years graduate student life: Hao Shen, I-Chu Wu, Lynn Liang, Shu-Ching Ou, Ruizhi Xie, Han Zhang, Jinlin Jiang, Lynn Liang, Chin-Chen Kuo, Twins Lin, Chia-Yi Tsai, Hao-Yun Lei, Chen-Yu Chou, Shen Wang, Wangying Zhao, Hsu-Ying Chen, Chun-Yen Hsu, Ching-Lung Chen, Sunny Yang, Wei-Fan Kuan, Jenn Fang Su, Ken-Hsuan Liao, Sun Hui, Yang Zhou.

I would like to thank my parents and parents-in-law for their understanding and support on my graduate study. I am greatly indebted to my wife, Jo-Chin, who always stands by me and gives me her love.

Finally, I want to thank my lovely baby, Lucas, who tried to turn off my laptop and to delete my writing all the time when I was trying to meet the deadline of this dissertation.

TABLE OF CONTENTS

LIST OF TABLES

LIST OF FIGURES

ABSTRACT

The prevalence of legacy and emerging contaminants has increasingly stressed our limited water resources, and caused impaired water quality in many parts of the world. To meet our growing demand for clean water in this century, it is of the utmost importance to develop more effective means to remove/degrade pollutants in water. In this research, three novel materials/processes were investigated for the adsorption or degradation of three important contaminants: arsenic, fluorinated alkenes, and nitrate. Arsenic is a common groundwater contaminant that poses a serious health threat to populations in the U.S. and other countries. Fluorinated organics are widespread in consumer and industrial products, and many of them are persistent due to the high stability of the carbon-fluorine bond. Nitrate is the most ubiquitous pollutant in U.S. groundwater. Nitrate is not only toxic at high concentrations, but is also a leading cause of water quality impairment. We have developed a new nano-magnetite-based sorbent to remove arsenic, investigated an effective catalyst for the reduction of fluorinated alkenes, and determined the capacity of a biochar to promote microbial nitrate reduction.

Magnetite nanoparticle composite (MNPC) was synthesized for the removal of arsenic from water. We have shown that magnetite nanoparticles (MNP) possess high capacities and superior kinetics for adsorption of arsenic. In addition, to enable treatment applications, a new method was developed to embed MNPs into a silica network (MNPC). MNPC exhibited high adsorption capacities for arsenite and arsenate, 159.7 and 165.1 mg g^{-1}, respectively, comparable to the adsorption capacity

of MNPs under anaerobic conditions. MNPC could retain over 99.99% of the MNPs in its structure. Moreover, the embedment prevented exposure of MNPC to oxygen and thereby extended its service life. Our results suggest that MNPC may represent a viable technology for arsenic removal from groundwater and drinking water.

Rhodium on alumina was used as a catalyst to activate hydrogen gas for the reduction of vinyl fluoride (VF) as a model compound for fluorinated alkenes. VF is the monomer of fluoropolymer, a high production volume compound, and a probable (group 2A) carcinogen. We studied the kinetics of VF reduction in the presence of water. The rate-limiting step for the reduction was determined to be the mass transfer of VF from bulk water to the catalyst surface. Based on the product distribution, the reaction paths were found to consist of reductive defluorination, followed by hydrogenation, and hydrogenation only, producing ethane and fluoroethane, respectively, as final product. When water was absent, the kinetics was too fast to be measured producing mainly fluoroethane as the final product. The experiment with humidified hydrogen gas showed that even layers of adsorbed water molecules on the surface of the catalyst would dramatically shift the reaction rate and product distribution. By revealing the crucial role of water in controlling both the reaction kinetics and pathway, this study could be an important step toward the development of effectively catalytic treatment for fluorocarbons.

We demonstrated for the first time that biochar could serve as an electron donor to support microbial nitrate reduction. This new discovery could be a basis of novel engineered treatment/remediation systems to degrade nitrate, the most prevalent pollutant in the U.S. groundwater. *Geobacter metallireducens* (GS-15) was used to investigate the role of redox active functional groups in biochar to nitrate reduction by

exoelectrogenic bacteria. We showed that both biologically and chemically reduced biochar could support nitrate reduction. Results of this study suggest that biochar could be a bioaccessible electron storage medium in bioretention cells and other engineered systems, and this finding may also be applied to other black carbon.

Each approach in this dissertation represents a breakthrough in contaminant treatment. Results of each investigation either form a basis for new and improved treatment methods or have implications, for the fate of contaminants in natural systems. Both are discussed in Chapter 5.

Chapter 1

INTRODUCTION

The prevalence of legacy and emerging contaminants has increasingly stressed our limited water resources and caused impaired water quality in many parts of the world. To meet our growing demand for clean water in this century, it is of the utmost importance to develop more effective means to remove/degrade pollutants in water. In this dissertation, three environmental contaminants, arsenic, nitrate and vinyl fluoride, were selected as the target compounds to illustrate the three new approaches to remove or degrade these contaminants. The selection of three contaminants was based on their increasing importance and ubiquity in the environment. Adsorption, biological transformation and catalytic reduction were used in this dissertation for the removal and degradation of the three pollutants in water.

1.1 Arsenic

Arsenic (As) is naturally occurring in the lithosphere with an average concentration of 1.5 to 3 $\mu g\ g^{-1}$ in the earth's crust[1]. Inorganic As is commonly present in many water bodies. Minerals and geothermal activities are the major sources of As[2]. The prevalent forms of As in water are arsenite (As(III)) and arsenate (As(V)), which have different physicochemical properties and toxicity[3].

The inorganic As exposure to a human body could come from air, water, soil and food and intake through drinking water and food is the predominant route[3]. Recently, due to bioaccumulation, crops such as rice have been found to contain high

inorganic As content when the soil or irrigation water is contaminated with As[4,5]. The use of groundwater as drinking water is another concern for As exposure in the U.S. Based on the data from United States Environmental Protection Agency (USEPA), around 78% of community water systems use groundwater as the water source, providing approximately 32% of the country's drinking water[6]. USEPA also estimated that about 15% of the population in the U.S. utilizes private groundwater wells for the domestic consumptions[7]. Because the prevalence of As has threatened populations in the U.S. and other countries[8], it is imperative that we develop effective methods to remove As from water.

1.1.1 Adsorption of Arsenic on Magnetite Nanoparticle Composite (MNPC)

The removal of As from water can be achieved by using ion exchange, reverse osmosis, membrane filtration, adsorption and the combination of coagulation, flocculation, sedimentation and filtration[9-12]. For point-of-use drinking water treatment, the use of ion exchange, reverse osmosis, membrane filtration and adsorption may be more feasible options.

In recent years, it has been shown magnetite nanoparticles (MNPs) have high As adsorption rates and capacities and they have been increasingly studied as an adsorbent for As removal from water[13-18]. However, because of the small size of NMPs, they cannot be easily applied as an adsorption in a flow-through water purification unit.

In Chapter 2, a new method for embedding MNPs into a silica network was created to produce magnetite nanoparticle composite (MNPC). We hypothesized that (1) the MNPC can retain MNPs inside the silica structure during treatments; (2) the embedment may contribute a higher stability of MNPs; and (3) MNPC will have a

comparable As adsorption capacities comparing with MNPs. The detail of experimental setup and result and discussion are provided in Chapter 2.

1.2 Fluoroalkene

In recent years, fluorinated organics have been widely used as surfactants, stain-resistant agents, refrigerants and fluoroplastic monomers[19-21]. Because of the high stability of the carbon-fluorine bond, many fluorinated organics resist chemical and biological treatment[22-24]. Many fluorinated hydrocarbons are toxic, bioaccumulative and/or carcinogenic[25-28]. Therefore, their prevalence has raised growing ecological and human health concerns[19,29].

Although the toxicity of fluoroalkene is lower than that of chloroalkene, many of studies have reported the brain, lungs, spleen and renal damage due to exposure to fluoroalkene[30]. In addition to the health effects, the release of fluoroalkenes has also raised environmental concerns, due to one of their atmospheric degradation products, trifluoroacetic acid (TFA). TFA is a widely sprayed environmental contaminant on a global scale, and it has raised ecological concerns of the seasonal accumulation in wetlands, with adverse environmental impacts[31,32]. A recent study by Mashino et al. suggested that the atmospheric oxidation of fluoroalkenes, such as hexafluoropropene, could produce TFA as the final product[33]. Based on the health risks and environmental impacts, it is necessary to treat fluoroalkenes effectively.

1.2.1 Catalytic Reduction of Fluorinated Alkenes over Rhodium

In the studies by Baumgartner and McNeill, the ability of a commercially available rhodium on alumina catalyst to activate hydrogen for the reduction of fluorinated benzene has been shown[34,35]. Since both fluorinated benzene and alkene

consist of sp2 hybridized carbon-fluorine bond, we proposed that rhodium on alumina catalyst can also reduce fluoroalkene by hydrogen. To verify our hypothesis, vinyl fluoride (VF), the simplest fluorinated alkenes, was chosen. The experimental setups and the discussions of the experimental result are provided in Chapter 3.

1.3 Nitrate

Nitrate is a common contaminant in many groundwater aquifers. The sources of nitrate include the biotransformation of ammonium from agricultural runoffs and mineralization of organic wastes. The major impacts of nitrate contamination of natural waters and drinking water are eutrophication and health concerns, respectively. Eutrophication is one of the most widespread problems of surface water bodies in the U.S.[36]. The main effect of eutrophication is algal blooms, which would reduce the clarity of the water, decrease the dissolved oxygen concentrations, create taste and odor issues and other problems that impact the water quality and local ecosystem.

The crucial health concern associated with nitrate is methemoglobinemia. The reduction of nitrate to nitrite would cause the oxidation of haemoglobin (Hb) to methaemoglobin (metHb); i.e. the Fe^{2+} in the haemoglobin is oxidized to Fe^{3+} and thereby loses its ability to bind oxygen[37].

1.3.1 Microbial Nitrate Reduction Supported by Biochar

In recent studies, bioretention cells have been applied to remove nitrate in storm water. In these studies, although the mechanism has not been fully discovered yet, biochar has been proposed as a matrix material to facilitate nitrate removal[38-40]. Based on the study of Klüpfel et al., the quinone functional groups on biochar have been suggested to be redox active material with rechargeable nature[41]. Since humic substances, that

also have redox active quinone functional groups, can be the electron donor to support soil nitrate reduction[42], we hypothesize that the role of biochar for the nitrate reduction in bioretention cells may be analogue to that of humic substances in soil. To uncover the biotic role of biochar for nitrate reduction, an exoelectrogenic bacterium, *Geobacter metallireducens*, was used. The details of this study are documented in Chapter 4.

In this dissertation, three environmental contaminants, arsenic, fluoroalkene and nitrate, were studied due to their health concerns and prevalence in water. By obtaining knowledge from other disciplines, the improvement and better understanding of existing environment processes have been achieved. In Chapter 2, to remove arsenic from water, composite approach was used with MNPs. In Chapter 3, vinyl fluoride was used with rhodium on alumina catalyst in the presence of hydrogen gas for the development of the catalytic process for treating fluoroalkenes. In Chapter 4, the role of biochar in the nitrate reduction was studied for improving the design of bioretention cells. In each chapter, the description of experimental procedures, discussion of experimental results and implications and applications are documented. Finally, the suggestions and summary for the approaches of this dissertation are provided in Chapter 5.

REFERENCES

(1) Ning, R. Y. (2002). Arsenic removal by reverse osmosis. Desalination, 143(3), 237–241.

(2) Schmidt, K. D.; Sherman, I. Journal of irrigation and drainage,1987, 113, 16-29.

(3) Agency for Toxic Substances and Disease Registry. (2007). Toxicological Profile For Arsenic, 1–559.

(4) Sun, G.-X., Williams, P. N., Carey, A.-M., Zhu, Y.-G., Deacon, C., Raab, A., et al. (2008). Inorganic Arsenic in Rice Bran and Its Products Are an Order of Magnitude Higher than in Bulk Grain. Environmental Science & Technology, 42(19), 7542–7546. http://doi.org/10.1021/es801238p

(5) Aitio, A.; Becking, G. Arsenic and arsenic compounds, 2001.

(6) United States Environmental Protection Agency. (2008). Factoids: Drinking Water and Ground Water Statistics for 2007, 1–16.

(7) United States Environmental Protection Agency. Private drinking water wells. Retrieved from Private Drinking Water Wells.

(8) Fawell, J. K., & Mascarenhas, R. (2011). Arsenic in Drinking-water. Background document for development of WHO Guidelines for Drinking-water Quality. Guidelines for Drinking-water Quality.

(9) Ficklin, W. H. *Talanta*,1983, 30, 371–373.

(10) Ning, R. Y. *Desalination*,2002, **143**, 237–241.

(11) Brandhuber, P.; Amy, G. *Desalination*. Elsevier 1998, **117**, 1–10.

(12) Mohan, D.; Pittman, C. U., Jr. *Journal of Hazardous Materials*, 2007, **142**, 1–53.

(13) Auffan, M.; Rose, J.; Proux, O.; Borschneck, D.; Masion, A.; Chaurand, P.; Hazemann, J.-L.; Chaneac, C.; Jolivet, J.-P.; Wiesner, M. R.; van Geen, A.; Bottero, J.-Y. *Langmuir*,2008, 24, 3215–3222.

(14) Shipley, H. J.; Yean, S.; Kan, A. T.; Tomson, M. B. *Environmental toxicology and chemistry*, 2009, 28, 509–515.

(15) Yean, S.; Cong, L.; Yavuz, C.; Mayo, J. *Journal of materials research*, 2005, **20**, 3255-3264.

(16) Yavuz, C. T.; Mayo, J. T.; Yu, W. W.; Prakash, A.; Falkner, J. C.; Yean, S.; Cong, L.; Shipley, H. J.; Kan, A.; Tomson, M.; Natelson, D.; Colvin, V. L. *Science*, 2006, **314**, 964–967.

(17) Farrell, J. W.; Fortner, J.; Work, S.; Avendano, C.; Gonzalez-Pech, N. I.; Zárate Araiza, R.; Li, Q.; Álvarez, P. J. J.; Colvin, V.; Kan, A.; Tomson, M. *Environmental Engineering Science*, 2014, **31**, 393–402.

(18) Abid, A. D.; Kanematsu, M.; Young, T. M.; Kennedy, I. M. *Aerosol Science and Technology*, 2013, **47**, 169–176.

(19) National Toxicology Program. *Report on carcinogens: carcinogen profiles*. 2011, 437–442.

(20) Lewandowski, G.; Meissner, E.; Milchert, E. *Journal of Hazardous Materials*, 2006, **136**, 385–391.

(21) Barber, J. L.; Berger, U.; Chaemfa, C.; Huber, S.; Jahnke, A.; Temme, C.; Jones, K. C. *Journal of Environmental Monitoring*, 2007, **9**, 530–541.

(22) Ma, R.; Shih, K. *Environmental Pollution*, 2010, **158**, 1354–1362.

(23) Boulanger, B.; Vargo, J. D.; Schnoor, J. L.; Hornbuckle, K. C. *Environmental Science & Technology*, 2005, **39**, 5524–5530.

(24) Sawama, Y.; Yabe, Y.; Shigetsura, M.; Yamada, T.; Nagata, S.; Fujiwara, Y.; Maegawa, T.; Monguchi, Y.; Sajiki, H. *Advanced Synthesis & Catalysis*, 2012, **345**, 777–782.

(25) Blake, D.; Howell, R. D.; Criddle, C. S. *Environmental Science & Technology*, 1997, **31**, 2445–2454.

(26) Pirkanniemi, K.; Sillanpää, M. *Chemosphere*, 2002, **48**, 1047–1060.

(27) Turner, J. C. R. *Catalysis science and technology*, Springer Verlag, 1981.

(28) Zhang, X.-J.; Lai, T.-B.; Kong, R. Y.-C. In *Topics in Current Chemistry*, 2011, **308**, 365–404.

(29) Adams, D. E. C.; Halden, R. U. *ACS Symposium Series*, 2010, **1048**, 539–560.

(30) Clayton, J. W. *Environmental Health Perspectives*, 1977, **21**, 255–267.

(31) Tromp, T. K.; Ko, M. K.; Rodriguez, J. M.; Sze, N. D. *Nature*, 1995, **367**, 327–330.

(32) Boutonnet, J. C.; Bingham, P.; Calamari, D.; Rooij, C. de; Franklin, J.; Kawano, T. *Human and Ecological Risk Assessment: an International Journal*, 1999, **5**, 59–124.

(33) Mashino, M.; Ninomiya, Y.; Kawasaki, M.; Wallington, T. J.; Hurley, M. D. *The Journal of Physical Chemistry A*, 2000, **104**, 7255–7260.

(34) Baumgartner, R.; McNeill, K. *Environmental Science & Technology*, 2012, **46**, 10199–10205.

(35) Baumgartner, R.; Stieger, G. K.; McNeill, K. *Environmental Science & Technology*, 2013, **47**, 6545–6553.

(36) Carpenter, S. R.; Caraco, N. F.; Correll, D. L.; Howarth, R. W.; Sharpley, A. N.; Smith, V. H. *Ecological applications*, 1998, **8**, 559-568.

(37) Jaffe, E. R. *Clinics in haematology*, 1981, **10**, 99-122.

(38) Beck, D. A.; Johnson, G. R.; Spolek, G. A. *Environmental pollution*, 2011, **159**, 2111–2118.

(39) Mohanty, S. K.; Boehm, A. B. *Environmental Science & Technology*, 2014, **48**, 11535–11542.

(40) Reddy, K. R.; Xie, T.; Dastgheibi, S. *Journal of Environmental Engineering*, 2014, **140**, 04014043.

(41) Klüpfel, L.; Keiluweit, M.; Kleber, M.; Sander, M. *Environmental Science & Technology*, 2014, **48**, 5601–5611.

(42) Van Trump, J. I.; Wrighton, K. C.; Thrash, J. C.; Weber, K. A.; Andersen, G. L.; Coates, J. D. *Mbio*, 2011, **2**, e00044-11.

Chapter 2

HIGHLY EFFICIENT ARSENIC REMOVAL USING A MAGNETITE NANOPARTICLE COMPOSITE

2.1 Introduction

2.1.1 Background of Arsenic

Arsenic (As) is a common groundwater contaminant and is known for its acute and chronic toxicity. Acute poisoning is caused by uptake of high dosage (above 60,000 ppb) of As, which would usually lead to death[1]. Long-term exposure to As may lead to cancer (skin, lungs, and bladder), systemic toxicity (respiratory, circulatory, and renal), reproductive toxicity and neurotoxicity[1-5] (Table 2.1).

A common As exposure pathway is through the intake of polluted groundwater and grains, which is a major problem in many parts of the world[8,9]. In the United States, As contaminated groundwater has been found in many areas including Southwest, Northwest, Northeast and Alaska[10]. For people living in these areas, the daily inorganic As intake for an adult can be as high as 40 μg day^{-1}, which is two times higher than the average value is the U.S.[6].

Table 2.1. Health effect for arsenic exposure

Exposure dosage mg kg-1 day-1	Health effects	Reference
1-2.6	Death	6 and 7
0.5	Serious effects on gastrointestinal, neurological and cardiovascular systems or death.	
0.05-0.3	Serious effects on gastrointestinal, neurological and cardiovascular systems.	
0.001-0.1 (chronic exposure)	Effects on neurological system, liver and skin.	
0.011 (chronic exposure)	Effects on cardiovascular system and skin (blackfoot disease).	2

Because As has two different oxidation states (Figure 2.1), in different waters the predominant As species may be different. In surface water, most of the As is arsenate with a valence of 5+ (As(V)). In reduced environments such as groundwater, the dominant form of As would be arsenite (As(III)), which is more toxic that As(V). Although the toxicity of As(V) is higher than As(III), the environmental effect of these As species is similar[6]. The As in groundwater could be derived from anthropogenic and natural sources. The anthropogenic sources are typically localized because the geochemical conditions in an aquifer would limite As mobilization[11]. For the natural sources, the major contributions of As in groundwater are from geothermal activities and mineral sources[11]. Since As(III) and As(V) are ubiquitous in groundwater all over the world, and groundwater has been used as the source of drinking and irrigation water by a huge population[8], the prevalence of As(III) and As(V) in groundwater has had a significant impact on water and food security. Therefore, there is an urgent need to have an effective As removal process for drinking and irrigation water.

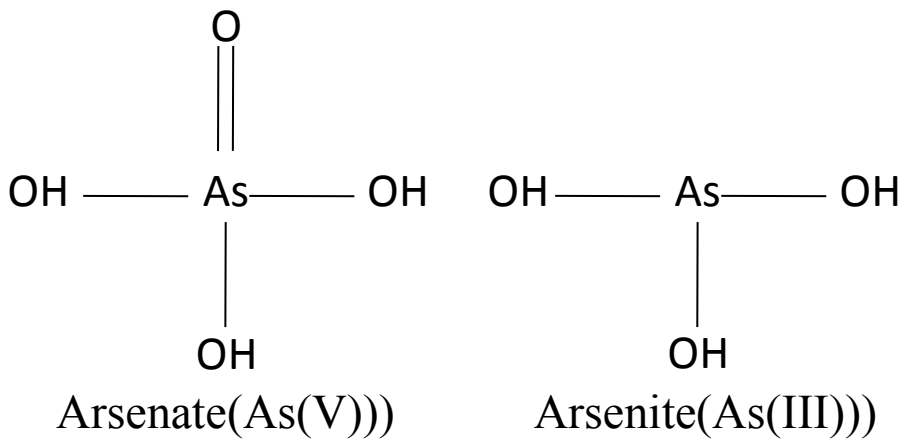

Figure 2.1: Arsenate (As(V)) and Arsenite (As(III)).

2.1.2 Arsenic Removal by Magnetite Nanoparticle

In the conventional environmental processes, the low concentration As removal from water can be achieved via the use of ion exchange, reverse osmosis, membrane filtration, adsorption and the combination of coagulation, flocculation, sedimentation and filtration[12-15]. In recent years, the improvement of nanotechnology has led to the development of many novel applications for environmental processes[16-18]. When the size of a nonporous adsorbent particle reduces to nano-scale, the surface-area-to-volume ratio would dramatically increase, resulting in the increase of the adsorption capacity. Because of high As adsorption capacity, magnetite nanoparticle (MNPs) has become a popular research topic in recent years[19-24]. In many cases, because of ferromagnetism, coagulation could happen during the use of MNPs, leading to the decrease of surface area to further lower the adsorption capacity. To avoid coagulation, the particle size of MNP has to be reduced below 16 nm to have superparamagnetic property to allow dispersing in a water[22].

2.1.3 Health Risk From Exposure to Iron Oxide Nanoparticles

Although MNP has a high As adsorption capacity,its toxicity can limit the use of MNP in an environmental process. Many studies have suggested the possible toxicity for the exposure of MNP and its oxidized products, such as maghemite and hematite, and the toxicity includes cytotoxicity, genotoxicity, developmental toxicity and neurotoxicity[25].

2.1.3.1 Cytotoxicity

Although the results between different type of cells were inconsistent, many studies indicate that the cytotoxicity for MNP was caused by the increase of oxidative stress and reactive oxygen species (ROS) production[26-29]. For human microvascular endothelial and porcine aortic endothelial cells the intracellular ROS formation is dose- and time- dependent for maghemite nanoparticle[27,30]. For human alveolar epithelial A549 cells, the cytotoxicity of hematite nanoparticle was reported.

2.1.3.2 Genotoxicity

In vitro DNA damage chromosome mutation assays is a common technique for testing genotoxicity[25]. Although different results were obtained from the studies using similar doses of iron oxide nanoparticles (IONPs) or MNPs, concentration-dependent DNA damage was found[31,32]. Based on the studies of Karlsson et al. [33,34], Fe_2O_3 nanoparticles showed no inductively primary DNA damage, but the damage was observed from the MNPs (Fe_3O_4) assay.

2.1.3.3 Developmental Toxicity

To evaluate the developmental toxicity, Frog Embryo Teratogenesis Assay Xenopus (FETAX) is the most widely used technique. A study from Nations et al.

suggested within the first 96 hours, the developmental or teratogenic effect for IONPs to *X. laevis*'s embryo is relatively minor[35]. Although a strong correlation between developmental effect and IONP treatment of embryo and fetal has not been found, the contribution of IONPs to the lag of offspring growth and maturation after birth was observed for mice, which would also lead to about 70% of death before the puberty[36].

2.1.3.4 Neurotoxicity

The increase of oxidative stress has been shown to lead to neurodegenerative diseases such as Parkinson's and Alzheimer's diseases[37]. Since one of the sources for INOPs toxicity has been identified to be the formation of ROS[25], studying neurotoxicity would be an important task for the evaluation of MNPs. The toxic effect of IONPs would vary between different types of nervous cells. For example, a toxic effect was not observed from the treatment of IONPs to microglia and oligodendrocyte; however, it was found to have toxic effects on pheochromocytoma cell[38-42]. In the study of Wu et al.[43], the authors indicated that after incubating with MNPs, a dose-dependent oxidative damage was found for rat pheochromocytoma cell. Also, the treatment of Fe_2O_3 was found to decrease the cell viability and ability to differentiate[44].

Although the nature of IONPs such as particle size, surface coating and reactivity could contribute to the inconsistent results between studies, the evaluation can still provide an insight into the potential risks of applying engineered MNP to drinking water treatments. Because of the potential health effects, preventing MNPs from leaching out of the treatment system has become an important issue. In this study, 3.02±0.32 nm (mean ± CI 95%) MNPs were embedded into a silica-based gel

for the development of MNP-composite (MNPC). To evaluate the adsorption capacity of the MNPC, the adsorption experiment of MNPs was also conducted.

2.2 Materials and Methods

2.2.1 Preparation of Magnetite Nanoparticle (MNPs)

1.99g of $FeCl_2 \cdot 4H_2O$ (J.T. Baker, Chu-Bei City, Taiwan) and 2.703g of $FeCl_3 \cdot 6H_2O$ (Riedel-de Haën, Seelze, Germany) were dissolved in 100ml deoxygenated deionized water (Millipore, Billerica, MA) in an amber glass bottle sealing with a cap and PTFE liner. The pH value of the solution was adjusted to 12 by using sodium hydroxide (Riedel-de Haën, Seelze, Germany). The bottle was then placed in a temperature-adjustable sonicator (Ultrasonic Cleaner DC600H, Delta New Instrument Co., New Taipei City, Taiwan) for 30min under 80˚C. The produced particles were rinsed by using deoxygenated deionized water for at least five times before vacuum drying. Except during sonication, MNPs and reagents were stored in an anaerobic chamber (Coy Laboratory Products, Grass Lake, MI) wrapped with aluminum foil to avoid exposure to light and oxygen.

2.2.2 Characterization of MNPs

A Transmission Electron Microscopy, TEM, (JEM-1400, JEOL, Tokyo, Japan) was first used to identify the morphology and size of MNPs. The result of TEM analysis showed that the size of individual nanoparticles and the aggregates were 1.15 nm and 3.02±0.32 nm (mean ± CI 95%), Figure 2.2. In order to characterize the crystalline structure of MNPs, a powder X-ray diffractometer (XRD, X'pert Pro, Panalytical, Almelo, The Netherlands) was used. Comparing the XRD result with JCPDS card for magnetite (NO. 19-629), the synthesized particles could be identified

as magnetite, Figure 2.3. The surface area of the MNPs was measured by using a Brunauer-Emmett-Teller (BET) surface area analyzer (ASAP 2020, Micromeritics, Norcross, GA), and the specific surface area was 65.8 $m^2 g^{-1}$.

2.2.3 As Adsorption Experiment by MNPs

As(III) and As(V) solution for the adsorption experiment were prepared weekly from 1000 mg L^{-1} stock solutions using pH 8, 10 mM tris buffer solution (tris(hydroxymethylamino)methane, 99%, Fluka, St. Louis, MO). The stock solutions which were monthly made from sodium arsenite ($NaAsO_2$, 99%, Fluka, St. Louis, MO) for As(III) and sodium arsenate ($Na_2HAsO_4 \cdot 7H_2O$, 98%, Alfa Aesar, Ward Hill, MA) for As(V) in the same tris buffer solution. The As(III) and As(V) concentrations for the adsorption experiment were 10, 50, 100, 250, 500, 1,000, 1,500, 2,500, 5,000, 10,000, and 25,000 ppb in pH 8, 10 mM tris buffer solution. The volume of solution in each experimental reactor was 40 ml with 2 mg MNPs. A temperature-adjustable anaerobic chamber was used for the preparation of solutions and anoxic adsorption experiments to prevent oxygen exposure and to keep the temperature at 30˚C. For the aerobic adsorption experiment, the preparation of reactors and solution was done in a hot room under 30˚C. During the adsorption experiment, the reactors were shaken orbitally under 120 rpm. After the adsorption experiments, 2 ml of supernatant water sample was taken from each reactor and transferred into a PFA digestion tube to digest before analyzing by using an inductively coupled plasma mass spectrometer (ICP-MS; ELAN DRC II, Perkin-Elmer, Waltham, MA).

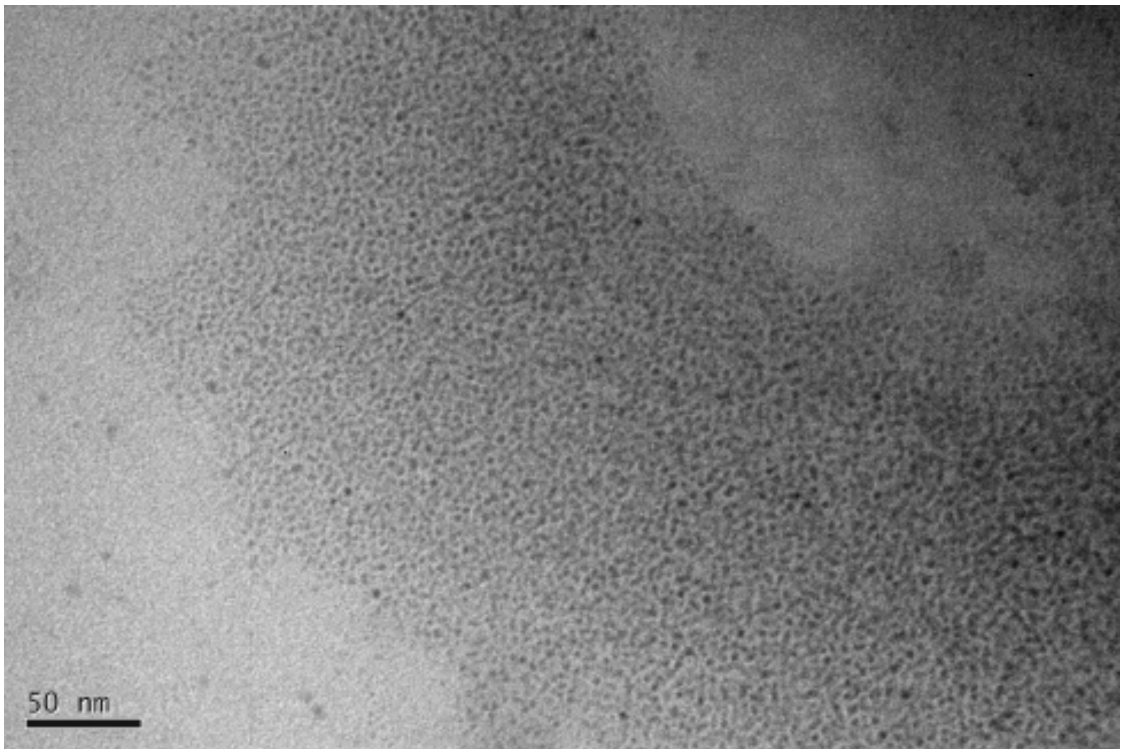

Figure 2.2: TEM image for the MNPs. Reprinted with permission from reference 60. Copyright 2012, Molecular Diversity Preservation International.

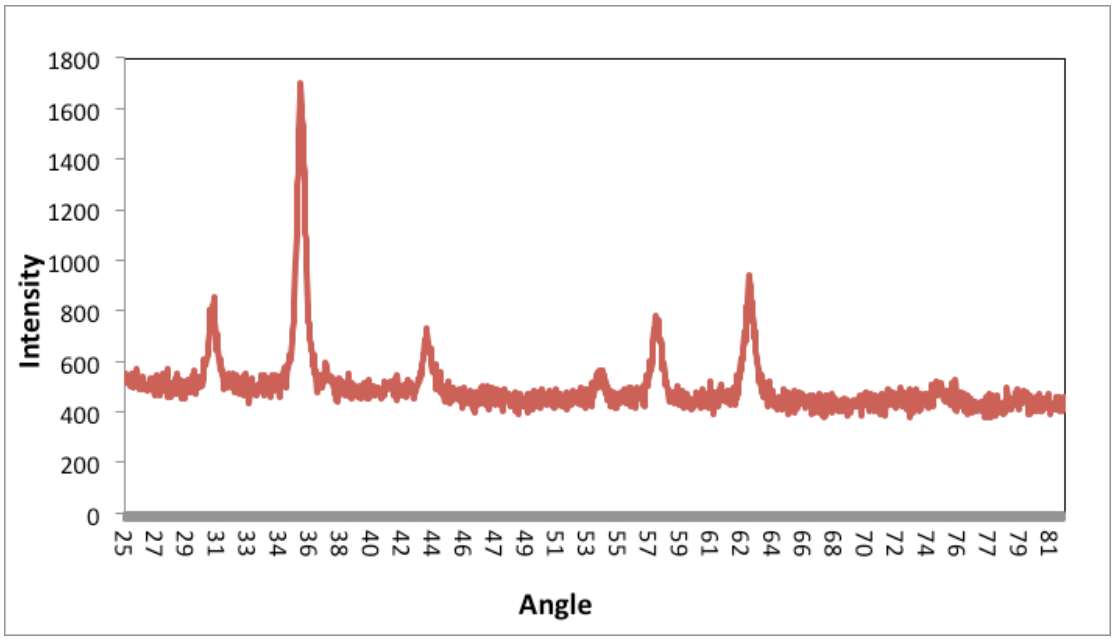

Figure 2.3: The XRD analysis of the MNPs, which matches the profiles of JCPDS Card (# 19-629) of magnetite

2.2.4 Synthesis of MNPC

For the preparation of silica gel, 21.6 ml deionized water was mixed with 0.14 ml of hydrogen chloride (J.T. Baker, Zhu-Bei City, Taiwan) to adjust to pH 1.2 before adding 14.2 ml of isopropyl alcohol. The solution was mixed with 58.3 ml of tetraethoxysilane (TEOS, Sigma-Aldrich, New Taipei City, Taiwan) to start the hydrolysis reaction. Under pH 1.2 and aerobic condition, TEOS would undergo hydrolysis and polymerization reaction and form a three-dimensional (3-D) network-like structure[45] to be the silica skeleton of MNPC.

After 2.5 h reaction, 3.02±0.32 nm (mean ± CI 95%) MNP was added into the gel to decorate the silica network. In order to make MNPs bond to the silica skeleton and solidify the gel, 1 ml of aminopropyltriethoxysilane (APTES, Sigma-Aldrich, New Taipei City, Taiwan) was added, which the reaction for APTES to the surface of

MNPs was silanization reaction to modify the surface forming a covalent bond with surface OH groups[46], Figure 2.4a

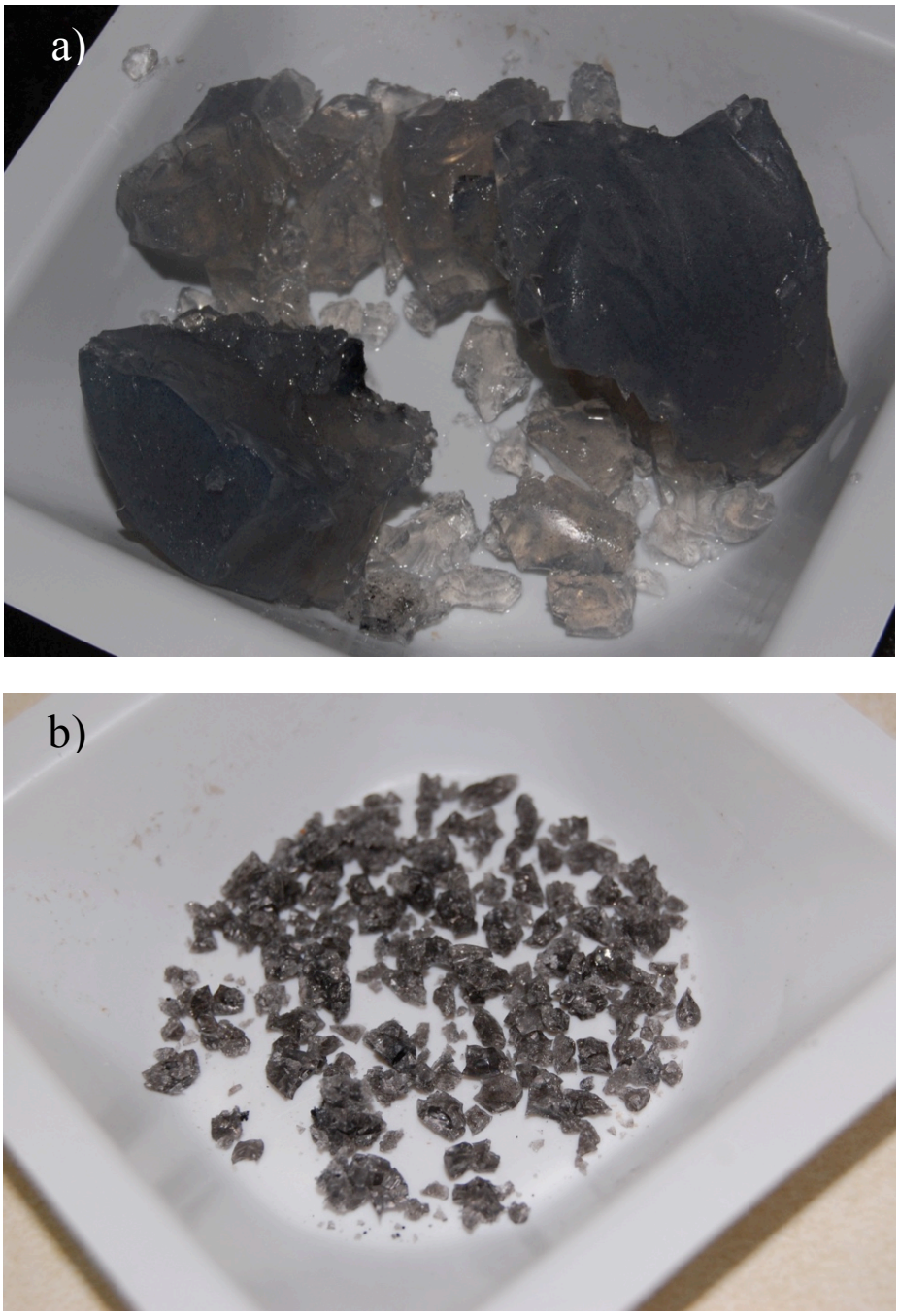

Figure 2.4: (a) After adding 1ml of APTES into the solution that contained silica gel and MNPs, the gel was transformed into solid MNPC. (b) The size and shape were changed for MNPC after vacuum drying for 48 h. Note that the (a) and (b) is the same sample before and after vacuum drying.

2.2.5 Characterization of MNPCs

To characterize the structure of MNPCs, a Transmission Electron Microscopy, TEM, (JEM-1400, JEOL, Tokyo, Japan) was used. To use the TEM, MNPC samples was dried in a vacuum chamber for over 48 h with drierite. Since pore water, which provides the support for the 3-D structure, was removed during the drying, collapse of MNPC was observed, which reduced the size of MNPC to about 5% of the original size, Figure 2.4a and b. After drying, MNPC was ground to fine particles for the analysis. Based on the TEM image, Figure 2.5, the MNPs were embedded into silica structure, and the size variation of the silica fraction was between 20 and 100 nm. In addition, because of the superparamagnetic property of MNPs, MNPC grains were not attracted to each other, but had a strong attraction to a neodymium magnet (NdFeB magnet).

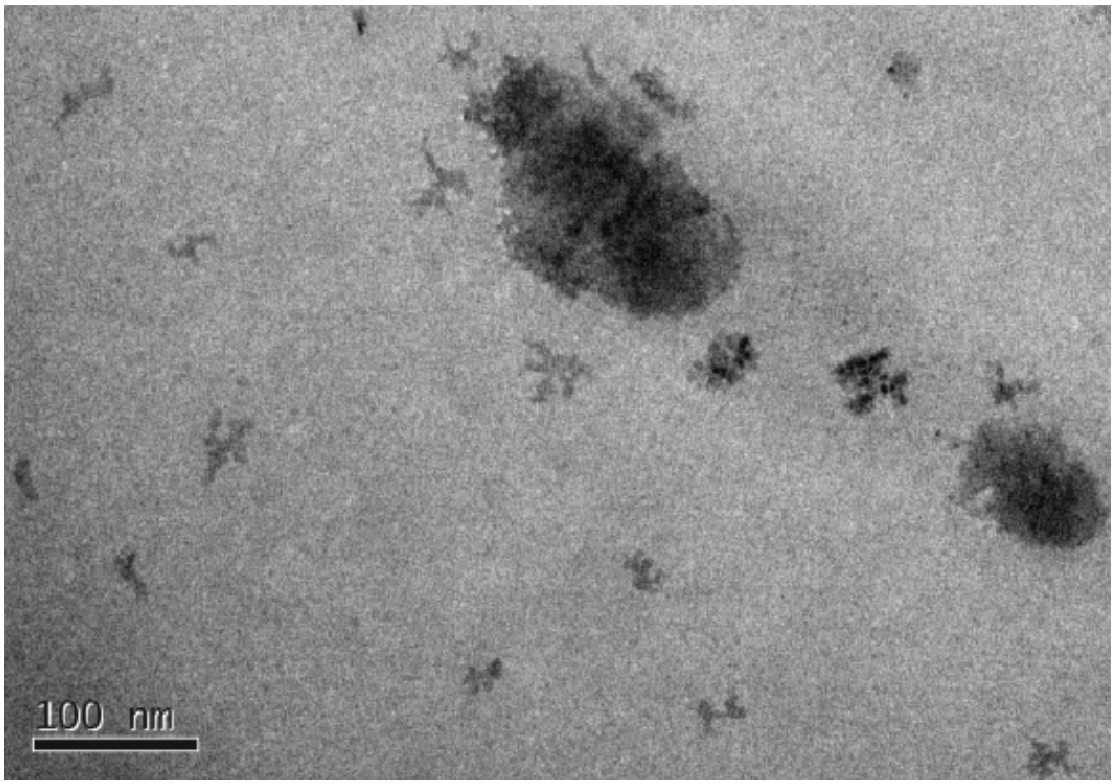

Figure 2.5: The TEM image for ground MNPCs. Reprinted with permission from reference 60. Copyright 2012, Molecular Diversity Preservation International.

2.2.6 As Adsorption Experiment by MNPC

The procedure for the preparation of As solution is described above. The same pH 8, 10 mM tris buffer solution was also used for the adsorption experiment, which the concentrations of As(III) and As(V) were 10, 50, 100, 250, 500, 1000, 1500, 2500, 5000, 10000, and 25000 ppb. Because the preparation of MNPC was under the aerobic condition, the adsorption experiment was conducted in a hot room under 30˚C. For each experimental reactor, the total iron content and liquid volume were 2 mg and 40 ml respectively. The determination of 2 mg of MNPs was based on the calculation from the total mass of MNPC and the amount of embedded MNPs. For the analysis of

aqueous As concentration, 2 ml solution was taken for each reactor after the reactor settled for 30s. The analysis procedure by using ICP-MS was described above.

2.3 Result and Discussion

2.3.1 Anaerobic and Aerobic Adsorption Experiments by Using MNPs

Under anaerobic condition, the adsorption capacities of MNPs reached 168.8 mg g^{-1} and 206.9 mg g^{-1} for As(III) and As(V) respectively, Figure 2.6a. For the aerobic experiments, the adsorption capacities were 108.6 mg g^{-1} for As(III) and 138.1 mg g^{-1} for As(V), Figure 2.6b. The result indicated that under anaerobic conditions, the adsorption capacity of MNPs was about 23-47% higher than the one under aerobic conditions for both As(III) and As(V). This phenomenon can be explained by, that under aerobic conditions, the presented oxygen in the solution would oxidize MNPs to maghemite nanoparticle, which has a much lower adsorption capacity[21]. For the MNP adsorption isotherms, the experimental result suggests that the adsorption curves for As(III) and As(V) consist of at least three Langmuir isotherms, which is different from other studies that only have two plateaus in the curves[21,47].

Comparing with other As adsorption studies conducted at around pH 8 by using sub 20 nm iron oxide nanoparticles, our MNPs under anaerobic conditions showed the highest adsorption capacity[19,21,22,48]. However, this result was somehow contradicting with the BET measurement of the MNPs since the specific surface area (SSA) for the MNPs was only 65.8 m^2 g^{-1}. Based on the observed particle size from the TEM analysis, Figure 2.2, with the much higher adsorption capacity than 20 nm of magnetite[21], the SSA seemed to be too low for the MNPs. This contradiction between the SSA and particle size can be rationalized by that the use of drily aggregated solid

for BET measurement might provide a much smaller SSA than the one that dispersed in water. This statement can be supported by a relationship between SSA and adsorption site density. If the measured SSA were correct, the site density would be high as 13.3 and 25.2 sites nm^{-2}. This number was much higher than the maximum site density 8 sites nm^{-2}, which was determined by using extended X-ray absorption spectroscopy (EXAFS) for the [111] facet of magnetite or maghemite nanocrystals[19,49-51]. Based on the experimentally determined site density, it can be concluded that the BET measurement for MNPs was underestimated about 6.65 to 12.6 times, and the reasonable SSA would be at least 438 $m^2 g^{-1}$.

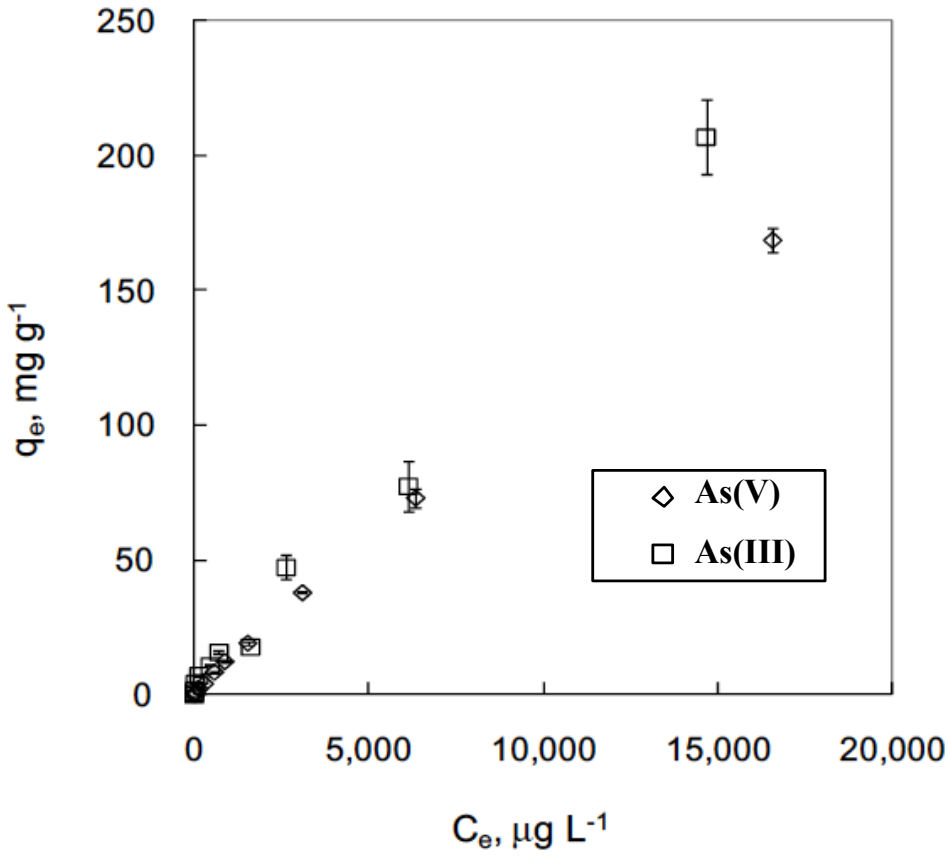

Figure 2.6a: Anaerobic adsorption of As(V) and As(III) over MNPs. pH 8, 10 mM tris buffer solution was used in the experiment, and reactors were shaken orbitally under 120 rpm in an anaerobic chamber under 30˚C. The error bars represent 95% confidence interval. Reprinted with permission from reference 60. Copyright 2012, Molecular Diversity Preservation International.

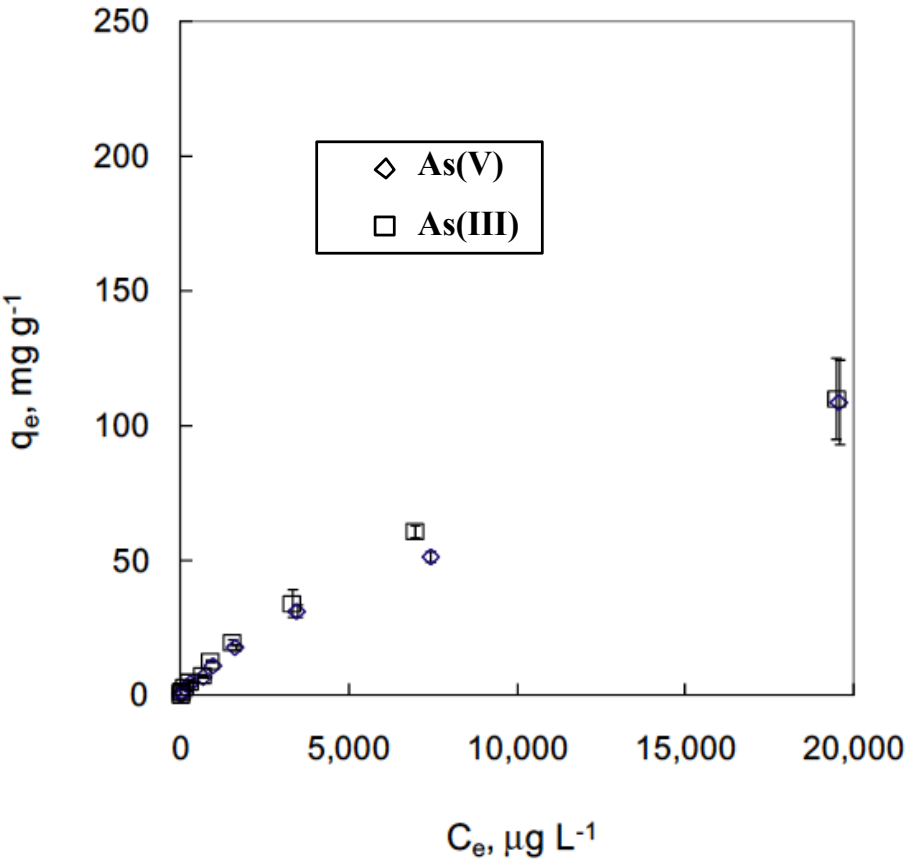

Figure 2.6b: Aerobic adsorption of As(V) and As(III) over MNPs. pH 8, 10 mM tris buffer solution was used in the experiment, and reactors were shaken orbitally under 120 rpm in a hot room under 30˚C. The error bars represent 95% confidence interval. Reprinted with permission from reference 60. Copyright 2012, Molecular Diversity Preservation International.

The experimental result also indicated that the adsorption capacity of MNPs was much higher for As(V) than As(III) under anaerobic condition. Under an anoxic environment, the adsorption mechanism of As to magnetite has been suggested to be the effect of electrostatic interaction, surface complexation and site density[52,53]. In this study, because the surface charge for MNPs at pH 8 was negative, it can be expected the adsorption would be contributed mainly from surface complexation and the density of specific sites.

Since the experimental conditions such as pH, temperature and adsorbent are consistent through this study, it is reasonable to conclude that the dominant species of As(III) and As(V) during the adsorption would be $H_3AsO_3^{(0)}$ and $H_3AsO_4^{2-}$ separately, appendix A. From the aspect of surface complexation, the major bonding for a pyramid structure of As(V) ($H_3AsO_4^{2-}$) would be ^{2}C bidentate bonding or forms outer-sphere complex[49]. However, because the coordination configuration for As(III) ($H_3AsO_3^{(0)}$) is different from As(V), which would form mainly hexanuclear ^{3}C tridentate bonding to the surface of MNPs[50,51]. The difference of surface complexation species, therefore, contributed to the difference in the adsorption capacity of two As species. The bonding type for As(V) on the surface is more versatile and allows a higher surface coverage; on the other hand, since a complex for an As(III) molecule on the MNPs requires more surface sites, there is a lower adsorption capacity.

Under an aerobic environment, because the oxidation of magnetite is inevitable, the formation of maghemite (γ-Fe_2O_3) at room temperature and hematite (α-Fe_2O_3) at much higher temperature[54] can easily be found, and the adsorption capacity would unsurprisingly be changed. For maghemite, the most likely oxidized product of magnetite in the experiment, a study showed that under pH 7.0 and pH 9.0,

the adsorption capacity of As(V) by maghemite nanoparticle (size between 3.8 and 18.6 nm) was lower than 25 mg g^{-1} [55]. Yet, for the As(III) adsorption capacity, a study of Auffan et al. indicated that the adsorption capacity of 6 nm maghemite at pH 7.0 was comparable to 11 nm magnetite at pH 8.0. This finding suggested that the oxidation of MNPs would impact the As(III) adsorption capacity less than the As(V)[19]. In this study, although the adsorption capacities for As(III) and As(V) were both decreasing once the experimental environment changed from anaerobic to aerobic condition, a larger impact on the adsorption capacity of As(V) than with As(III) was found, which is also supported by other studies.

To test the capability of MNPs for As adsorption under environmentally relevant conditions, a kinetic study was conducted at pH 8.1 under an anaerobic environment with 10, 50, 100 and 500 μg L^{-1} As concentrations, Figure 2.7. Based on the adsorption profiles, most of the reactions reached the equilibrium within 5 min. By applying first-order kinetics[56], the calculated rate constants under 95% C.I. are 12.32±1.00 h^{-1} for As(III) and 23.13±3.12 h^{-1} for As(V), Table 2.2. Because each sample required a magnetic separation by using a rare earth magnet for at least 3 min before sampling, it was impossible to obtain any data points within the first 5 min of adsorption. For the result of the sampling at 5 min, poor R^2 values were obtained for all experiments, Table 2.2. This result could be explained by the poor mixing conditions since there was only 2 min for MNPs to react with As(III) and As(V), and the rate constants in Table 2.2 could be underestimated.

In this study, the observed rate constants were about 11.0 - 13.4 times higher than the study using 20 nm MNPs at 100 μg L^{-1} of As concentration[20]. Although the observed rates in this study was much greater than the reported rates[20], the trend of

adsorption kinetics between As(V) and As(III) was in a good agreement with the literature, which the rate constant for As(V) was about 1.54 times higher than the rate for As(III) at the low MNPs dosage, 0.05g L^{-1} [20].

Table 2.2. Adsorption rate constants of MNPs, Reprinted and reproduced with permission from reference 60. Copyright 2012, Molecular Diversity Preservation International.

Initial concentration ($\mu g\ L^{-1}$)	K_{ads} in min^{-1} (R^2)	
	As(III)	As(V)
10	0.222 (0.768)	0.422 (0.677)
50	0.201 (0.721)	0.400 (0.871)
100	0.193 (0.999)	0.334 (0.839)

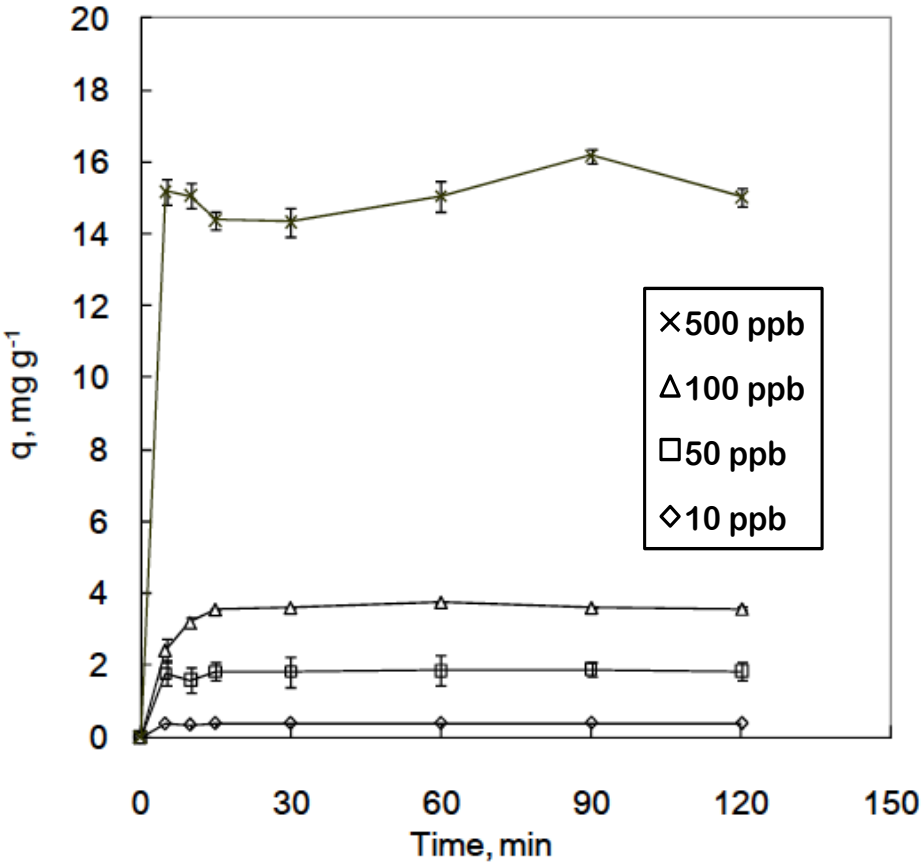

Figure 2.7a: Anaerobically kinetic adsorption profiles for As(III). pH 8, 10 mM tris buffer solution was used in the experiment, and reactors were shaken orbitally under 120 rpm in an anaerobic chamber under 30˚C. The error bars represent 95% confidence interval. Reprinted with permission from reference 60. Copyright 2012, Molecular Diversity Preservation International.

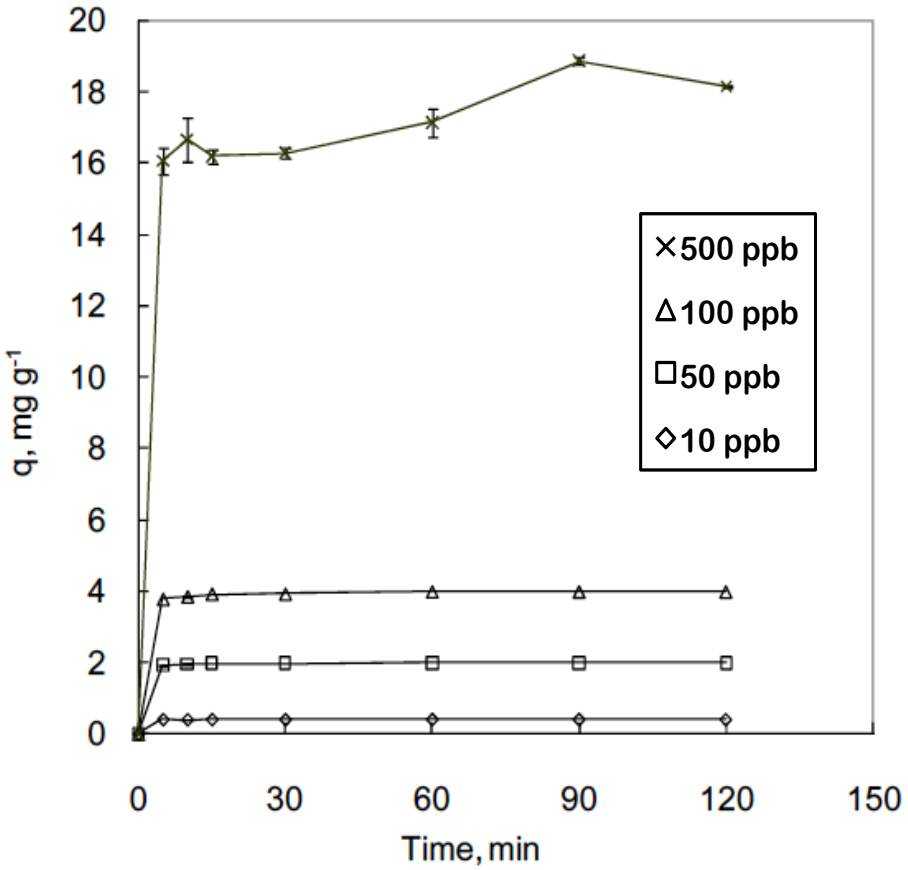

Figure 2.7b: Anaerobically kinetic adsorption profiles for As(V). pH 8, 10 mM tris buffer solution was used in the experiment, and reactors were shaken orbitally under 120 rpm in an anaerobic chamber under 30˚C. The error bars represent 95% confidence interval. Reprinted with permission from reference 60. Copyright 2012, Molecular Diversity Preservation International.

2.3.2 Aerobic As Adsorption by Using MNPC

Although the composite type approach for iron oxides has been reported in other research, which can be seen from, for example, the synthesis of iron oxide coated sand[57] and iron oxide clothed activated carbon[58], none of them embed MNPs in a 3-D tree-like silica structure.

The adsorption capacities for MNPC were 157.9 mg g^{-1} for As(III) and 165.1 mg g^{-1} for As(V), figure 2.8. Comparing this result with other studies, the adsorption capacities of MNPC were close to or higher than the maximum capacities of others[19,21,22,48],Table 2.3. Comparing with As adsorption to 300 nm magnetite particles at pH 8.0[21], the capacity of MNPC was about 105 times greater for As(III) and about 220 times greater for As(V). Comparing the adsorption capacities with previous experiments, the capacities of MNPC were in between the results of MNPs under anaerobic and aerobic conditions. Under aerobic condition and the same concentration range, 10 mg L^{-1} and 25 mg L^{-1}, the adsorption capacity of MNPC for As(V) was about 1.16 to 2.25 times greater than MNPs. For As(III) under the same condition, MNPC was 1.02 to 2.87 times greater. The adsorption behavior of MNPC seemed to be described well by Langmuir and linear isotherms. However, because of insufficient data points at the high As concentration, an unrealistic q_{max}, 1981 mg g^{-1} was obtained from the fitting.

Different from MNPs, MNPC can resist oxygen exposure, and this feature can be rationalized by the use of APTES in the synthesis of MNPC. The APTES created a silica coating on the surface of MNPs[46], which could prevent the oxidation of nanoparticles due to direct contact with dissolved oxygen in a solution. In addition, by doing the adsorption experiment, no significant different between As(III) and As(V) capacities was observed.

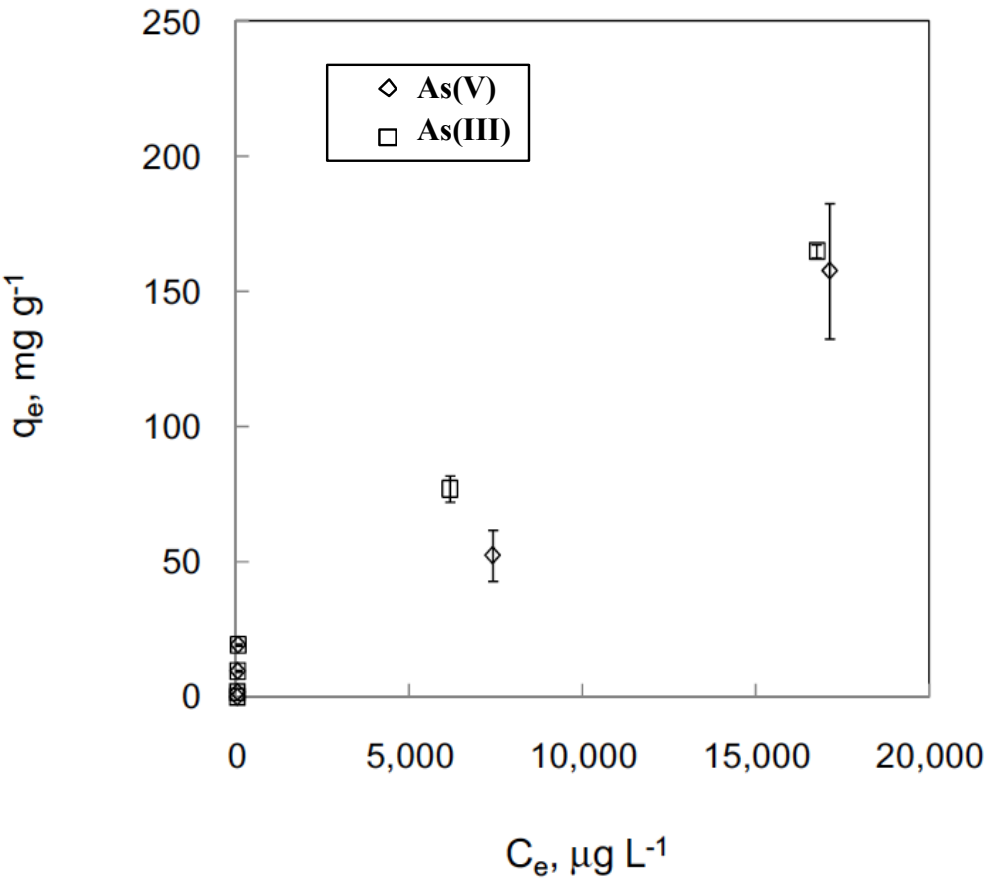

Figure 2.8: The adsorption result for MNPC to As(III) and As(V) under aerobic condition. pH 8, 10 mM tris buffer solution was used in the experiment, and reactors were shaken orbitally under 120 rpm in a hot room under 30˚C. The error bars represent 95% confidence interval. Reprinted with permission from reference 60. Copyright 2012, Molecular Diversity Preservation International.

Table 2.3. Comparison of As adsorption with different iron oxide. Reprinted and reproduced with permission from reference 60. Copyright 2012, Molecular Diversity Preservation International.

Adsorbent	Particle size (nm)	pH	q_e, max (mg g^{-1})		Ref
			As(III)	As(V)	
MNPs	3.02±0.32	8.0	168.8	206.9	Anaerobic*
			108.6	138.1	Aerobic*
MNPC	-	8.0	157.9	165.1	Aerobic*
Maghemite	6	7	172.5	-	19
Magnetite	12	8	-	~200**	22
	11.72		114.9	172.5	
Magnetite	20	8	29.2	5.9	21
	300	6.1	1.5	0.75	
Maghemite	3.8±0.8	7.0	-	20	59
		9.0		12.5	

*This study
** Estimated by the authors
*** Calculated by Yean et al. [21]

2.3.3 Stability of MNPC

In the past, due to the fast dissolving nature at pH below 4, MNPs cannot be applied to an acidic wastewater treatment such as mine waste. In this study, by modifying MNPs with silica, and because the particles would not be directly exposed to water while in use, we proposed that MNPC would be stable in a lower pH (lower than 4) aqueous environment.

To test the hypothesis, a separate experiment was conducted by immersing ground MNPC into a pH 1 hydrogen chloride solution to identify the change in

physical properties such as color, shape and size. After 40 days immersion, the result showed that no observable change was found, figure 2.9, which suggested that MNPC might have good applications in the lower pH range.

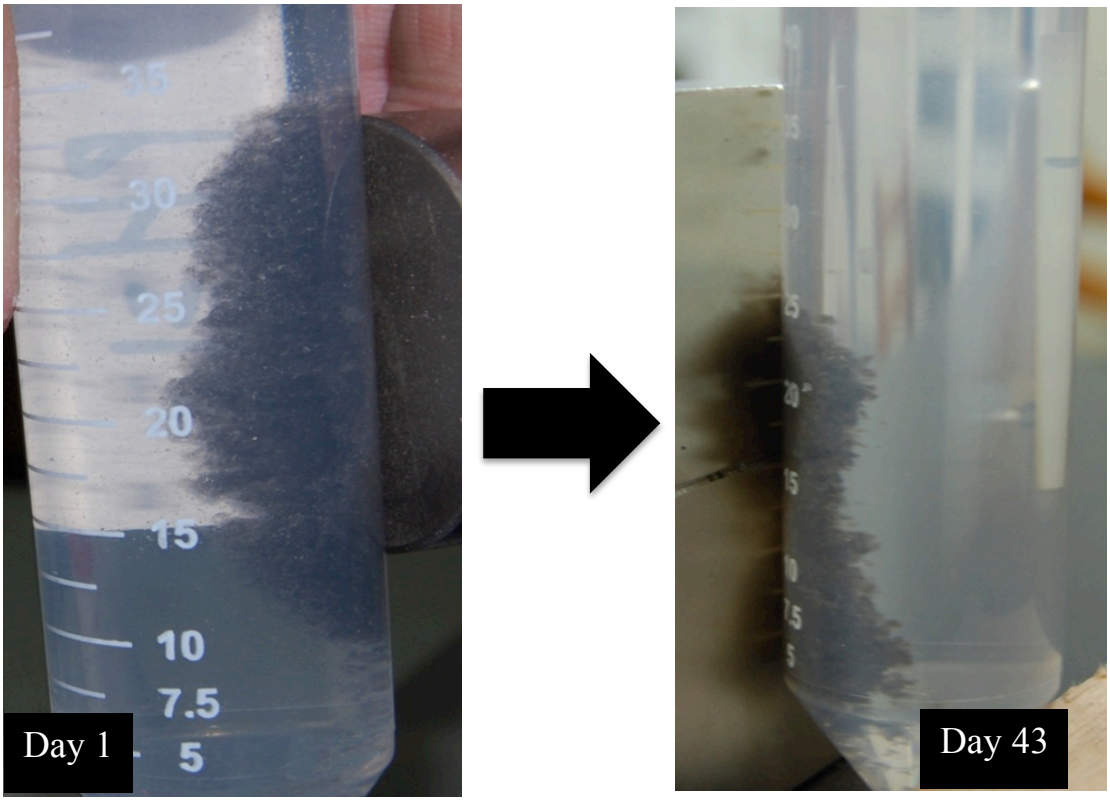

Figure 2.9: MNPC in pH 1 hydrogen chloride after 43 days under ambient environment. The significant change of physical property was not observed

2.3.4 Residual Iron and Iron Leaching Tests

Considering the potential health risks for using MNPs and the adsorbed As along with it, an iron recovery test was conducted for MNP and MNPC. By dispersing 0.1 g L^{-1} MNP in 40 ml of pH 8, 10 mM tris buffer solution in a serum bottle and

placing the bottle on a neodymium magnet for 30 min, the residual iron concentration in the water sample was 602.5 ppb. Even though the iron recovery was high as 99.2% recovery, by applying MNPs to a high As concentration wastewater, e.g. 25000 μg L^{-1}, the remaining MNPs would still contribute 172 μg L^{-1} and 139 μg $L^{-1}$of As(V) and As(III) in treated water. In other words, based on the adsorption isotherm, if the goal for remaining As concentration in treated water is below 10 ppb, the As concentration for untreated water cannot be in excess of 7900 μg L^{-1}. By considering the possible toxicities for MNPs, the potential health risk would be even greater. In contrast, by using MNPC containing the same amount MNPs under the same experimental condition without treating with a neodymium magnet, the result from the ICP-MS analysis showed that the remaining iron concentration was 8.5 ppb, which the recovery was above 99.99% (about 71 times lower than MNPs with the magnet). Considering low iron leaching and the high adsorption capacities of MNPC to As(III) and As(V), it can be applied to not only point-of-use applications, but also to a large-scale reactor type of treatments such as permeable reactive barrier (PRB). For drinking water treatment, high As removal rate and adsorption capacity, low leaching of MNPs, the resistance to oxygen and high compatibility with traditional sedimentation processes are the advantages of using MNPC.

2.4 Summary

The result of this study suggested that ultra-small MNPs could effectively remove As from water; the adsorption capacities under anaerobic conditions are 168.8 mg g^{-1} and 206.9 mg g^{-1} for As(III) and As(V), respectively. These values were much higher than the capacities that were obtained under aerobic condition (108.6 mg g^{-1} for As(III) and 138.1 mg g^{-1} for As(V)). For the MNPC under aerobic conditions, the

adsorption capacities (157.9 mg g^{-1} and 165.1 mg g^{-1} for As(III) and As(V) respectively) were in between the two conditions for MNPs.

Because of the potential health effects of MNPs, the approach for embedding MNPs into the silica gel was developed and used in this study, to minimize the concern for using MNPs to remove As from water. Based on the experimental result, feasibility for synthesizing a composite to retain the magnetic characteristics, adsorption capacity, and lower release of MNPs has been shown. With the nature of oxygen resistance, MNPC could be a promisingly alternative material for As removal in a drinking water or groundwater treatments.

REFERENCES

(1) Agency for Toxic Substances and Disease Registry. *ATSDR Case Studies in Environment Medicine - Arsenic Toxicity*, 2010, 1–125.

(2) Tseng, W. P. *Environmental health perspectives*,1977, **19**, 109–119.

(3) Chen, C. J.; Chuang, Y. C.; Lin, T. M.; Wu, H. Y. *Cancer research*,1985, **45**, 5895–5899.

(4) Chattopadhyay, S.; Bhaumik, S.; Purkayastha, M.; Basu, S.; Nag Chaudhuri, A.; Gupta, Das, S. *Toxicology letters*, 2002, **136**, 65–76.

(5) Shalat, S. L.; Walker, D. B.; Finnell, R. H. *Journal of Toxicology and Environmental Health*,1996, **48**, 253–272.

(6) Agency for Toxic Substances and Disease Registry. *Toxicological Profile For Arsenic*, 2007, 1–559.

(7) Ratnaike, R. N. *Postgraduate medical journal*, 2003, **79**, 391–396.

(8) Aitio, A.; Becking, G. *Arsenic and arsenic compounds,* 2001.

(9) Committee on Toxicology Board on Environmental Studies and Toxicology Division on Earth and Life Studies National Research Council. *Arsenic in Drinking Water*; National Academies Press, 2001.

(10) Ryker, S. J. *Geotimes*. 2001, **46**, 34–36.

(11) Smedley, P. L.; Kinniburgh, D. G. *Applied Geochemistry*, 2002, **17**, 517-568.

(12) Ficklin, W. H. *Talanta*,1983, 30, 371–373.

(13) Ning, R. Y. *Desalination*,2002, **143**, 237–241.

(14) Brandhuber, P.; Amy, G. *Desalination*. Elsevier 1998, **117**, 1–10.

(15) Mohan, D.; Pittman, C. U., Jr. *Journal of Hazardous Materials*, 2007, **142**, 1–53.

(16) Swaminathan, V. V.; Gibson, L. R.; Pinti, M.; Prakash, S.; Bohn, P. W.; Shannon, M. A. *Journal of Nanoparticle Research*, 2012, **14**, 17–31.

(17) Chang, C.-Y.; Hsieh, Y.-H. *Journal of Nanomaterials*. 2012, **2012**, 1–6.

(18) Park, S.-J.; Cheedrala, R. K.; Diallo, M. S.; Kim, C.; Kim, I. S.; Goddard, W. A. *Journal of Nanoparticle Research*, 2012, **14**, 1-14.

(19) Auffan, M.; Rose, J.; Proux, O.; Borschneck, D.; Masion, A.; Chaurand, P.; Hazemann, J.-L.; Chaneac, C.; Jolivet, J.-P.; Wiesner, M. R.; van Geen, A.; Bottero, J.-Y. *Langmuir*,2008, 24, 3215–3222.

(20) Shipley, H. J.; Yean, S.; Kan, A. T.; Tomson, M. B. *Environmental toxicology and chemistry*, 2009, 28, 509–515.

(21) Yean, S.; Cong, L.; Yavuz, C.; Mayo, J. *Journal of materials research*, 2005, **20**, 3255-3264.

(22) Yavuz, C. T.; Mayo, J. T.; Yu, W. W.; Prakash, A.; Falkner, J. C.; Yean, S.; Cong, L.; Shipley, H. J.; Kan, A.; Tomson, M.; Natelson, D.; Colvin, V. L. *Science*, 2006, **314**, 964–967.

(23) Farrell, J. W.; Fortner, J.; Work, S.; Avendano, C.; Gonzalez-Pech, N. I.; Zárate Araiza, R.; Li, Q.; Álvarez, P. J. J.; Colvin, V.; Kan, A.; Tomson, M. *Environmental Engineering Science*, 2014, **31**, 393–402.

(24) Abid, A. D.; Kanematsu, M.; Young, T. M.; Kennedy, I. M. *Aerosol Science and Technology*, 2013, **47**, 169–176.

(25) Valdiglesias, V.; Kiliç, G.; Costa, C.; Fernández-Bertólez, N.; Pásaro, E.; Teixeira, J. P.; Laffon, B. *Environmental and Molecular Mutagenesis*, 2014, **56**, 125-148.

(26) Auffan, M.; Achouak, W.; Rose, J.; Roncato, M.-A.; Chaneac, C.; Waite, D. T.; Masion, A.; Woicik, J. C.; Wiesner, M. R.; Bottero, J.-Y. *Environmental Science & Technology*, 2008, **42**, 6730–6735.

(27) Buyukhatipoglu, K.; Clyne, A. M. *Journal of Biomedical Materials Research Part A*, 2010, **96A**, 186–195.

(28) Dwivedi, S.; Siddiqui, M. A.; Farshori, N. N.; Ahamed, M.; Musarrat, J.; Al-Khedhairy, A. A. *Colloids and surfaces. B: Biointerfaces*, 2014, **122**, 209–215.

(29) Malvindi, M. A.; De Matteis, V.; Galeone, A.; Brunetti, V.; Anyfantis, G. C.;

Athanassiou, A.; Cingolani, R.; Pompa, P. P. *PLoS ONE*, 2014, **9**, 1-11.

(30) Apopa, P. L.; Qian, Y.; Shao, R.; Guo, N. L.; Schwegler-Berry, D.; Pacurari, M.; Porter, D.; Shi, X.; Vallyathan, V.; Castranova, V.; Flynn, D. C. *Particle and Fibre Toxicology*, 2009, **6**, 1-14.

(31) Hong, S. C.; Lee, J. H.; Lee, J.; Kim, H. Y.; Park, J. Y.; Cho, J.; Lee, J.; Han, D.-W. *International journal of nanomedicine*, 2011, **6**, 3219–3231.

(32) Könczöl, M.; Ebeling, S.; Goldenberg, E.; Treude, F.; Gminski, R.; Gieré, R.; Grobéty, B.; Rothen-Rutishauser, B.; Merfort, I.; Mersch-Sundermann, V. *Chemical research in toxicology*, 2011, **24**, 1460–1475.

(33) Karlsson, H. L.; Cronholm, P.; Gustafsson, J.; Möller, L. *Chemical research in toxicology*, 2008, **21**, 1726–1732.

(34) Karlsson, H. L.; Gustafsson, J.; Cronholm, P.; Möller, L. *Toxicology letters*, 2009, **188**, 112–118.

(35) Nations, S.; Wages, M.; Cañas, J. E.; Maul, J.; Theodorakis, C.; Cobb, G. P. *Chemosphere*, 2011, **83**, 1053–1061.

(36) Noori, A.; Parivar, K.; Modaresi, M.; Messripour, M.; Yousefi, M. H.; Amiri, G. R. *African Journal of Biotechnology*, 2011, 10, 1221–1227.

(37) Kim, J.-E.; Shin, J.-Y.; Cho, M.-H. *Archives of Toxicology*, 2011, **85**, 685–700.

(38) Luther, E. M.; Petters, C.; Bulcke, F.; Kaltz, A.; Thiel, K.; Bickmeyer, U.; Dringen, R. *Acta biomaterialia*, 2013, **9**, 8454–8465.

(39) Na, H. B.; Palui, G.; Rosenberg, J. T.; Ji, X.; Grant, S. C.; Mattoussi, H. *ACS Nano*, 2012, **6**, 389–399.

(40) Wang, Y.; Wang, B.; Zhu, M.-T.; Li, M.; Wang, H.-J.; Wang, M.; Ouyang, H.; Chai, Z.-F.; Feng, W.-Y.; Zhao, Y.-L. *Toxicology letters*, 2011, **205**, 26–37.

(41) Hohnholt, M.; Geppert, M.; Dringen, R. *Neurochemical Research*, 2010, **35**, 1259–1268.

(42) Hohnholt, M. C.; Geppert, M.; Dringen, R. *Acta biomaterialia*, 2011, **7**, 3946–3954.

(43) Wu, H.-Y.; Chung, M.-C.; Wang, C.-C.; Huang, C.-H.; Liang, H.-J.; Jan, T.-

R. *Particle and Fibre Toxicology*, 2013, **10**, 1–11.

(44) Pisanic, T. R., II; Blackwell, J. D.; Shubayev, V. I.; Fiñones, R. R.; Jin, S. *Biomaterials*, 2007, **28**, 2572–2581.

(45) Iler, R. K. *The chemistry of silica: solubility, polymerization, colloid and surface properties, and biochemistry*, Wiley 1979.

(46) Yamaura, M.; Camilo, R. L.; Sampaio, L. C.; Macêdo, M. A.; Nakamura, M.; Toma, H. E. *Journal of Magnetism and Magnetic Materials*, 2004, **279**, 210–217.

(47) Dixit, S.; Hering, J. G. *Environmental Science & Technology*. September 2003, **37**, 4182–4189.

(48) Tuutijärvi, T.; Lu, J.; Sillanpää, M.; Chen, G. *Journal of Hazardous Materials*, 2009, **166**, 1415-1420.

(49) Wang, Y.; Morin, G.; Ona-Nguema, G.; Juillot, F.; Calas, G.; Brown, G. E., Jr. *Environmental Science & Technology*, 2011, **45**, 7258–7266.

(50) Wang, Y.; Morin, G.; Ona-Nguema, G.; Menguy, N.; Juillot, F.; Aubry, E.; Guyot, F.; Calas, G.; Brown, G. E., Jr. *Geochimica Et Cosmochimica Acta*, 2008, **72**, 2573–2586.

(51) Morin, G.; Wang, Y.; Ona-Nguema, G.; Juillot, F.; Calas, G.; Menguy, N.; Aubry, E.; Bargar, J. R.; Brown, G. E., Jr. *Langmuir*, 2009, **25**, 9119–9128.

(52) Gimenez, J.; Martinez, M.; Depablo, J.; Rovira, M.; Duro, L. *Journal of Hazardous Materials*, 2007, **141**, 575–580.

(53) Mahdavi, S.; Jalali, M.; Afkhami, *Journal of Nanoparticle Research*, 2012, **14**, 171–188.

(54) Cornell, R. M.; Schwertmann, U. *The iron oxides: structure, properties, reactions, occurrences and uses*, John Wiley & Sons, 2006.

(55) Tuutijärvi, T.; Lu, J.; Sillanpää, M.; Chen, G. *Journal of Hazardous Materials*, 2009, **166**, 1415–1420.

(56) Shipley, H. J.; Yean, S.; Kan, A. T.; Tomson, M. B. *Environmental Science and Pollution Research*, 2009, **17**, 1053–1062.

(57) Herbel, M.; Fendorf, S. *Chemical Geology*, 2006, **228**, 16–32.

(58) Zhang, Q. L.; Lin, Y. C.; Chen, X.; Gao, N. Y. *Journal of Hazardous Materials*, 2007, **148**, 671–678.

(59) Sen, T.; Magdassi, S.; Nizri, G.; Bruce, I. J. *Micro & Nano Letters*, 2006, **1**, 39-42.

(60) Chang, S.-C.; Yu, Y.-H.; Li, C.-H.; Wu, C.-C.; Lei, H.-Y. *International Journal of Environmental Research and Public Health*, 2012, **9**, 3711–3723.

Chapter 3

CATALYTIC REDUCTION OF VINYL FLUORIDE OVER ALUMINA SUPPORTED RHODIUM

3.1 Introduction

3.1.1 Property of fluorine

Fluorine is a halogen with an atomic weight of 18.998 g mol^{-1},. It has not been found in the elemental state in nature[1]. Fluorine has the highest electronegativity of all elements. Because of no inner shell electron and the large positive charge of the nuclei, the valence shell orbital of fluorine (2s and 2p) is very stable, which gives a low 2p energy level, -1.86 eV (5 eV lower than the 1s orbital of a proton)[1]. In contrast to the non-fluorinated hydrocarbons, fluorination would give a lower highest occupied molecular orbital (HOMO) and lowest unoccupied molecular orbital (LUMO) to a fluorocarbon[1]. This suggests that the electrons in the valence shell would not fluctuate markedly rendering the size of the molecule small and electronic polarizability low (van der Waals attraction)[1].

3.1.2 Background of Fluorinated Organic Compounds

Fluorocarbons are more chemically inert than their structurally analogous hydrocarbons and chlorocarbons because of the higher stability of carbon-fluoride bond [2-4]. Early research on fluorocarbon focused on making nontoxic, inert, low boiling liquid for refrigerants and propellants. Based on the combination of carbon, chlorine and fluorine, many chlorofluorocarbons (CFCs) were created. In 1938, polytetrafluoroethylene (PTFE) was discovered during a refrigerant research by

Plunkett in the laboratories of the E. I. du Pont de Nemours & Company[5], which contributed the development of fluoropolymers.

In recent decades, fluorinated hydrocarbons have been increasingly used as surfactants, stain-resistant agents, refrigerants, and fluoroplastic monomers [6-8]. Because of their high stability, these compounds are ubiquitous in the environment and the biota[9-13]. Many fluorocarbons are also toxic, bioaccumulative, carcinogenic, and persistent[3,14-16], and hence their prevalence has raised growing ecological and human health concerns[3,17]. Although the toxicity of fluoroalkene is generally lower than that of chloroalkene, many studies have reported brain, lungs, spleen, kidney and renal damage due to exposure to fluoroalkene[18].

In recent years, the environmental fate of trifluoroacetic acid (TFA) has been studied intensively. TFA is a strong organic acid with low pK_a value (0.23) and is miscible with water (~1.45 g cm^{-3}). Because of the low Henry's law constant, log K_{ow} and the recalcitrant nature, the accumulation of TFA in the aqueous environments can be expected. TFA is a widely sprayed environmental contaminants on a global scale, which has raised the ecological concerns to the seasonal accumulation in wetlands with adverse environmental impacts[19,20]. A recent study by Mashino et al. suggested that the atmospheric oxidation of fluoroalkenes such as hexafluoropropene, the raw material for the production of one of most common commercial fluoropolymers: fluorinated ethylene propylene, could produce TFA as the final product[21].

Based on the possible health risk and environmental impact, it is necessary to treat fluoroalkene effectively. To develop a catalytic process that can treat fluorocarbons effectively and efficiently, vinyl fluoride (VF) was assigned to be the target compound in this study.

In 1901, Swarts first prepared VF through the reaction between zinc and 1,1-difluoro-2-bromoethane[22]. VF is the simplest fluoroalkene and a high production volume (HPV) chemical used primarily for the production of polyvinyl fluoride (PVF) and other fluoropolymers[9]. PVF has outstanding mechanical properties and resistance to weather and a wide variety of chemicals[23], which has been increasingly applied to the surfaces of pipes, buildings and aircraft cabins[24,25]. VF has been regulated by the U.S. EPA under the Toxic Substance Control Act (TSCA) and was recently added to the Toxic Release Inventory (TRI)[6]. Because of the structural similarity to vinyl chloride, VF has a comparable toxic effect[6-8] and is classified as a probable (IARC Group 2A) carcinogen[9-13].

3.1.3 Catalytic Reduction of Vinyl Fluoride

From the past, many chemical and biological processes have been invested and used to deal with chlorinated carbons such as pesticides, biphenyls, solvents and disinfection byproducts. In contrast, excluding processes requiring high temperature, high pressure, and/or non-aqueous solvents, no agent or microorganism have been found that can reductively defluorinate efficiently[2,26-28]. However, in recent years, studies on catalytic activation of the carbon-fluorine bond have suggested the possibility of reduction of fluoroalkene[2,29,30], and both homogeneous and heterogeneous catalysts have shown the promising feature.

A catalyst is a material that alters the reaction kinetics by lowering the activation energy of the reaction without being substantially consumed. It would accelerate the reaction rates for both directions equally, and with or without the use of a catalyst, the reaction equilibrium would not change. Based on whether the catalyst is

presenting in the same phase with the reactant(s), it can be catalogued as a homogeneous or heterogeneous catalyst.

3.1.3.1 Homogeneous Catalyst and the Reduction of Monohaloalkene

For a reaction being homogeneous catalysis, five criteria need to be satisfied[31]: (1) the catalyst molecules are dispersed in the same phase as the reactant(s); (2) the structure and property of the catalyst has been characterized by using chemical and spectroscopic methods; (3) the permitting kinetics is clearly showed in the reaction; (4) the catalytic cycle of the catalyst is detectable; and (5) the catalyst can be tuned (e.g. by changing the ligand(s) of the catalyst) to meet the reaction needs. To fulfill these qualifications, a homogeneous catalyst must be presenting in the same phase as the reactant, and the property of the catalyst must be fully understood.

Although the use of homogeneous catalysts is common in many chemical industries[31], research on catalytic defluorination to degrade environmental contaminants is rare. In 2009, Peterson, Thoreson and McNeill suggested the mechanism of catalytical reductive dehalogenation by using $(PPh_3)_3RhCl$ complexes in the presence of H_2[30], Figure 3.1. In the proposed mechanism, the final product for the reduction of fluoroethene could be ethene or fluoroethane[30]. Although the production of the non-defluorinated fluoroalkane can occur, this may be overcome by modifying the property of the catalyst. For example, by switching to a ligand that is harder than PPh_3, the reaction could become more favorable for ethene production.

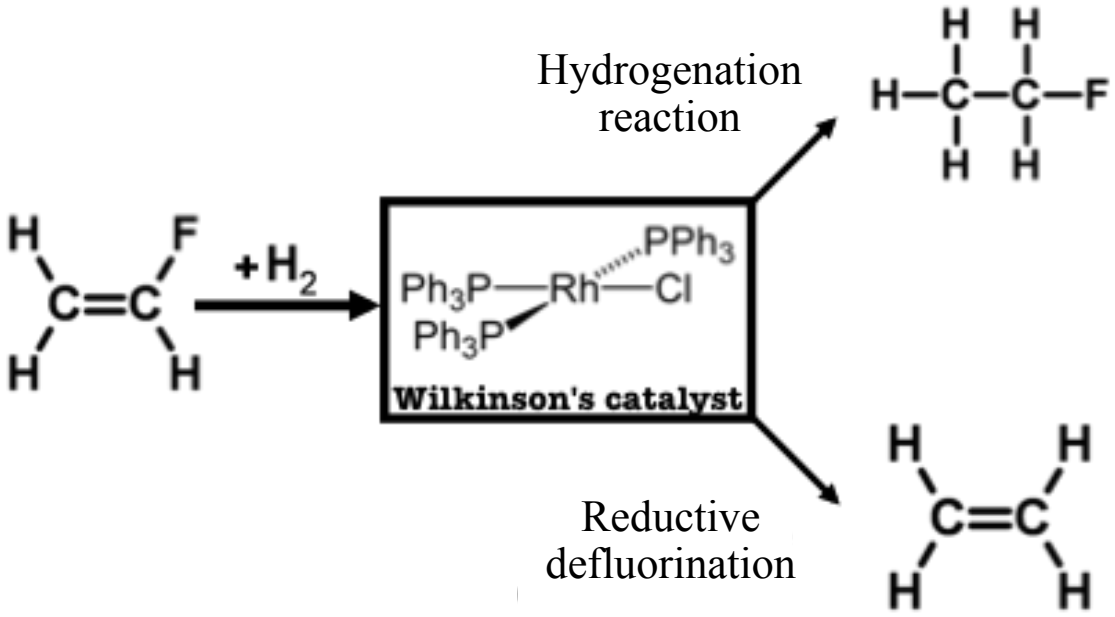

Figure 3.1: Catalytic reduction of vinyl fluoride by the homogeneous catalyst

3.1.3.2 Heterogeneous Catalyst and the Reduction of Fluorinated Organics

Unlike a homogeneous catalyst, heterogeneous catalysis means the catalyst and the reactant present in the different phases. For a solid catalyst, the reaction happens on the surface. Therefore, the surface complexity would largely affect the reaction kinetics. For example, for a porous catalyst the pore structure, size and distribution would affect the mass transfer of the reactant(s) to further influence the reaction rate. Also, because the reaction happens on the active site of a catalyst, the surface density would also affect the reaction kinetics.

In addition to the nature of the catalyst, environmental factors also largely control the reaction kinetics of heterogeneous catalysis. When a catalyst particle is used in a solution, the catalytic process can be divided into several elementary steps[3,14-16]: (1) the mass transfer of a reactant from bulk solution to the hydration layer

of the catalyst; (2) the mass transfer of the reactant through the hydration layer to the surface of the catalyst; (3) the adsorption of the reactant on the surface of the catalyst; (4) the complexation for the reactant and the active site; (5) the catalytic reaction; and (6) the desorption of products. Regarding the mass transfer of the reactant (step (1) and (2)), the mixing efficiency would be the dominant factor influencing the reaction kinetics. For the step (3) to (6), the reaction temperature would be the main factor.

In recent decades, because of the demand of industries, the activation of a carbon-fluorine bond has mainly focused on homogeneous catalysis[4]. Although a homogeneous catalyst has a higher reactivity and selectivity and no mass transfer issue[31], the unstable service time and recycling problem (almost impossible to reuse) largely decrease the possibility using a homogeneous catalyst in an environmental process, Table 3.2.

Table 3.1. General comparison of homogeneous and heterogeneous catalysts[31]

	Homogeneous catalyst	Heterogeneous catalyst
Activity (related to content of active material)	High	Variable
Selectivity	High	Variable
Service life of catalysts	Variable	Long
Diffusion problems	No	Yes
Catalyst recycling	Expensive	Unnecessary
Mechanistic understanding	Plausible under random conditions	More or less impossible

A recent study by Baumgartner and McNeill[2,29] showed that a rhodium on alumina catalyst could effectively break down fluorinated benzenes to cyclohexane by H_2 under ambient (room temperature and 1 atm) conditions. The authors demonstrated that the preferred reaction pathway for fluorinated benzenes in water was hydrodefluorination followed by hydrogenation with a half-life of 10 to 70 min. Since fluorobenzenes are sp2-hybridized fluorinated carbons, the experimental result suggested the possibility of developing a catalytic reduction process by using the rhodium on alumina catalyst for the degradation of fluoroalkene. Therefore, in this study, VF, the simplest fluoroalkene, was used as the target compound to verify the capability of the catalyst.

In this study, the rate law and rate-limiting step were determined. The role of water in controlling both the kinetics and pathway of VF reduction was elucidated. Based on these experimental data and evidence, the capability of rhodium on alumina

catalyst was evaluated, which provided insight for the reduction of other fluoroalkenes.

3.2 Materials and Methods

Compressed air, hydrogen (99.999%), nitrogen (99.999%) and helium gas (99.999%) were purchased from Keen Compressed Gas (Wilmington, DE). Ethane and ethene were obtained from Stotty gas (Houston, Texas), vinyl fluoride (C_2H_3F, 98%) and fluoroethane (C_2H_5F, 99%) were from SynQuest Laboratories (Alachua, FL). Tris(hydroxymethyl)-aminomethane, tris, was obtained from Bio-Rad (Hercules, California). Deionized water (>18 MΩ) was using for all experiments. Rhodium on γ-alumina catalyst (Rh/Al_2O_3, 5wt. %) was purchased from Sigma-Aldrich (St. Louis, MO). The specific surface area of the catalyst obtained from Nova 2000 (Quantachrome; Boynton Beach, FL) by using N_2 adsorption is 153.2 ± 3.0 m^2 g^{-1}, and the shape of the pores are cylindrical[32].

A gas chromatography (Agilent 6890; Santa Clara, CA) with a flame ionization detector, GC-FID, was used for the analysis of vinyl fluoride, flurorethane, ethene, and ethane. For the detection of the water vapor concentration in a gas phase reactor, a gas chromatography (Agilent 6890N) with a mass spectrometry (Agilent 5973N), GC-MS, was utilized. During the experiment, four points external calibration was applied for the quantification.

3.2.1 Experimental Setup

Aqueous experiments were performed in 250 ml amber glass bottles (Fisher Scientific, Pittsburgh, PA) containing 50 ml pH 8.2, 10 mM tris buffer solution with predetermined amount of catalyst. The headspace and solution were purged with

hydrogen for 1.5 hours before the bottle was sealed by using mininert valves (Vici, Houston, TX) and vinyl tape (3M, Saint Paul, MN). The reaction was initiated by introducing a known quantity of VF into reactor headspace. During the experiment, the reactors were shaken at 240 rpm under 24±1.5 ˚C, and 25 µl of headspace samples were taken by using a 250 µl gas-tight syringe (Vici, Houston, TX) and introduced into GC-FID for the analysis. The setups for control and blank bottles were identical to the reactors, with the absence of catalyst or hydrogen, respectively.

The setup for the gas phase experiment was identical to the aqueous phase experiment, with the omission of tris buffer solution. After purging predetermined amount of catalyst in 250 ml amber glass bottles with hydrogen under ambient pressure for over one hour, the bottles were sealed with crimp mininert valves and vinyl tape. Multiple headspace samples were taken and analyzed at predetermined elapsed times. Different from the liquid phase reactors, the gas phase experiments reactors each received five doses of vinyl fluoride (each dose is equivalent to 10.4 µmole vinyl fluoride) separately.

For the humidity experiment, the same setup as for the gas phase reaction was applied, except the pure hydrogen were passed through a humidifier to create different humidity levels for the experiment, 96±0.1%, and calibration curve for the humidity measurement, 53.0±0.1, 67.5±0.1, 80.5±0.1 and 100%. The humidifier was composed by using a 2000 ml serum bottle filled with 400 ml D.I. water, and an air stone was submerged into the D.I. water connected with a tube going through a crimp cap to be the inlet of hydrogen. The relative humidity (RH) level was controlled by adjusting the flow rate of the hydrogen. During the trial, the temperature for the reaction was set to 22± 0.05˚C by using a double jacket with a temperature-adjustable water bath to

prevent the fluctuation of room temperature affecting the RH. For the analysis, GC-FID was used for determining the concentration of VF and its daughter compounds, and GC-MS was utilized for monitoring the shift of relative humidity in the reactors during the reaction.

3.2.2 Analytical Method

Ethane, ethene, and vinyl fluoride were monitored by the GC-FID with GS-GasPro column (0.32mm × 30m, Agilent, Santa Clara, CA). The temperature program for the oven starts from 40 ˚C and held for 2 min, and ramped up 30˚C min^{-1} to 130 ˚C and held for 2.5 min. Five-point calibration curves for ethane, ethene, and vinyl fluoride were also built by using the GC-FID in amber glass bottles and mininert valves with the same water-to-headspace ratio. For relative humidity measurement, the GC-MS was utilized with DB-5ms column (0.25 mm × 30 m × 0.5 μm film thickness Agilent, Santa Clara, CA.), and the oven temperature and run time were 50 ˚C and 2 min. For the quantification of RH, SIM mode with 18 m/z for the mass spectrometry was applied. The RH calibration curve was built based on the identical procedure for setting up a gas phase reactor without introducing vinyl fluoride and rhodium catalyst. During the experiment, a bottle contained only hydrogen with 83±0.1 RH was used as the blank.

3.3 Results and Discussion

3.3.1 Liquid-Phase Experiments

The degradation of vinyl fluoride was followed by the production of ethene, ethane and fluoroethane indicating that the rhodium catalyst was capable to reduce fluorinated alkene as well as fluorinated benzenes in the presence of water, Figure 3.2.

The experimental result suggested that ethane was the final product in the system, and based on the appearance of ethene and fluoroethane, the hydrodefluorination and hydrogenation were confirmed. Ethene, which presented at low concentrations throughout the experiment, was presumably the defluorination product of vinyl fluoride, which might undergo hydrogenation reaction to produce ethane. For fluoroethane, since the concentration did not approach zero at the last sampling, it could be another final product. To confirm the roles of ethene and fluoroethane and to investigate the reaction pathway, separate experiments using ethene or fluoroethane as the starting material under identical conditions were conducted. The results showed that ethene was quantitatively transformed to ethane, and there was no reduction reaction of fluoroethane over a month. Since the production of fluoroethane was observed, the reaction route for this experiment was different from the one for fluorobezenes, which would undergo exclusively reductive defluorination[2,29], suggesting the hydrodefluorination and hydrogenation for fluorinated alkene could be both parallel and sequential, Figure 3.3.

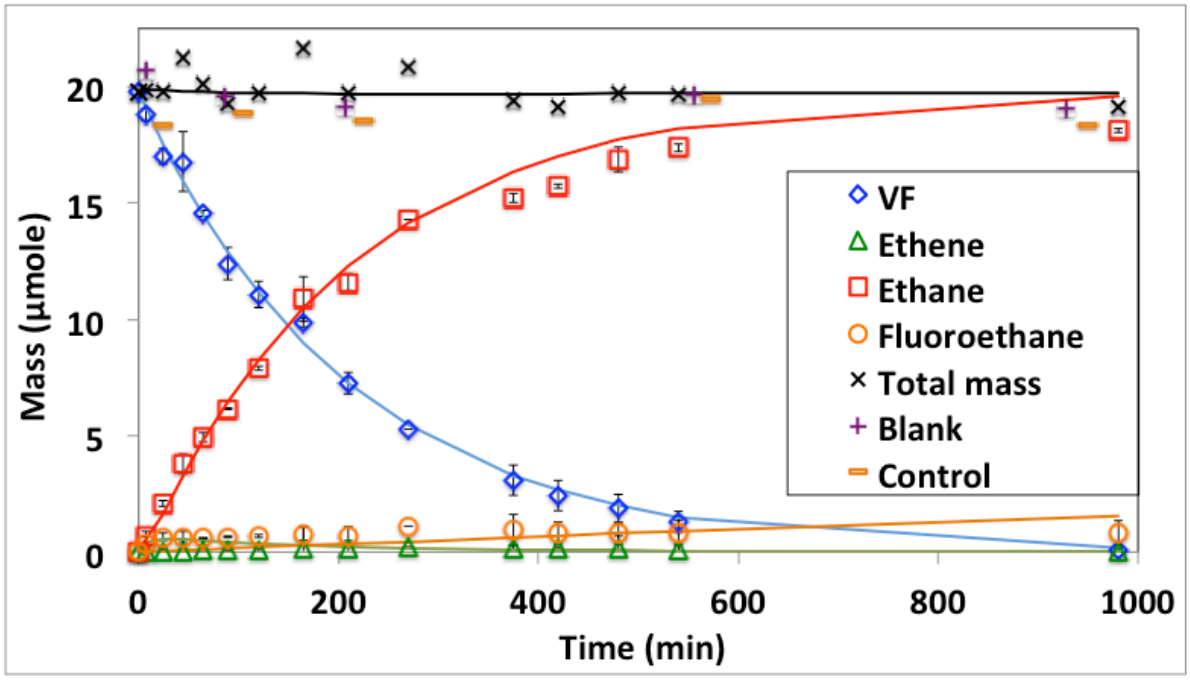

Figure 3.2: Concentration profiles of VF and its products during reduction of 20.8 µmole of VF in 250 mL reactors containing 50 mL of 10 mM Tris solution and 0.86 mg of Rh/Al_2O_3 catalyst (5% Rh, w/w) under 24±1.5 ˚C and 240 rpm shaking. The fitted curves are based on the pathway in Figure 3.3 and the assumption that all the reactions are pseudo-first-order. Reprinted with permission from reference 40. Copyright 2014, American Chemical Society.

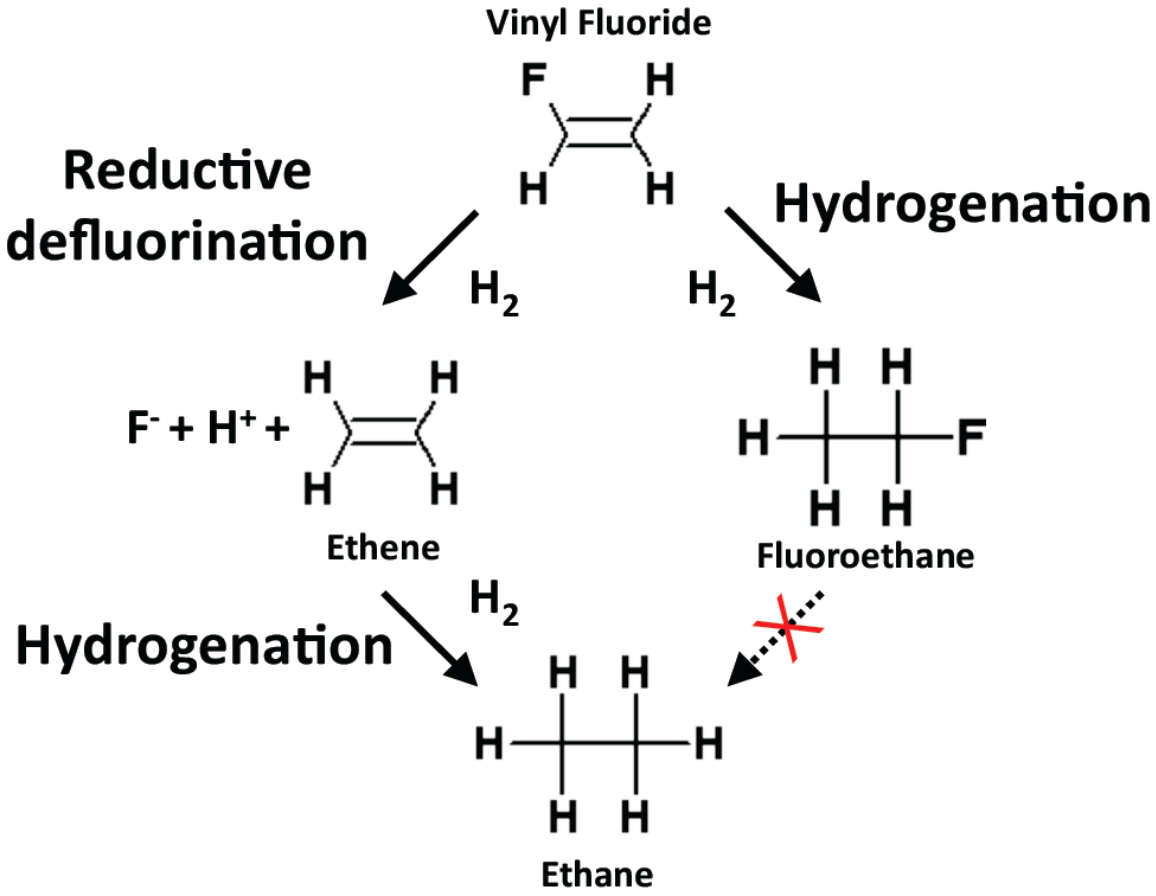

Figure 3.3: Proposed VF reduction pathway. Reprinted with permission from reference 40. Copyright 2014, American Chemical Society.

By fitting the experimental data with pseudo-first-order rate equations, solid lines in Figure 3.2, good R^2 values for VF and ethane profiles were obtained (> 0.99), and the rate of the disappearance of VF was 7.96×10^{-5} s^{-1}. However, for fluoroethane and ethene, the R^2 values were 0.31 and 0.15 respectively. For fluoroethane, the poor fitting could be rationalized by the observed concentration being too close to the detection limit. In addition, based on the fitted model for ethene, the hydrogenation

rate was 0.0024 s^{-1}, which was about 31 times faster than the reaction rate for the reductive defluorination of VF, 7.82×10^{-5} s^{-1}. With the pi electron bonding nature of rhodium[33], the reduction profile indicated that ethene was not only a fast reacting intermediate, but also a surface bounded species in the system. Based on these results, the pathway of VF reduction in the presence of water involves two parallel routes: hydrodefluorination followed by hydrogenation (to ethane); and hydrogenation (to fluoroethane). The mole ratio (R, fluoroethane/ethane) of the end products, was 0.022. The predominant route was analogous to the reaction sequence proposed by Baumgartner and McNeill[2-4], suggesting that, in water, fluorinated benzenes and alkenes probably react in a similar manner over Rh.

Because the rate constant for the removal of VF that was obtained from the experiment was strongly related to experimental parameters such as the amount of water and catalyst in a reactor, to apply the rate constant to other systems, a second-order rate constant of VF reduction was also obtained. To acquire the rate constant, 0.5, 1, 2 and 10 mg of the catalyst were used to reduce 20.4 μmole of VF with the same experimental procedure as previous experiments.

From the result of the experiment, a linear relationship with a high R^2 value, 0.999, was obtained, Figure 3.4. The profile showed that the reduction rate of vinyl fluoride increased along with increasing amount of the catalyst following the first-order kinetics. The pseudo-first-order rate constant k_1' was found to be first-order with respect to Rh concentration. Hence, the rate law of VF reduction in water was second-order, as shown in eq. 3.1. The second-order rate constant (k_2) obtained through linear regression was 9.36 s^{-1}(mole Rh/L)$^{-1}$. It suggested the reaction rate was a function of the catalyst usage and independent from the amount of vinyl fluoride in a reactor

meaning that the reduction rate could be estimated by knowing the amount of the catalyst in the system.

$$-\frac{d[VF]}{dt} = k_1'[VF]^1 = k_2[VF]^1[Rh]^1 \tag{3.1}$$

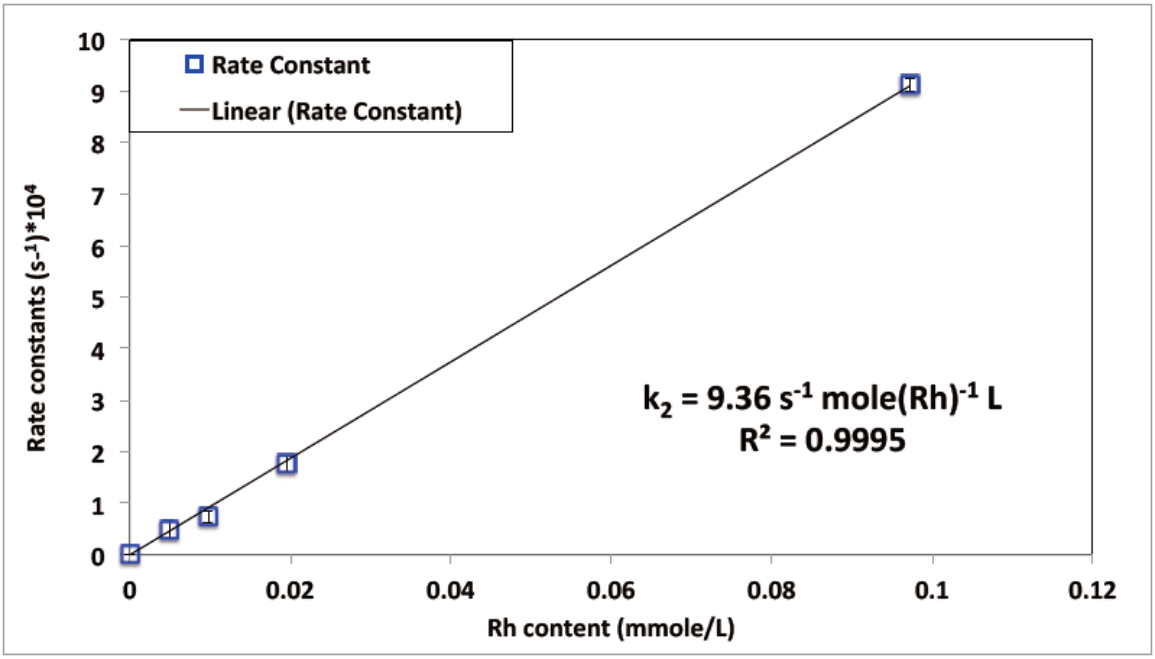

Figure 3.4: Pseudo-first-order rate constants for VF reduction in water was first-order in rhodium content. Second-order rate constant (k_2) was obtained via linear regression. The reactors containing 50 ml pH 8.2, 10 mM tris buffer solution were shaken at 240 rpm under 24±1.5 ˚C. Error bars represent 95% confidence intervals. Reprinted with permission from reference 40. Copyright 2014, American Chemical Society.

3.3.2 Gas-Phase Experiments

In an environmentally-related condition, vinyl fluoride is a gas with a high Henry's law constant, 4.83 at 20˚C (dimensionless), so it is reasonable to investigate the reduction of VF in the gas phase. The gas phase experiment was conducted

utilizing pure hydrogen (99.999%) with 0.86 mg rhodium on alumina catalyst. By re-spiking 10.4 µmole of VF for five times into gas phase reactors, the experimental profile was obtained, Figure 3.5.

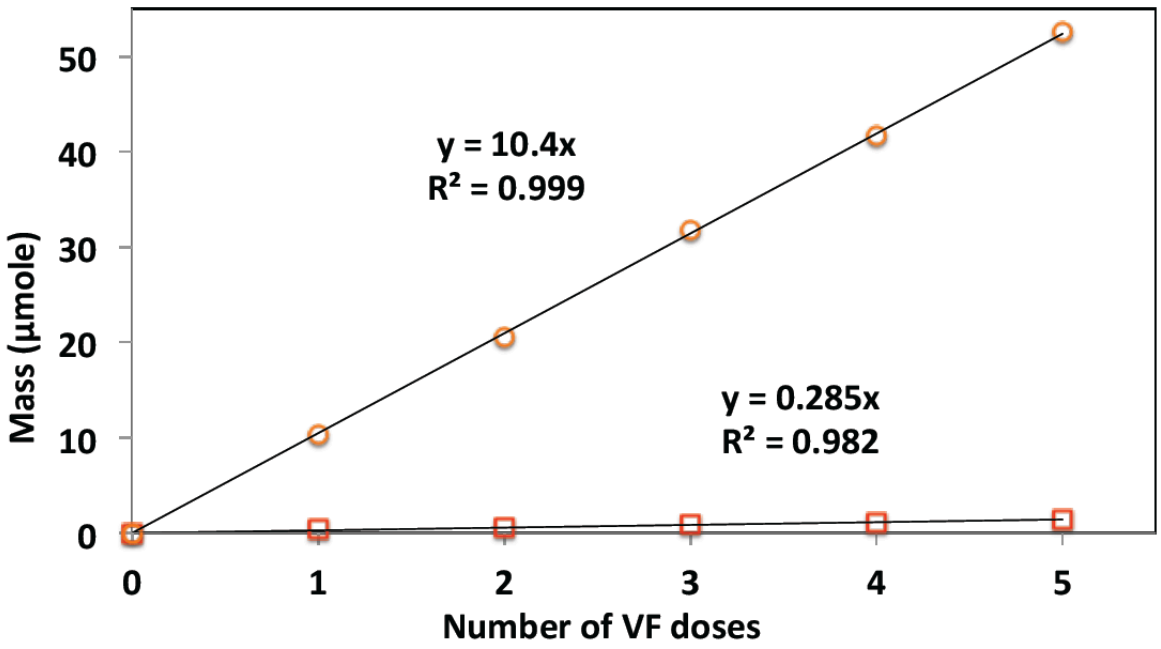

Figure 3.5: Cumulative masses of fluoroethane and ethane produced over five 10.4-µmole doses of VF added sequentially to gas-phase reactors, each containing pure H_2 and 0.86 mg of Rh/Al_2O_3 catalyst (5% Rh, w/w), and the experiment was conducted under room temperature. The orange circles represent the mass of fluoroethane, and the red squires show the mass of ethane. Reprinted with permission from reference 40. Copyright 2014, American Chemical Society.

Different from the liquid-phase experiment, the degradation profile, like Figure 3.2, was unable to be obtained because all the VF was reduced before the first sample was taken. During reaction with five doses of VF, a decrease of the rate was not observed, suggesting the catalyst did not deactivate. While reacting in water, VF

experienced both hydrodefluorination and hydrogenation, producing ethane and fluoroethane as the final products. However, fluoroethane, rather than ethane, was the main product in the gas-phase reactors. After all the VF was reduced, the fluoroethane-to-ethane mole ratio (R) was constant at 36.5. From the sharp contrast between gas- and liquid-phase experiment in reaction kinetics and product selectivity, it suggested that water played a critical role in controlling VF reduction over the catalyst.

3.3.3 Rate-Limiting Step

Because the monitoring of VF reduction in the liquid phase was based on the headspace measurement and the rate of the gas-phase reduction was much faster than the liquid-phase experiment, it could be expected that the rate constant that we obtained might not be the reduction rate. The observed VF transformation involved three elemental steps: (1) mass transfer of VF from the headspace into water, (2) mass transfer of VF from bulk water to catalyst surface, and (3) adsorption of VF to catalyst prior to reduction[3,14-16].

Since a good linear relation between reduction rate and different amount of catalyst was obtained, step 1 seemed not to be the rate-limiting step, or k_1' would be independent of Rh content, if the gas-to-liquid mass transfer were limiting. When water was absent in the system, a much faster reaction rate was observed, which suggested that the reduction of VF, could not be the slowest step (step 3) in the experiment. Based on the understanding of the system, the only remains candidate is step 2.

To assess whether step 2 could be the rate-limiting step, the liquid-to-particle mass transfer constant k_{MT}, Figure 3.6, was calculated using the method described by

Arnold et al.[3,17,34], which could be used under a situation of that a calculated Reynolds number (Re) is between 0 and 200, eq. 3.2.

$$Sh = \left(\frac{k_L^* d_p}{D}\right) = 2 + (0.6Re)^{\frac{1}{2}}(Sc)^{\frac{1}{3}} = 2 + \left(0.6\frac{d_p u_t}{\upsilon}\right)^{\frac{1}{2}}\left(\frac{\upsilon}{D}\right)^{\frac{1}{3}} \quad (3.2)$$

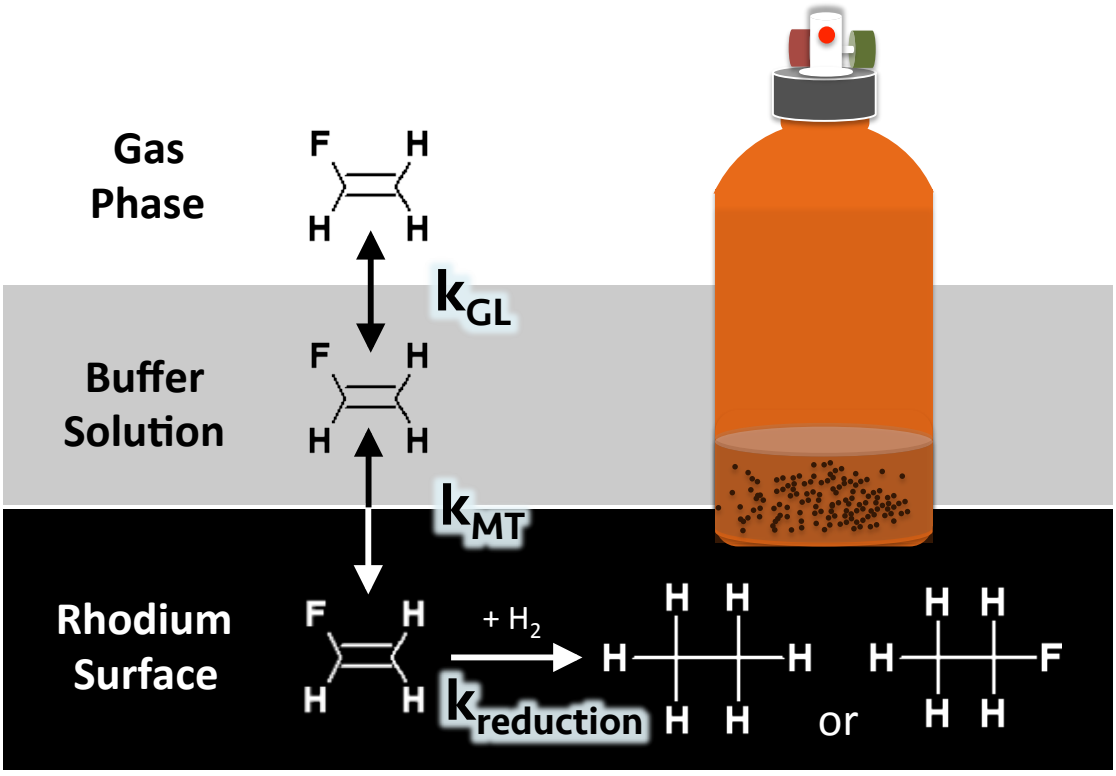

Figure 3.6: The illustration of possible rate limiting step in the reduction of vinyl fluoride. k_{GL} represents the mass transfer for VF from gas phase to water; k_{MT} shows the mass transfer from water to the surface of the catalyst; and $k_{reduction}$ is the reduction rate of VF.

In eq. 3.2, Sh and Sc are dimensionless Sherwood numbers, which are 1171.31 and 0.313 for this system; D is the diffusion coefficient for vinyl fluoride in water, $1.4\times10^{-9}m^2s^{-1}$; d_p is the diameter of the catalyst, 50 μm; υ is viscosity of the fluid, $1\times10^{-6}m^2s^{-1}$; u_t is the terminal velocity of the catalyst, 3.8×10^{-3} ms^{-1}. For the data in Figure 3.2, the geometric surface area-to-liquid volume ratio (a) was 0.54 m^2/m^3. After the calculation, the mass transfer coefficient was obtained, $k_L^* = 1.2\times10^{-4}m\ s^{-1}$. However, because the assumption for the equation, which the shape of the particle is the sphere, was different from the catalyst used in the experiment. The correction factor of 1.2 proposed by Harriott[2,28,35] was utilized in the calculation. After the calculation, the $k_{MT} = 1.2\ k_L^*\ a = 7.8\times10^{-5}s^{-1}$. This value is practically identical to the observed pseudo-first-order rate constant (k_1' = 7.96E-5 s^{-1}). Therefore, results of the experiments and calculations supported that transport of VF molecules from bulk water to catalyst surface was the rate-limiting step in liquid-phase reactors.

3.3.4 Humidified Gas-Phase Experiments

By conducting the liquid- and gas-phase experiments, the dramatic change of reaction rate and pathway was explored indicating the critical role of water in the system. To have a further investigation, humidified gas-phase experiments using H_2 with a 96±0.1% RH at a constant temperature of 22±0.05 ^oC were conducted. The choice of 96% RH was to ensure a high adsorbed water content on the surface of the catalyst and to avoid water condensation due to the fluctuation of room temperature. Under the experimental condition, the surface of the catalyst would be covered by 8 and 23 layers of adsorbed water molecules[2,36,37]. By using 1.68Å as the van der Waals radius for a water molecular[29,38], the amount of surface-bound water that accumulated on 0.86 mg catalyst was about 20-57 mmol.

From the result of the experiment, Figure 3.7, it can be seen that for the first dose of VF, the reaction rate was still too fast to be measured. However, by introducing more doses of VF, the reaction rate became slower, Figure 3.8, and gradually approaching the reaction rate of the liquid phase reactors, red solid line. Note that no discernable change in rate occurred over the same time and VF dosage in the liquid- and gas-phase reactors. In addition to the decrease of the reaction rate, the final product distribution was also changed. The R value for the humidified experiment was 2-6, which was in between dry H_2, 36.5, and aqueous reaction, 0.022. The result in Figure 3.7 proved the essential role of water affecting the reduction kinetic and pathway for the VF: even layers of surface-bound water molecules posed a pronounced mass transfer barrier that limited the overall VF reaction rate and altered the reaction route and final product distribution dramatically.

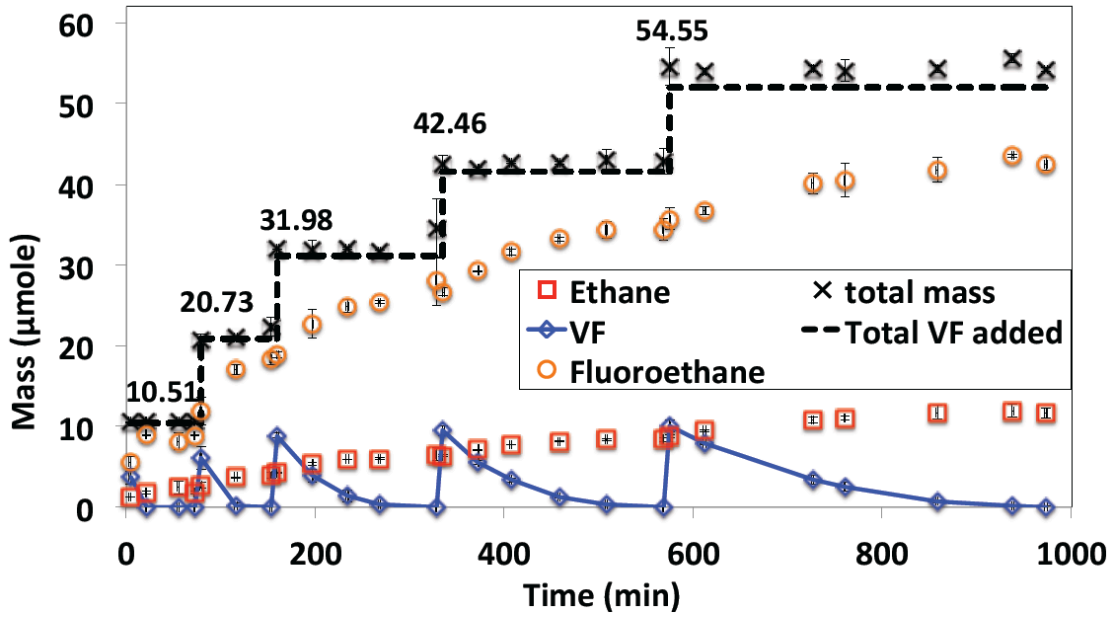

Figure 3.7: Concentration profiles and mass balance during reduction of five doses of VF (10.4±0.3 µmole/dose) in 250-mL reactors containing pre-humidified H_2 and 0.86 mg of Rh/Al_2O_3 catalyst (5% Rh, w/w). The temperature of reactors was maintained at 22±0.05 ^oC throughout experiment. Reprinted with permission from reference 40. Copyright 2014, American Chemical Society.

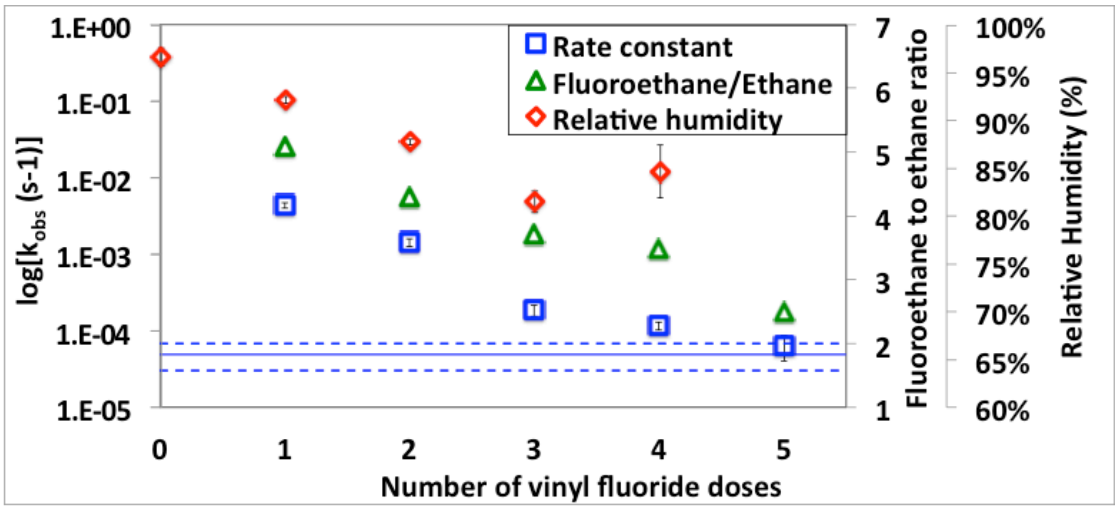

Figure 3.8: First-order rate constants of VF reduction, fluoroethane-to-ethane mole ratio, and water vapor concentration (expressed as relative humidity) during reduction of five (10.4 µmole±0.3) doses of VF over 0.86 mg of Rh/Al_2O_3 catalyst (5% Rh, w/w). The temperature of reactors was maintained at 22±0.05 ^{o}C throughout experiment. The solid line represents the first-order rate constant for VF reduction in water (i.e., from Figure 3.2) and the dashed lines represent one standard deviation. Reprinted with permission from reference 40. Copyright 2014, American Chemical Society.

For the decreasing k_1' and R in Figure 3.8, it probably caused by the production of hydrodefluorination products, H^+ and F^-. Because the hydration of the ions are highly exothermic (-1090 for H^+ and -506 kJ/mol for F^-[24,25,39]), their production would create a local osmotic imbalance at/near Rh, which would drive the migration of surface water from the vicinity and draw water molecules from gas-phase toward Rh to lower the overall water fugacity in the system. The continuing production of ions during the experiment would lead to creating increasingly thicker water layer on the surface of the catalyst, resulting in a greater mass transfer barrier and further shifted product distribution, Figure 3.8. This hypothesis could be used to explain the

selectivity of two products, ethene and fluoroethane. Since the presence of water on Rh could stabilize the relatively polar/partially charged transition state for hydrodefluorination, the reaction would be more favorite forming ethene, H^+ and F^-, and this also demonstrated low, high, and intermediate R values in liquid water, dry H_2, and humidified H_2 experiments.

This hypothesis was proved by monitoring the change of relative humidity (RH) in the reactors in the experiment. At the beginning of the experiment, the RH was 96%, and the total amount of water vapor was 260 mmol in the reactor corresponding to 2564 Pa of partial pressure, which was the initial fugacity of the water in the system. After three additional doses of VF, the RH decreased to 81%, which reflected the decrease of 400 Pa in water fugacity and removal of 41 mmol of water vapor, and it was equivalent to 0.7-2 times the initial mass of adsorbed water. By knowing the amount of accumulated water, H^+ and F^-, the ionic strength of bonded water was calculated, between 7 and 11 M at the end of the experiment. This observation could be used to explain the similar reduction rates between aqueous- and humidified gas-phase experiment. Although the water content in a humidified gas-phase reactor was far less than an aqueous reactor, the high ionic strength bonded water on the surface of the catalyst would contribute to extra mass transfer barrier to VF.

Comparing SEM images of fresh and used (for the humidified gas-phase experiment after vacuum-dried) catalyst particles, Figure 3.9a and 3.10a, the change in morphology could easily be seen after the reduction of vinyl fluoride. The results of elemental mapping (Figures 3.9b-d and 3.10b-d) showed that for the used one, fluorine that was presumably produced from HF formed during VF defluorination was

covering the surface. In the aqueous-phase reaction, the formed H^+ and F^- ions would be removed by water from the catalyst surface. In the dry gas-phase reaction, the formation of HF was minimal, and the effect of it was also limited. However, in the humidified H_2 reaction, H^+ and F^- would be absorbed by water in the vicinity to form hydrofluoric acid "solution" on the surface. It is known that HF can react with alumina to yield products such as aluminum hydroxyfluoride ($AlF_x(OH)_{3-x}\bullet 6H_2O$) and hydrated aluminum fluoride ($AlF_3\bullet 3H_2O$)[1]. If similar reactions occurred in the experiment, the aluminum fluorides could account for the surface deposits in Figure 3.10.

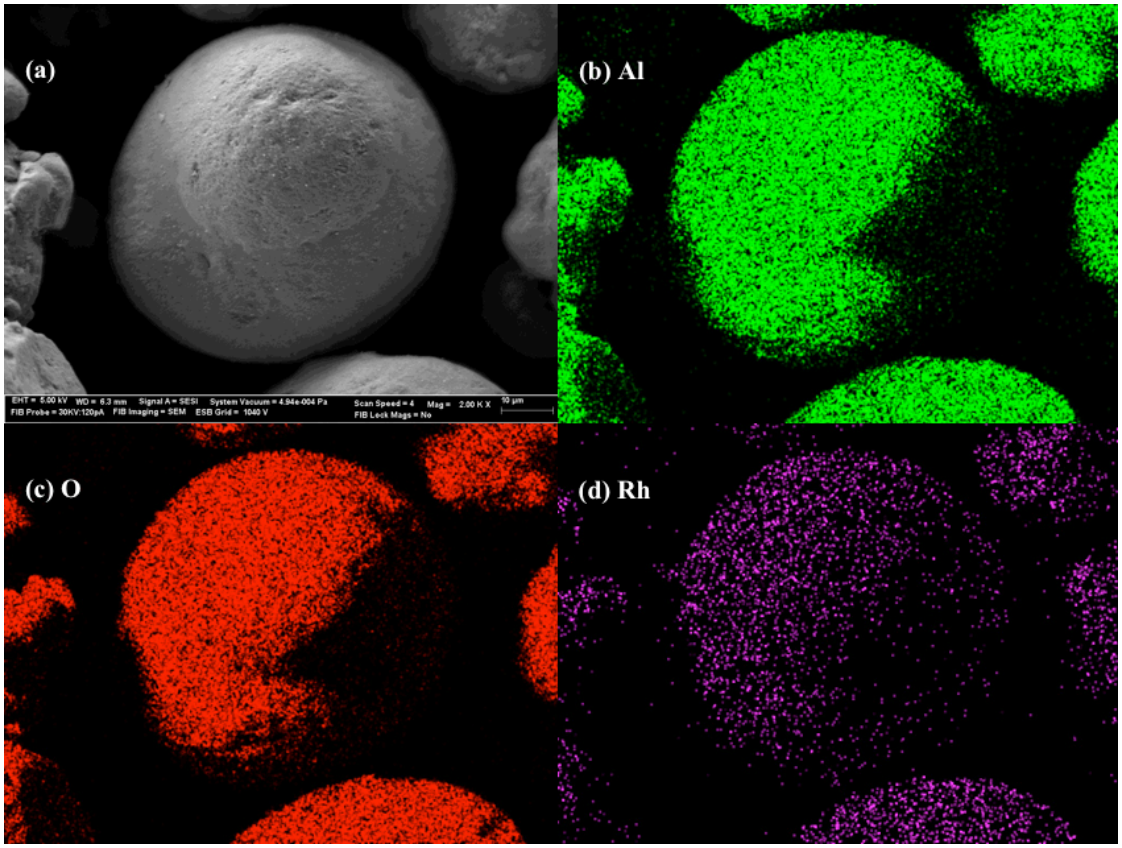

Figure 3.9: SEM and EDX images of fresh (unused) Rh/Al_2O_3 catalyst particles, illustrating the smooth morphology and uniform surface distribution of Al, O, and Rh. Reprinted with permission from reference 40. Copyright 2014, American Chemical Society.

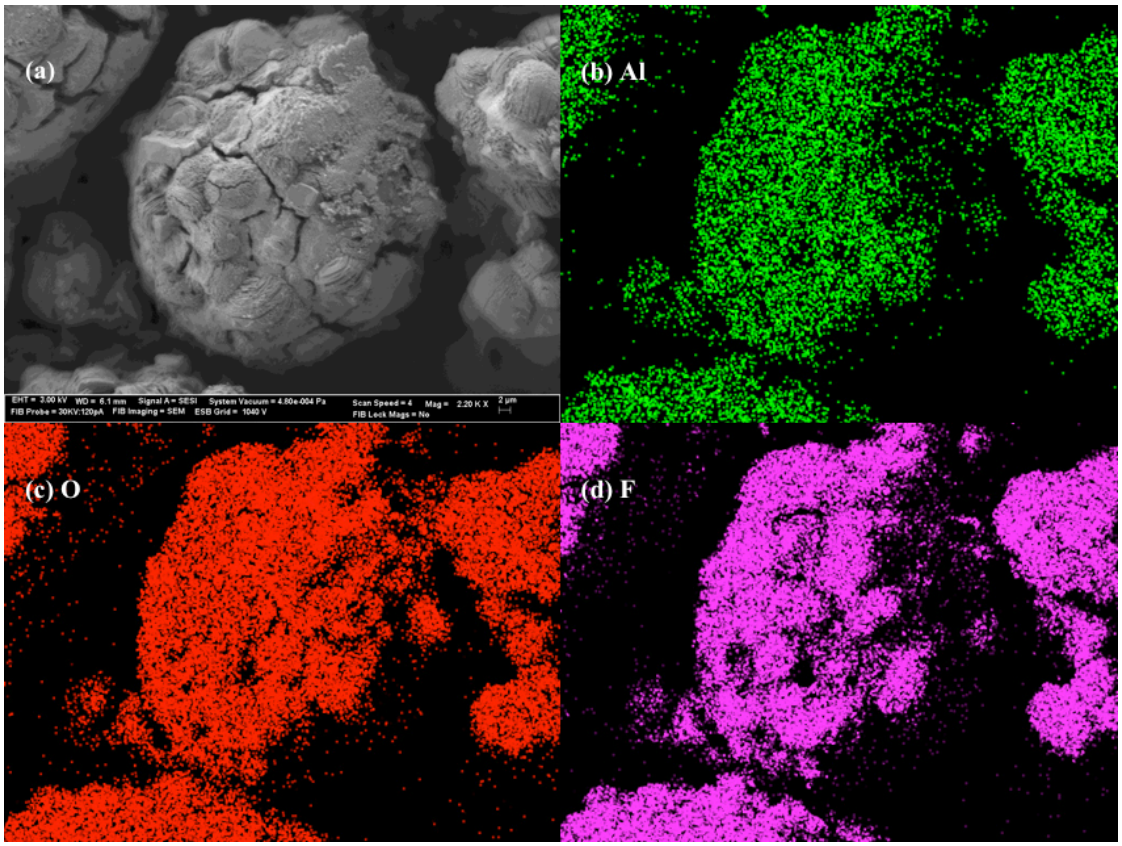

Figure 3.10: SEM and EDX images of used and vacuum dried Rh/Al_2O_3 catalyst particles, showing a crusty deposit with cracks on the surface after a humidified gas-phase experiment. Fluorine was present over the entire surface, whereas Rh was no longer detected. The crusty surface and cracks might be caused in part by the formation of aluminum fluorides and drying. Reprinted with permission from reference 40. Copyright 2014, American Chemical Society.

3.4 Summary

Many fluoroalkenes have been identified as having inhalation toxicity and carcinogenicity[41]. Because of the structural similarity to vinyl chloride, VF has been classified as a probable (IARC Group 2A) carcinogen[9-13] with a high production volume[9], which was assigned as the target compound in this study. By conducting the VF reduction experiments, the capability of the rhodium on alumina catalyst has been

verified. For the reduction pathway of VF, it would undergo both hydrodefluorination and hydrogenation. In the presence of liquid water, the hydrodefluorination was the dominant reaction route. In the absence of water, VF would experience mainly hydrogenation to produce fluoroethane as the final product. In a high relative humidity environment, the products' selectivities were in between the previous two reaction conditions. Based on the information that obtained from all three experiments and the calculations in this study, the aqueous phase experiment was mass transfer limited. By verifying the capability of rhodium on alumina catalyst and revealing the crucial role of water, this study can be an important step toward developing the first promising catalysis system to efficiently and effectively break down fluorocarbons.

REFERENCES

(1) Atkins, P.; De Paula, J. *Atkins' physical chemistry*, WH Freeman and Company Books, 2006.

(2) Baumgartner, R.; McNeill, K. *Environmental Science & Technology*, 2012, **46**, 10199–10205.

(3) Blake, D.; Howell, R. D.; Criddle, C. S. *Environmental Science & Technology*, 1997, **31**, 2445–2454.

(4) Braun, T.; Wehmeier, F. *European Journal of Inorganic Chemistry*, 2011, **2011**, 613–625.

(5) Plunkett, R. J. *Tetrafluoroethylene polymers*, US Patent Office, 1939.

(6) National Toxicology Program. *Report on carcinogens: carcinogen profiles*. 2011, 437–442.

(7) Lewandowski, G.; Meissner, E.; Milchert, E. *Journal of Hazardous Materials*, 2006, **136**, 385–391.

(8) Barber, J. L.; Berger, U.; Chaemfa, C.; Huber, S.; Jahnke, A.; Temme, C.; Jones, K. C. *Journal of Environmental Monitoring*, 2007, **9**, 530–541.

(9) National Toxicology Program. *Report on carcinogens background document for vinyl fluoride*, 2005, pp 1–42.

(10) Senthilkumar, K.; Ohi, E.; Sajwan, K.; Takasuga, T.; Kannan, K. *Bulletin of Environmental Contamination and Toxicology*, 2007, **79**, 427–431.

(11) Olsen, G. W.; Burris, J. M.; Ehresman, D. J.; Froehlich, J. W.; Seacat, A. M.; Butenhoff, J. L.; Zobel, L. R. *Environmental health perspectives*, 2007, **115**, 1298–1305.

(12) Houde, M.; Martin, J. W.; Letcher, R. J.; Solomon, K. R.; Muir, D. C. G. *Environmental Science & Technology*, 2006, **40**, 3463–3473.

(13) Prevedouros, K.; Cousins, I. T.; Buck, R. C.; Korzeniowski, S. H. *Environmental Science & Technology*, 2006, **40**, 32–44.

(14) Pirkanniemi, K.; Sillanpää, M. *Chemosphere*, 2002, **48**, 1047–1060.

(15) Turner, J. C. R. *Catalysis science and technology*, Springer Verlag, 1981.

(16) Zhang, X.-J.; Lai, T.-B.; Kong, R. Y.-C. In *Topics in Current Chemistry*, 2011, **308**, 365–404.

(17) Adams, D. E. C.; Halden, R. U. *ACS Symposium Series*, 2010, **1048**, 539–560.

(18) Clayton, J. W. *Environmental Health Perspectives*, 1977, **21**, 255–267.

(19) Tromp, T. K.; Ko, M. K.; Rodriguez, J. M.; Sze, N. D. *Nature*, 1995, **367**, 327–330.

(20) Boutonnet, J. C.; Bingham, P.; Calamari, D.; Rooij, C. de; Franklin, J.; Kawano, T. *Human and Ecological Risk Assessment: an International Journal*, 1999, **5**, 59–124.

(21) Mashino, M.; Ninomiya, Y.; Kawasaki, M.; Wallington, T. J.; Hurley, M. D. *The Journal of Physical Chemistry A*, 2000, **104**, 7255–7260.

(22) Kalb, G. H.; Coffman, D. D.; Ford, T. A. *Journal of Applied Polymer Science,* 1960, **4**, 55-61.

(23) Simril, V. L.; Curry, B. A. *Journal of Applied Polymer Science*. 1960, **10**, 62-68.

(24) McGregor, D. B.; Heseltine, E.; Møller, H. *Scandinavian journal of work, environment & health*, 1995, **21**, 310–312.

(25) Ebnesajjad, S. *Polyvinyl Fluoride*, William Andrew, 2012.

(26) Ma, R.; Shih, K. *Environmental Pollution*, 2010, **158**, 1354–1362.

(27) Boulanger, B.; Vargo, J. D.; Schnoor, J. L.; Hornbuckle, K. C. *Environmental Science & Technology*, 2005, **39**, 5524–5530.

(28) Sawama, Y.; Yabe, Y.; Shigetsura, M.; Yamada, T.; Nagata, S.; Fujiwara, Y.; Maegawa, T.; Monguchi, Y.; Sajiki, H. *Advanced Synthesis & Catalysis*, 2012, **345**, 777–782.

(29) Baumgartner, R.; Stieger, G. K.; McNeill, K. *Environmental Science & Technology*, 2013, **47**, 6545–6553.

(30) Peterson, A. A.; Thoreson, K. A.; McNeill, K. *Organometallics*, 2009, **28**, 5982–5991.

(31) Comils, B.; Herrmann, W. A.; Schlogl, R.; Wong, C. H. *Catalysis from A to Z*, Wiley, 2000.

(32) De Boer, J. H.; Everett, D. H.; Stone, F. S. *Butterworths*, 1958, **10**, 68.

(33) Amii, H.; Uneyama, K. *Chemical Reviews*, 2009, **109**, 2119–2183.

(34) Arnold, W. A.; Ball, W. P.; Roberts, A. L. *Journal of Contaminant Hydrology*, 1999, **40**, 183–200.

(35) Harriott, P. *AIChE Journal*, 1962, **8**, 93–101.

(36) Goodman, A. L.; Bernard, E. T.; Grassian, V. H. *The Journal of Physical Chemistry A*, 2001, **105**, 6443–6457.

(37) Yan, B.-D.; Meilink, S.; Warren, G. W.; Wynblatt, P. *Components, Hybrids, and Manufacturing Technology*, 1987, **10**, 247–251.

(38) Li, A.-J.; Nussinov, R. *Proteins: Structure, Function, and Bioinformatics*, 1998, **32**, 111–127.

(39) Atkins, P. W. *Physical chemistry*, Cambridge University Press, 1990.

(40) Yu, Y.-H.; Chiu, P. C. *Environmental Science & Technology Letters*, 2014, **1**, 448–452.

(41) Clayton, J. W. *Environmental health perspectives*, 1977, **21**, 255-267.

Chapter 4

WOOD-DERIVED BLACK CARBON (BIOCHAR) AS A MICROBIAL ELECTRON DONOR AND ACCEPTOR

4.1 Introduction

4.1.1 Sources of Nitrogen in Soil Environments

Nitrogen is essential for the growth of animals, microbes, crops and other plants. In soil environments, inorganic forms of nitrogen are present in such as ammonium (NH_4^+) and nitrate (NO_3^-), which can be easily used by plants[1]. Nitrogen can come from multiple sources: (1) Atmospheric deposition: Agricultural land receives a large quantity amount of nitrogen from the precipitation of nitrogen oxides (NO_x) and NH_3 from rainfalls. The major sources of NO_x comes from power plants and motor vehicles, while the sources NH_3, include industrial emissions, coal burning, livestock wastes and other agricultural sources[2]; (2) Biological fixation: Bacteria such as *Rhizobia* are able to use nitrogenase to convert dinitrogen gas (N_2) into NH_4^+. This process is central in the symbiosis of *Rhizobia* and the root systems of kudzu, clovers, soybeans, alfalfa, lupines and peanuts; (3) Fertilizers: Ammonia fertilizer is produced through industrial fixation of atmospheric N_2, typically via the Haber process. In this process, high pressure (200 atm) and temperature (>400˚C) are required, and methane (CH_4) and air are the sources of hydrogen and nitrogen, respectively; (4) Animal manures: Only a small portion of nitrogen in livestock operation is used for the production of meat or milk[3], while over 70% of nitrogen is excreted[4].

4.1.2 Production of Nitrate in Soil Environments

In a soil environment, microbial activities contribute to the main effort for the transformation of NH_4^+ to NO_3^-. When the available carbon source is limited in the environment, NH_4^+ would be rapidly converted into NO_3^-, a process in which *Nitrosomonas* and *Nitrobacter* are usually involved in tandem[5]. *Nitrosomonas* oxidizes NH_4^+ to NO_2^-, which is followed by the oxidation of NO_2^- to NO_3^- by *Nitrobacter*. Since the kinetics for NO_3^- formation is much faster than the production of NO_2^-, NO_3^- is usually the dominant nitrogen species[5]. Based on the research of Powlson, the oxidation of NH_4^+ is not the only source of NH_4^+; for the mineralization of organic N such as crop and plant residues is another major NO_3^- source in soil[6].

4.1.3 Nitrate and Eutrophication

Global nitrogen cycle has been dramatically altered by human activity, and the rate of N input in the terrestrial N cycle have about doubled and will continuously increase in the future[7,8]. In many cases, the applied as fertilizer usually exceed the need of plants for growth. This extra N would accumulate in soil or be discharged to surface water or groundwater[8,9]. The surplus N has been found to have a strong impact on the growth of algae and vascular plants in many water bodies causing eutrophication[10,11]. Eutrophication is one of the most widespread problems to surface waters in the U.S.[12]. The main effect of eutrophication is to cause algal blooms, which would have detrimental impacts on the ecosystem and the water quality[13]. The impacts include: (1) increasing biomass of phytoplankton and periphyton; (2) decreasing diversity of phytoplankton and periphyton species; (3) population shifting to the phytoplankton species that are toxic; (4) increasing water turbidity; (5) decreasing dissolved oxygen concentrations; and (6) taste and odor problems.

4.1.4 Nitrate in Drinking Water and Its Health Risks

Because NO_3^- is an anion with very high water solubility, it can easily move along with water following precipitation or irrigation, and migrates to surface water and groundwater. In the United States, the background level of NO_3^- in natural waters is lower than the USEPA drinking water standard (10 mg L^{-1}) [14]. However, shallow wells adjacent to farmlands could have much higher NO_3^- concentrations due to discharge of agricultural runoff[15]. Given that groundwater is an important source of drinking water in the U.S., about 2-3% of the total U.S. population is potentially exposed to NO_3^- concentrations higher than 50 mg L^{-1} [16].

The toxic effect of NO_3^- on the human body is mainly attributed to the production of NO_2^- [17]. When NO_3^- is ingested, it is absorbed rapidly by the small intestine and distributed to the tissues. In the distribution process, over 25% of NO_3^- would be transported and concentrated in the saliva. After the NO_3^- is transported, the oral microflora would reduce about 20% of NO_3^- to NO_2^-, and both of them would re-enter the gastrointestinal tract[18]. The absorbed NO_2^- in the human body would cause the oxidation of hemoglobin (Hb) to methemoglobin (metHb), which makes the Fe^{2+} in the heme become Fe^{3+}, rendering the heme unable to bind oxygen[19]. When the concentration of metHb is more than 10% of Hb, methaemoglobinaemia would occur causing cyanosis and even asphyxia[19]. In general, the presence of (NADH)–cytochrome b5–metHb reductase in the human body is able to reduce metHb to Hb. However, for infants below four months of age, the level of metHb reductase is low, and as a result, higher level of metHb would be found in infants than adults[17].

4.1.5 Nitrate Removal from Water

Methods to remove NO_3^- from water can be classified into three major categories: physical adsorption, chemical reduction and biological reduction. Physical adsorption of NO_3^- can be achieved by using adsorbents that have positive surface charge and/or anion exchange capacity. Several materials have been evaluated including ion-exchange resins[20], activated carbon[21], bamboo powder charcoal[22] and amine-modified coconut coir[23]. Although some of these materials showed promising NO_3^- removal efficiency, they may not be suitable for *in situ* application due to high cost. For chemical reduction, the removal of NO_3^- can be achieved by using, for example, bimetallic catalysts (e.g., Pd-Cu with hydrogen or formic acid) [24,25], zero valent iron (ZVI)[26], and aluminum (Al)[27]. However, because of the high cost of the catalyst, the chance is low to have *in situ* catalytic reduction of NO_3^-. For the use of ZVI and Al, since the final product is NH_4^+, post-treatment is required. Biological denitrification can be suitable for *in situ* applications, since denitrifying bacteria are ubiquitous in a natural environment[28]. The process is particularly advantageous since NO_3^- serves as the terminal electron acceptor for microbial respiration and the main final product is nitrogen gas (N_2). A wide spectrum of organic carbons such as methane[29], methanol, ethanol[30], vegetable oil[31,32] and agricultural wastes[33-35] have been used as carbon and electron sources to support microbial nitrate reduction. However, above electron donors are not regenerable and need to be supplied/replenished periodically, which would add to the labor and material costs. Also, because NO_3^- is a non-point source pollutant, it makes treatment challenging.

In recent studies of bioretention cells, the use of biochar as the matrix material has been suggested to be beneficial to the removal of total suspended solids (TSS), N, P, and bacteria from stormwater[36-38].

4.1.5.1 Biochar

Black carbon (BC), pyrogenic organic carbon produced through pyrolysis or incomplete combustion of biomass[36], has attracted much interest in environmental research areas. When the feedstock of BC is surplus biomass, it is specifically referred to as biochar (biomass-derived charcoal)[37]. In a natural environment, BC and natural organic matter (NOM) are the two major geosorbents controlling the transport and fate of hydrophobic environmental contaminants[38-40]. The early studies of BC such as biochar were mainly focused on adsorption, and BC was often assumed to be a chemically inert sorbent in sedimentary environments [41-43]. However, recent studies have shown that BC including biochar, soot, activated carbon, graphite, char, carbon nanotubes, and graphene oxide are able to mediate the reduction of nitrogenous compounds abiotically[44-47]. By physically separating nitro and azo aromatic compounds, heterocyclic nitramines, and nitrate esters from the reductant, high purity graphite is still able to mediate the reduction. It is suggested that electrical conductivity and the ability to transfer atomic hydrogen are the main mechanisms for the catalytic capability of the graphitic region of BC[48,49]. In addition to the highly graphitic carbons, the mechanism for the less graphitic carbon, such as soot and biochar may be different. Analogue to NOM, the functional groups on BC such as quinone groups may be able to undergo reversible redox reactions, which provides an explanation for the catalytic ability of biochar. However, these chemical reduction mechanisms would not extend to NO_3^- since it does not adsorb to biochar to a significant extend. Therefore, the mechanism for the biochar facilitated NO^3- reduction in bioretention[50-52] cells is still unclear.

4.1.5.2 *Geobacter Metallireducens*

Exoelectrogens such as *Geobacter spp.* are the anaerobic bacteria that can directly transfer electron in and out of the cell without using cell synthesized soluble compounds[53], and they are prevalent in sedimentary environments, such as aquatic sediments, wetlands, and subsurface environments[54-60]. *Geobacter spp*. are anaerobic prokaryotes, and they are well known by their ability to oxidize/reduce organic compounds and metals[61]. They can directly harvest electrons from organic compounds and then transfer the electrons to metals, such as Fe^{3+}, to complete the electron transport chain for the metabolic cycle[62]. In addition, recent studies on exoelectrogenic bacteria suggested that NOM, such as humic acid, is able to be both an electron donor[63] and acceptor[64,65] to support the microbial respiration of *Shewanella oneidensis* MR-1 and *Geobacter spp*. Similar to humic substances, biochar also has quinone groups that can undergo reversible redox reactions, and biochar may able to be both an electron donor and acceptor for quinone groups exoelectrogens.

A recent study on the electron storage capacity (ESC) of biochar has suggested that by varying the feedstock and pyrolysis temperatures the ESC of plant-based biochar could be up to 2 mmol e^-/g[66], which is comparable to the ESC of dissolved and particulate organic matter[67,68]. Since exoelectrogenic bacteria, such as *Geobacter spp.*, are able to use humic substances as electron donor and acceptor, it can be expected that this is the active role of biochar in a bioretention system. Note that the role of the functional groups in biochar involves storage of electrons, which is different from the mechanism based on the electroconductivity of the graphitic region. In this study *Geobacter metallireducens* (GS-15) was used to investigate the role of redox active functional groups in biochar to exoelectrogenic bacteria, even though the final product is NH_4^+. There are three main reasons that GS-15 was used in the study. (1) GS-15 can

use simple organic molecule such as acetate (AC) as electron donor for the reduction of NO_3^-; (2) GS-15 is able to utilize humic acid as both electron donor[63] and acceptor[64]; and (3) GS-15 does not use hydrogen gas (H_2) as electron donor for the reduction[61,69], and H_2 is present in our glovebox for removing oxygen from the inside environment.

4.2 Materials and Methods

4.2.1 Biochar

Soil reef biochar (The Biochar Company, PA) was used in this study. The production of biochar was from the pyrolysis of Southern Yellow hardwood chips at 550˚C. The properties of the biochar are listed in Table 4.1. The biochar was sieved, and only particle sizes between 250-500 μm were used. To oxidize the redox active functional groups in the biochar, the sieved biochar was placed in DI water (50 g L^{-1}) and subjected to low-pressure aeration and settlement cycles for 60 h. After the aeration, the biochar was dried by using a vacuum oven (Fisher, Pittsburgh, PA). All air-oxidized biochar was sterilized by autoclaving (121°C, 15 min) and degassed with 80:20 N_2:CO_2 gas mixture (Keen Compressed Gas, Wilmington, DE) prior to experiments. To quantify the soluble organic content of the biochar, water samples of rinsates/filtrates were analyzed. The result of total organic carbon (TOC) analysis suggested that the washed/oxidized biochar contained minimal soluble organic carbon (Table 4.2).

Table 4.1. Physical-chemical properties of Soil Reef biochar

	Value[a]	Units	Method
pH	8.71[b]		1:20 w/v in DI water, 24 hr
Electrical Conductivity (EC 20 w/w)	283	mmhos cm^{-1}	4.11 USCC:dil. Rajkovich
Total Ash	21.4	% of total mass	ASTM D-1762-84
Particle Density	1.816[b]	g cm^{-3}	
BET Surface Area	391±10[b]	m^2 g^{-1}	N_2 adsorption
Organic Carbon (org-C)	74.2	% of total mass	Dry Combustion-ASTM 4373
Total Nitrogen (N)	0.59	% of total mass	Dry Combustion-ASTM 4373
Hydrogen/Carbon (H/C) Ratio	0.26		Dry Combustion-ASTM 4374

[a]Data provided by The Biochar Company unless otherwise noted.
[b]Measured at the University of Delaware.

Table 4.1 Physical-chemical properties of Soil Reef biochar (continued)

Liming (neutral value as $CaCO_3$)	14.7	% $CaCO_3$	Rayment & Higinson
Total Potassium(K)	3566	mg/Kg dry mass	Enders & Lehman
Available K	4034	mg/Kg dry mass	Wang after Rajan
Total Phosphorous(P)	2528	mg/Kg dry mass	Enders & Lehman
Available P	1608	mg/Kg dry mass	Wang after Rajan
Total N	0.59	mg/Kg dry mass	KjN
Ammonia (NH_4-N)	4.1	mg/Kg dry mass	Rayment & Higinson
Nitrate (NO_3-N)	63	mg/Kg dry mass	Rayment & Higinson
Organic (Org-N)	5800	mg/Kg dry mass	
Volatile Matter	79	% dry mass	ASTM D-1762-84
Arsenic (As)	1.4	mg/Kg dry mass	EPA 3050B/EPA 6010
Cadmium (Cd)	<0.01	mg/Kg dry mass	EPA 3050B/EPA 6010
Chromium (Cr)	11	mg/Kg dry mass	EPA 3050B/EPA 6010
Cobalt (Co)	1.3	mg/Kg dry mass	EPA 3050B/EPA 6010
Copper (Cu)	24	mg/Kg dry mass	EPA 3050B/EPA 6010
Lead (Pb)	3	mg/Kg dry mass	EPA 3050B/EPA 6010
Molybdenum (Mo)	0.22	mg/Kg dry mass	EPA 3050B/EPA 6010
Mercury (Hg)	<0.2	mg/Kg dry mass	EPA 7471
Nickel (Ni)	5.1	mg/Kg dry mass	EPA 3050B/EPA 6010
Selenium (Se)	<0.3	mg/Kg dry mass	EPA 3050B/EPA 6010
Zinc (Zn)	15	mg/Kg dry mass	EPA 3050B/EPA 6010
Boron (B)	40	mg/Kg dry mass	TMECC
Chlorine (Cl)	325	mg/Kg dry mass	TMECC
Sodium (Na)	465	mg/Kg dry mass	EPA 3050B/EPA 6010

[a]Data provided by The Biochar Company unless otherwise noted.

[b]Measured at the University of Delaware.

Table 4.2. Dissolved organic carbon in biochar rinsate/filtrate

	Batch[a]	TOC (mg/L)		DOC content (mg/g biochar)	EEC[b] (mmol e^-/g biochar)
		Mean	Stdev		
First Rinsate	A	32.9	1.7	0.66	0.0022
	B	32.9	0.8	0.66	0.0022
	C	42.1	0.9	0.84	0.0028
Second Rinsate	A	28.3	2.4	0.57	0.0019
	B	28.6	0.8	0.57	0.0019
	C	42.1	0.9	0.84	0.0028
Vacuum Filtrate	A	15.5	1.2	0.31	0.0010
	B	20.2	1.9	0.40	0.0014
	C	15.7	0.7	0.31	0.0010

[a]Each batch contained 50 g of sieved biochar washed and aerated in 1 L of deionized water.

[b]Electron exchange capacity calculated using the carbon content (0.581) and electron capacity of Elliott soil humic acid (1.96 mmol/g humic acid), which had the highest electron capacity of all the humic and fulvic acids studied by Aeschbacher et al.[1]

4.2.2 Microorganism

GS-15, *Geobacter metallireducens* (ATCC 53774) was chosen for this study. GS-15 was grown in a modified ATCC 1768 medium (Table 4.3) with 5mM sodium nitrate as the electron acceptor and carbon source, and 5mM sodium acetate as the electron acceptor. After an 18 h incubation, the culture was washed 4 times by using blank medium (ATCC 1768 medium without electron donor, electron acceptor and NH_4^+). For each wash, the cells were centrifuged at 1100g for 15 min. The washed cell pellet was resuspended at a density of 5 to 9E10 cells mL^{-1} using the blank medium.

Table 4.3. Ingredients of 1 L modified ATCC 1768 medium

$NaHCO_3$	2.5g	$C_2H_3NaO_2$	0.41g
NH_4Cl	1.5g	$NaNO_3$	0.43g
$NaH_2PO_4 \cdot 2H_2O$	0.678g	Wolfe's mineral solution (10ml)	
KCl	0.1g	Nitrilotriscetic acid	15mg
Wolfe's vitamin solution (10ml)		$MgSO_4 \cdot 7H_2O$	30mg
Biotin	20µg	$MnSO_4 \cdot H_2O$	5mg
Folic acid	20µg	NaCl	10mg
Pyridoxine hydrochloride	100µg	$FeSO_4 \cdot 7H_2O$	1mg
Thiamine hydrochloride	50µg	$CoCl_2 \cdot 6H_2O$	1mg
Riboflavin	50µg	$CaCl_2$	1mg
Nicotinic acid	50µg	$ZnSO_4 \cdot 7H_2O$	1mg
Calcium D-(+)-pantothenate	50µg	$CuSO_4 \cdot 5H_2O$	0.1mg
Vitamin B12	1µg	$AIK(SO_4)_2 \cdot 12H_2O$	0.1mg
p-Aminobenzoic acid	50µg	H_3BO_3	0.1mg
Thioctic acid	50µg	$Na_2MnO_4 \cdot 2H_2O$	0.1mg

4.2.3 Experimental Setup

In this study, 125 mL serum bottles were used for the experiments. After the inoculation inside the anaerobic chamber ($N_2/CO_2/H_2$, 75:20:5), all reactors were sealed with butyl rubber stoppers and aluminum crimps, foil-wrapped, and were

incubated under 30˚C. Water samples were taken at predetermined time points, and then analyzed for AC, NO_2^-, NO_3^- and NH_4^+.

4.2.3.1 Acetate Utilization Experiment

Cell suspension (~2×10^8/mL) with two different amounts of oxidized biochar (2 and 4 g) was set up in quintuplicate 125 mL serum bottles, and each reactor contained 104 ml of blank medium, Figure 4.1. Additional sets of triplicate reactors were prepared as control groups: abiotic control (2 g of oxidized biochar without cells), biotic control (cells without biochar), and blank medium. Cysteine (TCI American, Portland, OR), 158 mmol, <5% of the electrons needed for acetate oxidation, was added to each bottle to scavenge oxygen. All reactors were spiked with 0.4 mmol of sodium acetate, and the pH was 6.9±0.1 throughout the experiments.

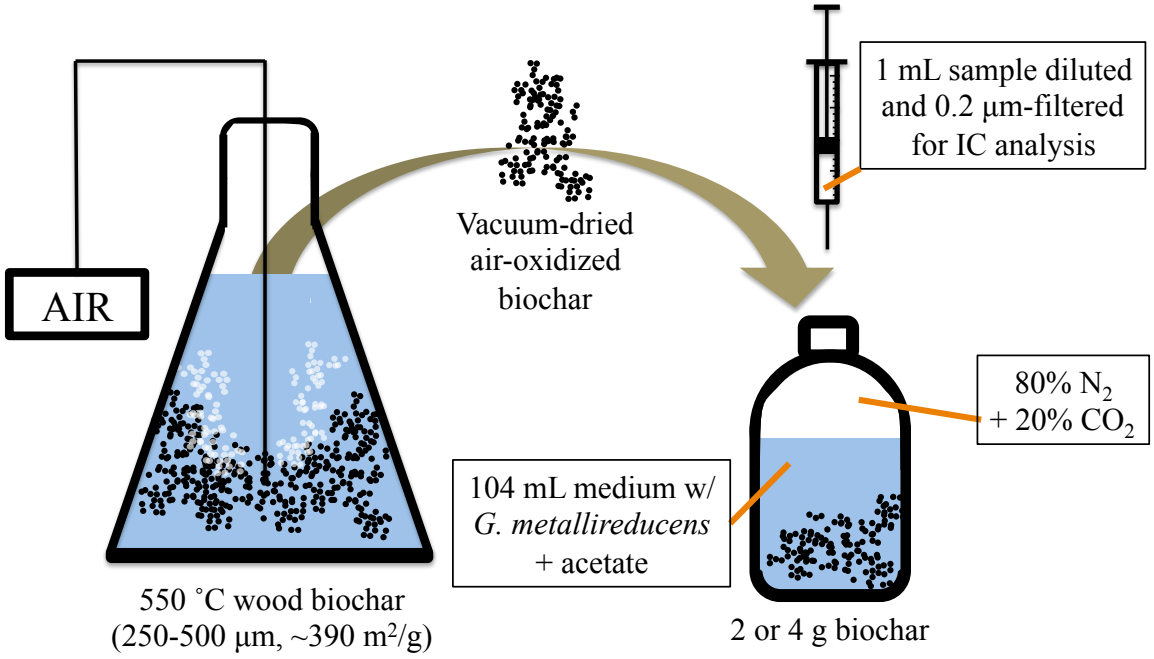

Figure 4.1: The setup for the acetate utilization experiments

4.2.3.2 Nitrate Reduction Experiment

Upon the completion of the acetate oxidation experiment, reactors containing 2 g of biologically-reduced was used. The reduced biochar was washed 5 times with 30 mM bicarbonate buffer and 2 times with blank medium to remove residual acetate and cells for the experiment. Reactors and controls were set up in triplicate as described in the acetate utilization experiment, except that either oxidized or biologically-reduced biochar was used, Figure 4.2. The comparable amount of cells was also used in this experiment, and ~0.45 mmol of nitrate was spiked in each reactor. However, because of failure to remove cells associated with biochar, abiotic controls (reduced biochar with NO_3^-) were not included in the experiment. To further test the hypothesis, dithionite-reduced biochar was used for the second nitrate reduction experiment. To produce dithionite-reduced biochar, 100 mL of 75mM sodium dithionite (Fisher, Pittsburgh, PA) solution was added to 2 g of air-oxidized biochar in serum bottle. After reacting overnight, the biochar was washed 6 times with 30 mM sodium bicarbonate buffer and 2 times with blank medium prior to use. The preparation of the experiment was the same as described above, but the cysteine was not used in this experiment.

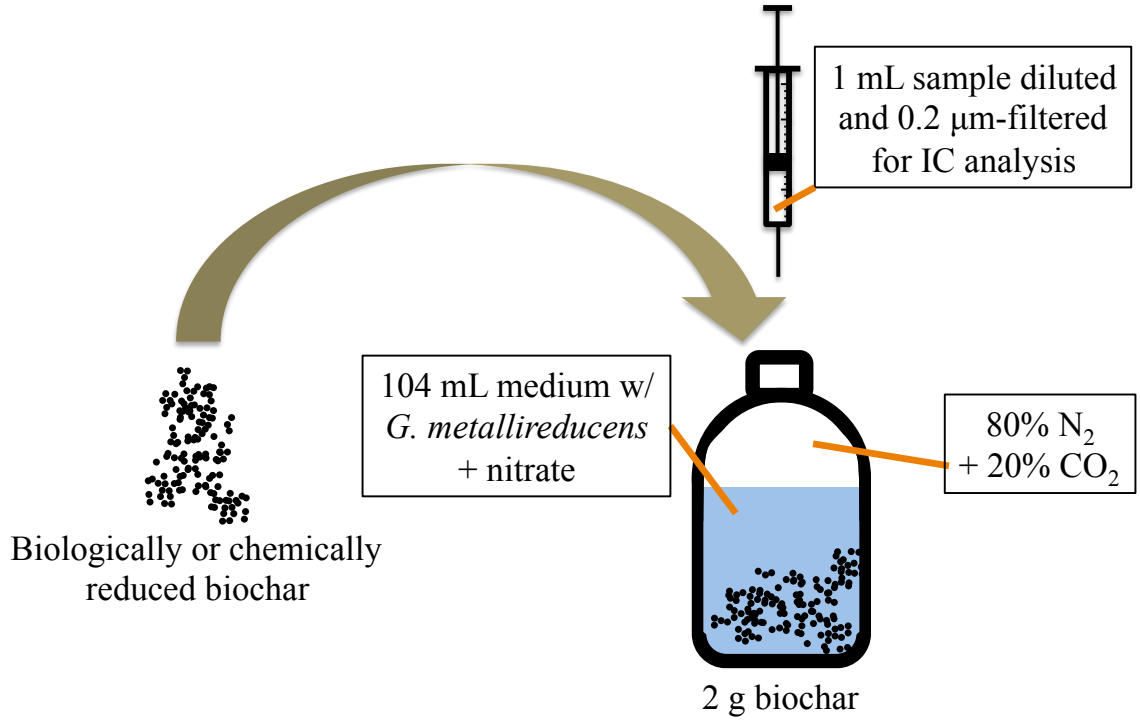

Figure 4.2: The setup for the nitrate reduction experiment

4.2.4 Sampling and Analytical Methods

Samples for the analyses of NH_4^+, AC, NO_2^- and NO_3^- were collected at predetermined times during batch experiments. The procedure for sampling followed a strict protocol to prevent microbial contamination and oxygen infusion. Before doing the sampling, the rubber stopper of a reactor was sterilized by using 70% ethanol. The glass syringe for sampling used sterile disposable needle and was flushed several times with N_2:CO_2 gas (80:20). One mL sample was drawn and diluted 10 times with deionized water in a 10 mL volumetric flask. After mixing, the diluted sample was immediately filtered with 25 mm diameter syringe filter (0.22-µm MCE, Millex - GS). The filtrate was transferred into two separate plastic vials (1.5 mL for NH_4^+ analysis and 8 mL for the anion analysis). Anion samples were analyzed immediately after

sampling by using an ion chromatograph (IC). The filtered NH_4^+ samples were stored under 4˚C, and the analysis was performed at the end of each experiment. To verify the issues of contamination or NH_4^+ loss during the storage, NH_4^+ standards were made in parallel under the same preparation methods and storage conditions for quality control, where the results suggested that the loss of NH_4^+ is negligible.

AC, NO_2^- and NO_3^- were analyzed by using a Metrohm 850 Professional IC with MagIC Net analytical software. The eluent was 6.5 % v/v acetone with 3.2 mM sodium carbonate and 1.0 mM sodium bicarbonate. The flow rate was 0.7 mL/min, and the column oven was set at 28˚C. For the analysis of NH_4^+, a Dionex IC (ICS-1100) equipped with an Ion PAC CS16 (5 x 250 mm) was used. The mobile phase was 38 mN sulfuric acid, with a flow rate of 1 mL/min. The concentrations of NH_4^+ were detected using a conductivity detector and quantified using Chromeleon 7.0 software.

The quantification of concentrations of AC, NO_2^-,NO_3^-, and NH_4^+ was based on the calibration curves. The preparation of calibration standards used sodium acetate, sodium nitrate, sodium nitrite and ammonium chloride, individually prepared for each analyte. The concentrations of the calibration standards were 0.1, 0.25 and 0.5 mM. Calibration standards were also used during IC analysis of each batch of experimental samples for quality control purposes.

4.3 Results and Discussion

4.3.1 Acetate Utilization Experiment

Figure 4.3 shows the results of the experiment, where AC was used as the electron donor supporting microbial activity and air-oxidized biochar was used as the electron acceptor. The AC utilization was observed in the blank, biotic and abiotic

controls, indicating that without an electron acceptor, GS-15 cannot use AC, and that the physical losses (e.g., sorption to biochar) of AC were minimal. In the presence of air-oxidized biochar and AC with GS-15, the consumption of AC was observed. The AC consumption rate with 2 g of biochar was 0.66±0.10 mM/d in the first 2 d and approached a plateau. This result suggested that the air-oxidized biochar could act as electron sink to support AC oxidation by GS-15. When the amount of air-oxidized biochar was doubled from 2 to 4 g, the initial degradation rate doubled, 1.3±0.1 mM/d, and the AC was completely consumed. This observation suggested that the amount of AC utilization was limited by the biochar loading in the 2 g reactors. Therefore, the result of AC oxidation supports the hypothesis that biochar can be the microbial electron acceptor.

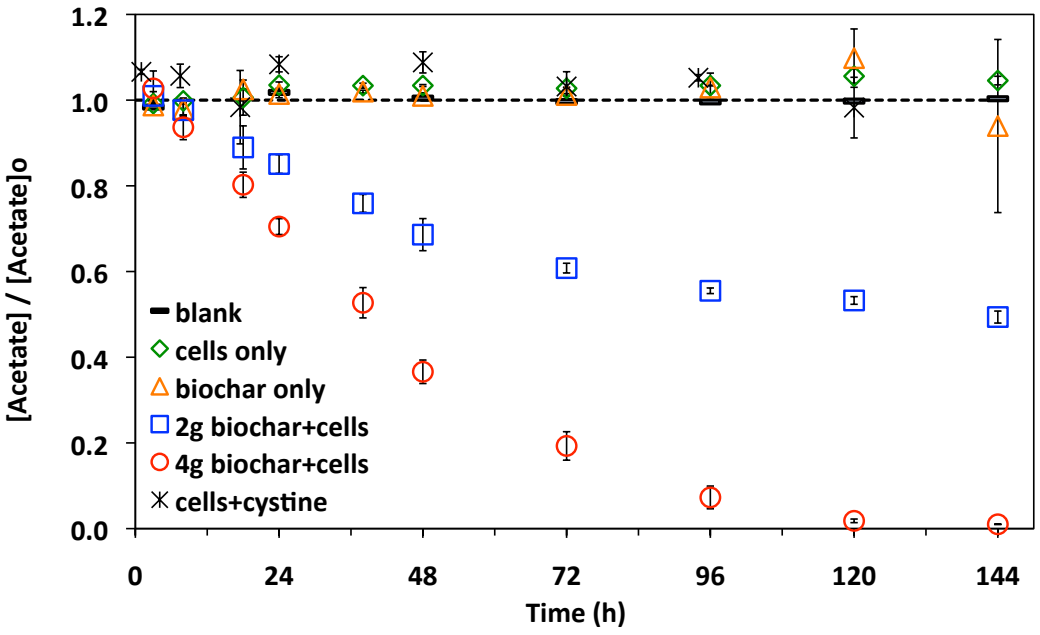

Figure 4.3: Acetate utilization in batch reactors containing blank (blank medium), cells only (without biochar), cells with 1.6 mmol of cystine (no biochar), biochar only (2 g of oxidized biochar without cells), and cells with 2 g or 4 g of oxidized biochar. For biotic biochar reactors and controls, error bars represent one standard deviation from quintuplicate and triplicate reactors, respectively. The initial acetate concentration was approximately 4 mM for all reactors, and the experiment was conducted under 30˚C. Reprinted with permission from reference 89. Copyright 2016, American Chemical Society.

It has been reported that cysteine/cystine couple could act as a mediator for the electron transfer in syntrophic acetate oxidation[70]. Although GS-15 cannot utilize cysteine and cystine as the substrate[61], the cysteine may be abiotically oxidized to cystine by the biochar, which could be a potential electron acceptor for GS-15 to oxidize AC. However, the loss of AC was not observed from a control containing cell, AC and stoichiometric amount (1.6 mmole) of cystine (Figure 4.3), which suggested

that cystine could not be the electron acceptor for the AC oxidation, and it also confirmed that GS-15 transferred electrons directly to biochar in the bioreactors.

Assuming the consumed acetate was converted to CO_2, eight electrons (per one molecule of acetate) would be transferred to biochar in our system. Based on stoichiometric calculation from the AC consumption, the electron storage capacity (ESC) of the air-oxidized biochar was 0.766 mmol e^-/g biochar. Compared to previously reported EAC for biochar (wood pyrolyzed at 500 °C) using electrochemical methods (0.54 mmole e^- g^{-1}biochar[66]), the EAC value of our air-oxidized biochar is higher (0.86 mmole e^- g^{-1} biochar). The difference in EAC values can be attributed to variation in process parameters such as feedstock and pyrolysis temperature during biochar production. However, the actual ESC of the biochar may be greater than 0.766 mmol e^-/g biochar, which is discussed below.

4.3.2 Nitrate Reduction Experiment

Figure 4.4 depicts the results of nitrate reduction experiment for the biologically reduced biochar. Without cells, the concentration of NO_3^- did not change in the blank and oxidized biochar reactors. For the cell-received controls, NO_3^- was consumed instantly to a limited extent, with or without the use of biochar. For these controls, NH_4^+ was detected indicating the reduction of NO_3^-, which suggested that the possible electron donors were added cells and cysteine. In the previous studies, *Geobacter spp.* has been suggested to have the ability to store electron in periplasmic and outer-surface cytochromes[61], and the ability was also showed in the study for the reduction of Pu(VI) and U(VI) by using rest cells of GS-15 without other electron donor[71]. For the electrons from the GS-15 and the added cysteine, based on nitrate losses in Figure 4.4 (assuming 8 electrons for the reduction of NO_3^- to NH_4^+), the total amount of

electrons from the biomass would be 0.173 mmol e^-/reactor. Based on the additional electrons from cysteine and cells, the actual ESC for the air-oxidized biochar in the AC utilization experiment would be around 0.85 mmol/g biochar. In contrast to the controls, reactors containing cells, NO_3^-, and biologically reduced biochar (from the AC utilization experiment) had a further consumption, which was followed by the production of NO_3^-, Figure 4.5.

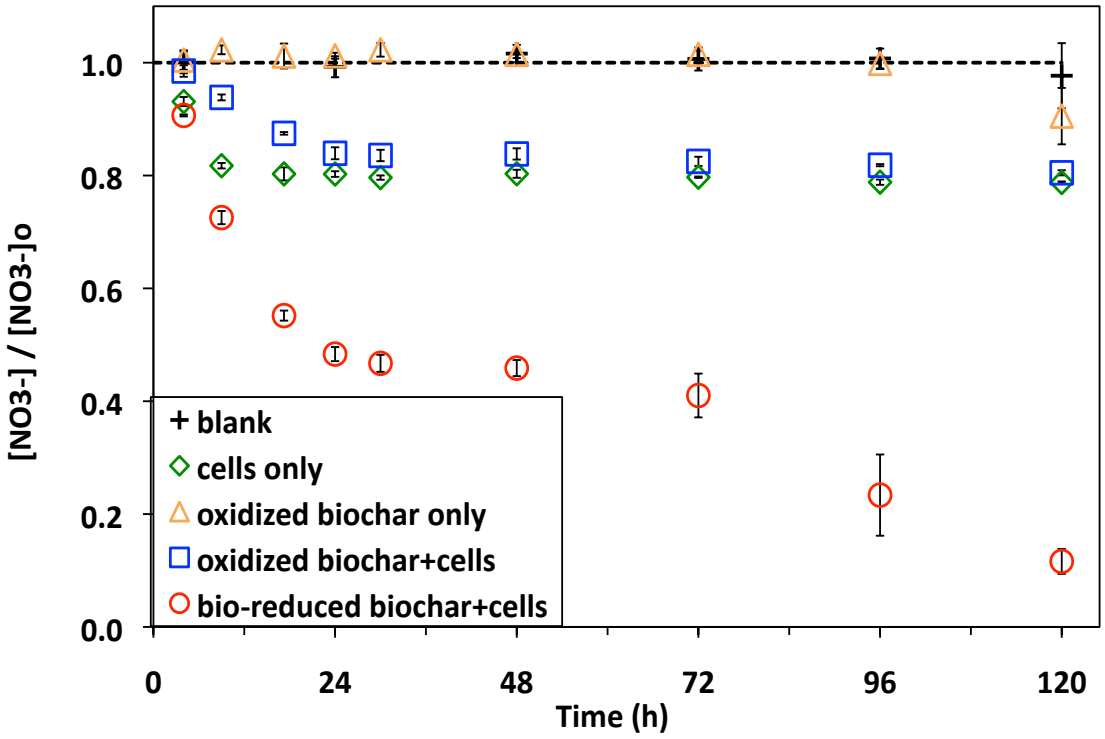

Figure 4.4: Nitrate reduction experiment with biologically reduced biochar, which contains blank (blank medium), cells only, 2 g of oxidized biochar with and without cells, and 2 g of biologically reduced biochar with cells. Initial nitrate concentration was approximately 4 mM for all reactors. Error bars represent one standard deviation from triplicate reactors. The experiment was conducted under 30˚C. Reprinted with permission from reference 89. Copyright 2016, American Chemical Society.

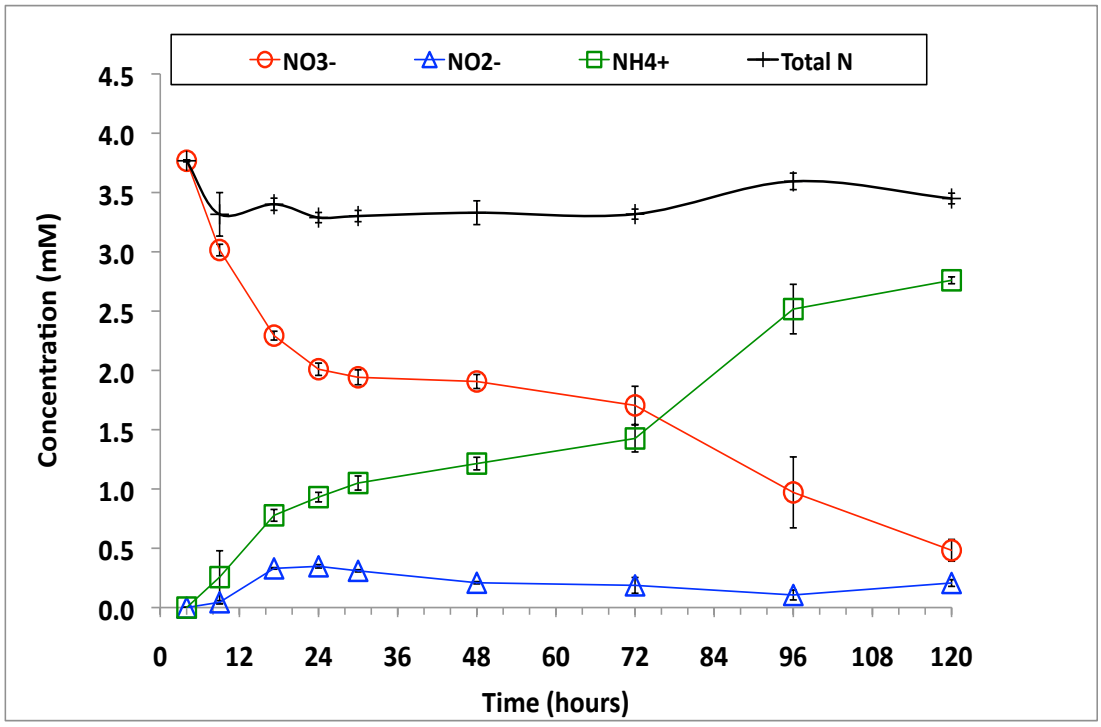

Figure 4.5: Biologically reduced biochar as the electron donor. Comparing with the initial nitrate concentration, the ammonium yield was 79.6%. Initial nitrate concentration was approximately 4 mM for all reactors, and the experiment was conducted under 30˚C. Reprinted with permission from reference 89. Copyright 2016, American Chemical Society.

The controls containing biologically reduced biochar and NO_3^- were compromised, appendix B. Because washing procedure cannot remove all the cells that are associated with biochar, Figure 4.6, the NO_3^- concentration reduced after the initial lag. To verify that the reduced biochar cannot reduce NO_3^- abiotically, and to confirm either biologically and chemically reduced biochar can be the electron donor

to support NO_3^- reduction by GS-15, another experiment using dithionite-reduced biochar was performed, Figure 4.7. The result of the experiment showed that without the use of cells, reduced biochar could not reduce NO_3^- abiotically. Same as the observation from the biologically reduced experiment, the cell only controls also showed the limited NO_3^- reduction. Based on the yield (25-30%) of NH_4^+ in all controls, the removed NO_3^- was only partially reduced. For the reactors containing both reduced biochar and GS-15, the further consumption of NO_3^- was observed. The NO_3^- concentration reached a plateau at 72 h, and interestingly, the formation of NH_4^+ plateaued at 192 h.

The NH_4^+ yields in all controls were 25–30%, suggesting the nitrate removed from solution was only partially reduced. Based on the assumption that 8 electrons were needed for the production of NH_4^+, the bioaccessible ESC of dithionite-reduced biochar was about 0.87 mmol/g (no cysteine was added to the reactors).

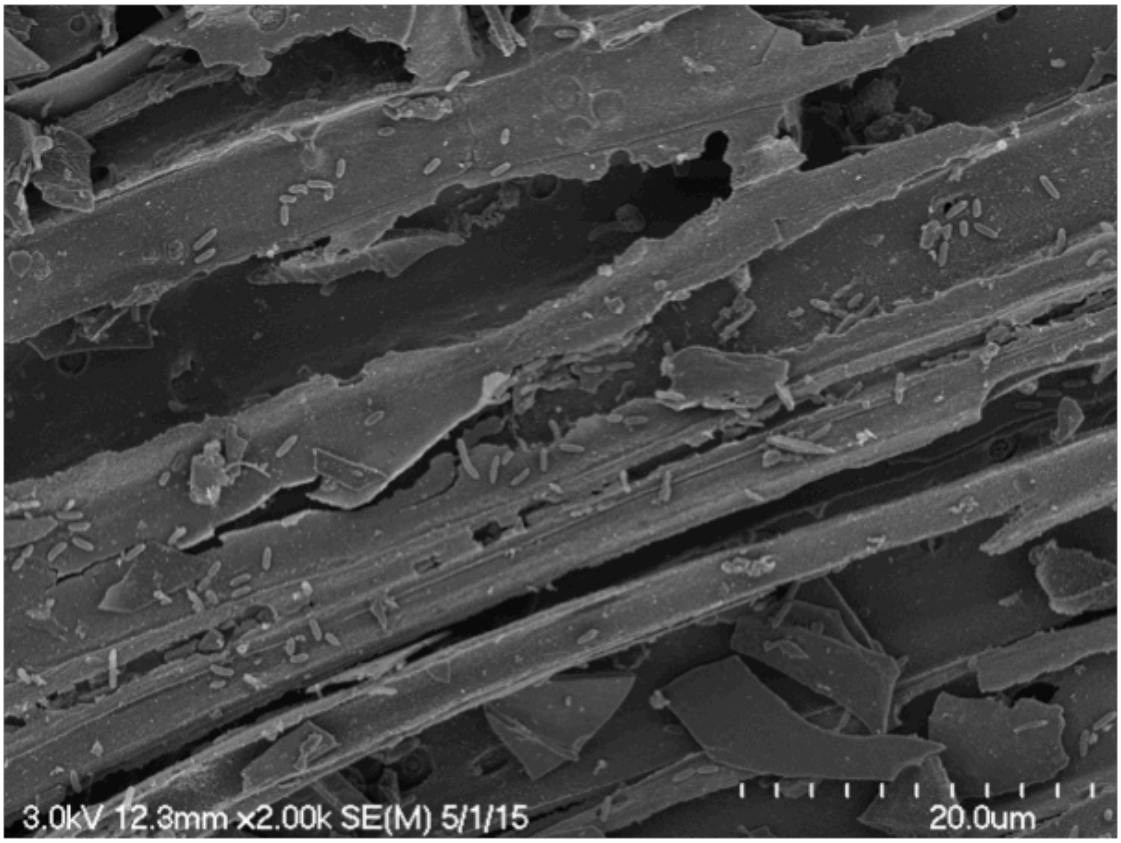

Figure 4.6: SEM image from the washed biologically reduced biochar from the acetate oxidation experiment, illustrating attachment of residual GS-15 cells to the surface of biochar. Reprinted with permission from reference 89. Copyright 2016, American Chemical Society.

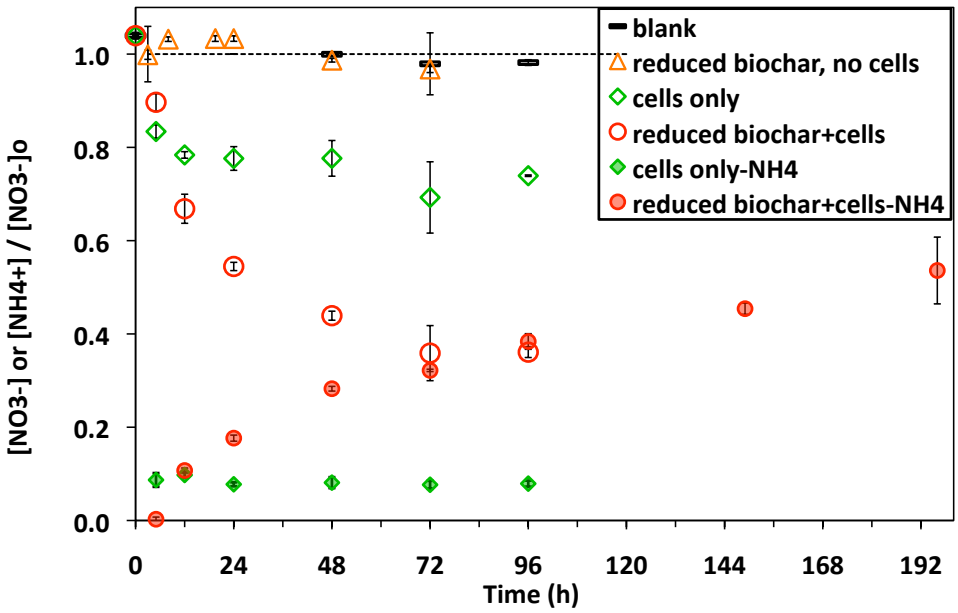

Figure 4.7: Nitrate reduction experiment with dithionite-reduced biochar, which contained blank (blank medium), cells only, 2 g of dithionite-reduced biochar (no cells), and 2 g of dithionite-reduced biochar with cells. NH_4^+ concentrations are for cells only controls and biotic biochar reactors. Error bars represent one standard deviation from triplicate reactors. Initial nitrate concentration was approximately 4.5 mM for all reactors, and the experiment was conducted under 30˚C. Reprinted with permission from reference 89. Copyright 2016, American Chemical Society.

The bioavailable ESC of Soil Reef biochar is comparable to the ESCs for wood and grass biochar, 0.59 and 1.04 mmol/g respectively (pyrolyzed under 500˚C)[66]. This result is somewhat surprising because the ESCs of the wood and grass biochar were measured by an electrochemical method, which involves the use of electron transfer mediators 2,2′-azino-bis(3-ethylbenzothiazoline-6-sulfonic acid) (ABTS, $E_H^{o'}$ = 0.70 V) and 4,4′-bipyridinium-1,1′-bis(2-ethylsulfonate) (ZiV, $E_H^{o'}$ = –0.41 V). In theory, the bioavailable ESC should be lower than the value from electrochemical measurement since: (1) the mediators are able to access all the redox functional groups including the groups that are sterically hindered for GS-15; and (2) the

electrochemical method can measure ESC (i.e., can reduce/oxidize quinone functions) over a wider range of redox potential than the microbes could achieve thermodynamically[72].

4.3.3 Mechanism

Similar to acetate, humic acid, and anthrahydro-quinone-2,6-disulfonate (a humic acid surrogate) [63,73], the use of biologically and chemically reduced biochar as electron donor for NO_3^- reduction would produce NH_4^+ as the final product, Figure 4.5 and 4.7. This result is different from using graphite electrodes as the sole electron donor to support GS-15 reduction of nitrate, which would produce only NO_2^- as the final product[69]. Based on the difference of the product distribution of NO_3^- reduction, the experimental result of this study suggests that the role of biochar is similar to humic acid (which stores electrons), and unlike graphite (which conducts electrons). This also indicates that the biochar supported microbial activity in this study is based on the redox reaction of the quinone groups, rather than by electron conduction through its graphene domains.

It is instructive to compare the result of this study to the study of Chen et al.[74]. In their study, the conductivity of biochar was used to explain the enhanced interspecies electron transfer (IET) between GS-15 and *Geobacter sulfurreducens*, and this IET has been observed from other black carbon such as activated carbon[75]. However, their experimental result showed that even with poorly conductive biochar, high consumption of ethanol was still observed. This contradiction suggests that the conductivity of biochar might not be the dominant mechanism. Comparing the stoichiometry calculation for the oxidation of ethanol to CO_2 and the reduction of fumarate, the number of transferred electrons did not match, which suggested that

biochar in their study acted as an electron sink (0.5 mmol/g biochar). If the above observations are true, the results of Chen et al. study actually supports the proposed electron storage mechanism in this study. Therefore, depending on its properties (e.g., abundance of redox-active groups and aromaticity), black carbon may support microbial activities through different mechanisms.

4.4 Summary

Being the important electron donor[63,76] and acceptor[65,77] in geomicrobiology, organic matter possesses an ESC between 0.5 and 7 mmol/g OC[67,77,78], which significantly affects anaerobic environments. A recent study by Kappler et al. shows that biochar could be an electron acceptor to facilitate the electron transfer from *Shewanella oneidensis* to ferric minerals[79]. In this study, the role of biochar being both electron donor and acceptor has been demonstrated, which the bioaccessible ESC of biochar is comparable to dissolved and particulate organic carbons. This suggests the role of biochar and black carbon in geomicrobiology should be seen as rechargeable reservoirs. Regarding the high annual global emission rate of black carbon (8.4 MT/y[80,81]) and the prevalence of them in sedimentary environments[41], the role of black carbon in anaerobic environments and the interaction with microbiota merit further investigations.

In recent years, biochar has been suggested as a beneficial soil amendment to reduce the mobility of N and P in agricultural soils[36,82-86]. In addition to the agricultural applications, the addition of biochar is also suggested to promote denitrification in soil[36,82,87]. Although the mechanisms of denitrification have been proposed[82,87,88], only few of them are supported by direct experimental evidence. The

results of this study provide a plausible mechanism describing how the interaction between biochar and bacteria can promote microbial denitrification.

Compared to humic substances, the high stability and low mobility of biochar demonstrate it to be suitable for environmental application. Regarding its ability to support microbial redox reaction, considerable ESC and rechargeable nature[66], biochar could be an electron storage medium for biodegradation of contaminants in bioretention and other engineered systems.

REFERENCES

(1) Whitehead, D. C. *Nutrient elements in grassland: soil-plant-animal relationships*, Cabi, 2000.

(2) Schlesinger, W. H. *Biogeochemistry, an Analysis of Global Change*, Academic Press, 1997.

(3) Whitehead, D. C.; Pain, B. F.; Ryden, J. C. *Journal of the Royal Agricultural Society of England*, 1986.

(4) Haygarth, P. M.; Chapman, P. J.; Jarvis, S. C.; Smith, R. V. *Soil Use and Management*, 1998, **14**, 160–167.

(5) Powlson, D. S. *Soil Use and Management*, 1993, **9**, 86–93.

(6) Powlson, D. S. *Soil Use and Management*, 2006, **16**, 141–141.

(7) Vitousek, P.M.; Mooney, H.A.; Lubchenko, J., Melillo, J.M. *Science*, 1997, **277**, 494-499..

(8) Vitousek, P.M.; Aber, J.; Howarth, R.W.; Likens, G.E.; Matson, P.A.; Schindler, D.W.; Schlesinger, W.H.; Tilman, G.D. *Ecological Applications*, 1997, **7**, 737-750.

(9) Nolan, B.T.; Ruddy, B.C.; Hitt, K.J.; Helsel, D.R. *Environmental Science and Technology*, 1997, **31**, 2229-2236.

(10) Hecky, R.E.; Kilham, P. *Limnology and Oceanography*, 1988, **33**, 796- 822.

(11) Howarth, R.W. *Annual Review of Ecology and Systematics*, 1988, **19**, 898-910.

(12) Carpenter, S. R.; Caraco, N. F.; Correll, D. L.; Howarth, R. W.; Sharpley, A. N.; Smith, V. H. *Ecological applications*, 1998, **8**, 559-568.

(13) Smith, V. H. *Successes, limitations, and frontiers in ecosystem science*, 1998, 7-49, Springer New York.

(14) Nolan, B. T.; Hitt, K. J. *Environmental Science & Technology*, 2006, **40**, 7834–7840.

(15) Kocher, A. M.; Loscalzo, J. *Nitrite and nitrate in human health and disease*, Springer Science & Business Media, 2011.

(16) van Grinsven, H. J. M.; Ward, M. H.; Benjamin, N.; de Kok, T. M. *Environmental health*, 2006, **5**, 26.

(17) World Health Organization. *Nitrate and nitrite in drinking-water*, World Health Organization, 2011.

(18) Alexander, J.; Benford, D.; Cockburn, A.; Cravedi, J. P. *The EFSA Journal*, 2008, **689**, 1-79.

(19) Jaffe, E. R. *Clinics in haematology*, 1981, **10**, 99-122.

(20) Boumediene, M.; Achour, D. *Desalination*, 2004, **168**, 187–194.

(21) Sato, Y.; Murayama, K.; Nakai, T.; Takahashi, N. *Water research*, 1995, **29**, 1267-1271.

(22) Mizuta, K.; Matsumoto, T.; Hatate, Y.; Nishihara, K.; Nakanishi, T. *Bioresource technology*, 2004, **93**, 255–257.

(23) Baes, A. U.; Okuda, T.; Nishijima, W.; Shoto, E. *Water Science and Technology*, 1997, **35**, 89-95.

(24) Pintar, A. *Catalysis Today*. October 15, 1999, **53**, 35–50.

(25) Prüsse, U.; Vorlop, K. D. *Journal of Molecular Catalysis A: Chemical*, 2001, **173**, 313-328.

(26) Huang, Y. H.; Zhang, T. C. *Water research*, 2004, **38**, 2631–2642.

(27) Luk, G. K.; Au-Yeung, W. C. *Advances in Environmental Research*, 2002, **6**, 441–453.

(28) Gamble, T. N.; Betlach, M. R.; Tiedje, J. M. *Applied and Environmental Microbiology*, 1977, **33**, 926-939.

(29) Islas-Lima, S.; Thalasso, F.; Gomez-Hernandez, J. *Water research*, 2004, **38**, 13-16.

(30) Gómez, M. A.; Hontoria, E.; González-López, J. *Journal of Hazardous Materials*, 2002, **90**, 267-278.

(31) Hunter, W. J. *Journal of Contaminant Hydrology*, 2003, **66**, 79–91.

(32) Hunter, W. J. *Journal of Contaminant Hydrology*, 2001, **53**, 119-131.

(33) Volokita, M.; Abehovich, A.; Soares, M. *Water Science & Technology*, 1996, **34**, 379-385.

(34) Schipper, L. A.; Barkle, G. F.; Hadfield, J. C.; Vojvodic-Vukovic, M.; Burgess, C. P. *Journal of Contaminant Hydrology*, 2004, 69, 263–279.

(35) Ovez, B.; Ozgen, S.; Yuksel, M. *Process Biochemistry*, 2006, **41**, 1539-1544.

(36) Masiello, C. A. *Marine Chemistry*, 2004, **92**, 201–213.

(37) Lehmann, J.; Gaunt, J.; Rondon, M. *Mitigation and Adaptation Strategies for Global Change*, 2006, **11**, 395–419.

(38) Cornelissen, G.; Gustafsson, Ö.; Bucheli, T. D.; Jonker, M. T. O.; Koelmans, A. A.; van Noort, P. C. M. *Environmental Science & Technology*, 2005, **39**, 6881–6895.

(39) Nguyen, T. H.; Ball, W. P. *Environmental Science & Technology*, 2006, **40**, 2958–2964.

(40) Armitage, J. M.; Cousins, I. T.; Persson, N. J.; Gustafsson, Ö.; Cornelissen, G.; Saloranta, T.; Broman, D.; Næs, K. *Environmental Science & Technology*, 2008, **42**, 3697–3703.

(41) United States Environmental Protection Agency. *Assessment and remediation of contaminated sediments (arcs) program risk assessment and modeling overview document* Washington, United States Environmental Protection Agency, 1993.

(42) Zimmerman, J. R.; Ghosh, U.; Millward, R. N.; Bridges, T. S.; Luthy, R. G. *Environmental Science & Technology*, 2004, 38, 5458–5464.

(43) Cho, Y.-M.; Ghosh, U.; Kennedy, A. J.; Grossman, A.; Ray, G.; Tomaszewski, J. E.; Smithenry, D. W.; Bridges, T. S.; Luthy, R. G. *Environmental Science & Technology*, 2009, **43**, 3815–3823.

(44) Oh, S.-Y.; Chiu, P. C. *Environmental Science & Technology*, 2009, **43**, 6983–6988.

(45) Oh, S.-Y.; Son, J.-G.; Chiu, P. C. *Environmental Toxicology and Chemistry*, 2013, **32**, 501–508.

(46) Xu, W.; Dana, K. E.; Mitch, W. A. *Environmental Science & Technology*,

2010, **44**, 6409–6415.

(47) Kemper, J. M.; Ammar, E.; Mitch, W. A. *Environmental Science & Technology*, 2008, **42**, 2118–2123.

(48) Oh, S.-Y.; Cha, D. K.; Chiu, P. C. *Environmental Science & Technology*, 2002, **36**, 2178–2184.

(49) Ye, J.; Chiu, P. C. *Environmental Science & Technology*, 2006, **40**, 3959–3964.

(50) Beck, D. A.; Johnson, G. R.; Spolek, G. A. *Environmental pollution*, 2011, **159**, 2111–2118.

(51) Mohanty, S. K.; Boehm, A. B. *Environmental Science & Technology*, 2014, **48**, 11535–11542.

(52) Reddy, K. R.; Xie, T.; Dastgheibi, S. *Journal of Environmental Engineering*, 2014, **140**, 04014043.

(53) Logan, B. E. *Microbial Fuel Cells*, John Wiley & Sons, 2008.

(54) Lovley, D. R. *Geomicrobiology Journal*, 1987, **5**, 375–399.

(55) Lovley, D. R. *Microbiological reviews*, 1991, **55**, 259-287.

(56) Lovley, D. R. *Annual Reviews in Microbiology*, 1993, **47**, 263–290.

(57) Lovley, D. R. *FEMS Microbiology Reviews*, 1997, **20**, 305–313.

(58) Lovley, D. In *The prokaryotes*, Springer, 2006, 635–658.

(59) Lin, B.; Westerhoff, H. V.; Röling, W. F. M. *Environmental Microbiology*, 2009, **11**, 2425–2433.

(60) Eickhoff, M.; Birgel, D.; Talbot, H. M.; Peckmann, J.; Kappler, A. *Organic Geochemistry*, 2013, **58**, 107–114.

(61) Lovley, D. R.; Ueki, T.; Zhang, T.; Malvankar, N. S.; Shrestha, P. M.; Flanagan, K. A.; Aklujkar, M.; Butler, J. E.; Giloteaux, L.; Rotaru, A.-E.; Holmes, D. E.; Franks, A. E.; Orellana, R.; Risso, C.; Nevin, K. P. *Geobacter: The Microbe Electric's Physiology, Ecology, and Practical Applications*, Elsevier Ltd., 2011, 1–100.

(62) Shi, L.; Squier, T. C.; Zachara, J. M.; Fredrickson, J. K. *Molecular*

Microbiology, 2007, **65**, 12–20.

(63) Lovley, D. R.; Fraga, J. L.; Coates, J. D.; Blunt-Harris, E. L. *Environmental Microbiology*, 1999, **1**, 89–98.

(64) Lovley, D. R.; Coates, J. D.; Blunt-Harris, E. L.; Phillips, E. *Nature*, 1996, **382**, 445-448.

(65) Klüpfel, L.; Piepenbrock, A.; Kappler, A.; Sander, M. *Nature Geoscience*, 2014, **7**, 195–200.

(66) Klüpfel, L.; Keiluweit, M.; Kleber, M.; Sander, M. *Environmental Science & Technology*, 2014, **48**, 5601–5611.

(67) Aeschbacher, M.; Sander, M.; Schwarzenbach, R. P. *Environmental Science & Technology*, 2010, **44**, 87–93.

(68) Roden, E. E.; Kappler, A.; Bauer, I.; Jiang, J.; Paul, A.; Stoesser, R.; Konishi, H.; Xu, H. *Nature Geoscience*, 2010, **3**, 417–421.

(69) Gregory, K. B.; Bond, D. R.; Lovley, D. R. *Environmental Microbiology*, 2004, **6**, 596–604.

(70) Kaden, J.; S Galushko, A.; Schink, B. *Archives of Microbiology*, 2002, **178**, 53–58.

(71) Icopini, G. A.; Lack, J. G.; Hersman, L. E.; Neu, M. P.; Boukhalfa, H. *Applied and Environmental Microbiology*, 2009, **75**, 3641–3647.

(72) Luan, F.; Gorski, C. A.; Burgos, W. D. *Environmental Science & Technology*, 2015, **49**, 3557–3565.

(73) Lovley, D. R.; Phillips, E. J. *Applied and Environmental Microbiology*, 1988, **54**, 1472–1480.

(74) Chen, S.; Rotaru, A.-E.; Shrestha, P. M.; Malvankar, N. S.; Liu, F.; Fan, W.; Nevin, K. P.; Lovley, D. R. *Scientific Reports*, 2014, **4**.

(75) Rotaru, A. E.; Shrestha, P. M.; Liu, F.; Markovaite, B.; Chen, S.; Nevin, K. P.; Lovley, D. R. *Applied and Environmental Microbiology*, 2014, **80**, 4599–4605.

(76) Coates, J. D.; Cole, K. A.; Chakraborty, R.; O'Connor, S. M.; Achenbach, L. A. *Applied and Environmental Microbiology*, 2002, **65**, 2445–2452.

(77) Lau, M. P.; Sander, M.; Gelbrecht, J.; Hupfer, M. *Biogeochemistry*. December

16, 2014, **123**, 49–61.

(78) Aeschbacher, M.; Graf, C.; Schwarzenbach, R. P.; Sander, M. *Environmental Science & Technology*, 2012, **46**, 4916–4925.

(79) Kappler, A.; Wuestner, M. L.; Ruecker, A.; Harter, J.; Halama, M.; Behrens, S. *Environmental Science & Technology Letters*, 2014, **1**, 339–344.

(80) Lamarque, J. F.; Bond, T. C.; Eyring, V.; Granier, C.; Heil, A.; Klimont, Z.; Lee, D.; Liousse, C.; Mieville, A.; Owen, B.; Schultz, M. G.; Shindell, D.; Smith, S. J.; Stehfest, E.; Van Aardenne, J.; Cooper, O. R.; Kainuma, M.; Mahowald, N.; McConnell, J. R.; Naik, V.; Riahi, K.; van Vuuren, D. P. *Atmospheric Chemistry and Physics*, 2010, **10**, 7017–7039.

(81) Sasser, E. *Report to Congress on Black Carbon: Department of the Interior, Environment, and Related Agencies Appropriations Act, 2010*, United States Environmental Protection Agency, 2012.

(82) Clough, T. J.; Condron, L. M. *Journal of Environment Quality*, 2010, **39**, 1218–1223.

(83) Nelson, N. O.; Agudelo, S. C.; Yuan, W.; Gan, J. *Soil Science*, 2011, **176**, 218-226.

(84) Anderson, C. R.; Condron, L. M.; Clough, T. J.; Fiers, M. *Pedobiologia*, 2011, **54**, 309–320.

(85) Lehmann, J.; Rillig, M. C.; Thies, J.; Masiello, C. A. *Soil biology and biochemistry*, 2011, **43**, 1812–1836.

(86) Laird, D.; Fleming, P.; Wang, B.; Horton, R.; Karlen, D. *Geoderma*, 2010, **158**, 436–442.

(87) Cayuela, M. L.; Sánchez-Monedero, M. A.; Roig, A.; Hanley, K.; Enders, A.; Lehmann, J. *Scientific Reports*, 2013, **3**, 1–7.

(88) Bock, E.; Smith, N.; Rogers, M.; Coleman, B.; Reiter, M.; Benham, B.; Easton, Z. M. *Journal of Environment Quality*, 2015, **44**, 605–613.

(89) Saquing, J. M.; Yu, Y.-H.; Chiu, P. C. *Environmental Science & Technology Letters*, 2016, 3, 62–66.

Chapter 5

SUMMARY AND RECOMMENDATIONS FOR FUTURE DIRECTIONS

5.1 Magnetite Nanoparticle Composite for Arsenic Adsorption

Magnetite nanoparticles were used to synthesize MNPC for the removal of arsenite (As-III) and arsenate (As-V) from water through adsorption. Based on the superior performance of MNPC, we propose that it may be a promising new material to support drinking water treatment and improve water safety. Research on the application of nanoparticles to water treatment systems has largely focused on membrane processes. The method we developed to incorporate nanoparticles into composites, such as MNPC, offers a different approach to apply nanomaterials to water purification processes. Nanoparticle composites such as MNPC may be used in existing small- and large-scale water treatment systems, including point-of-use water filters and municipal treatment plants for the removal of arsenic and potentially other anionic pollutants.

While MNPC exhibited high As-III and As-V adsorption capacities, the mechanism is not fully understood. MNPC showed comparable adsorption capacities for As-III and As-V, suggesting that the adsorption mechanism might be different from that for MNP. To investigate the mechanism, chemical characterization methods; e.g. Fourier transform infrared spectroscopy, FTIR, and electron spectroscopy for chemical analysis, ESCA, may provide useful information.

The silica framework of MNPC was made of tetraethyl orthosilicate (TEOS), which is relatively expensive and may present a cost barrier to the mass adoption of MNPC in the water treatment market. In the production of MNPC,

aminopropyltriethoxysilane (APTES) was added to be the cross-linking agent to bind MNPs to the silica framework. Since the surface of MNPs and silica is connected by APTES, it may be possible to use a cheaper material, such as zeolite or quartz sand, as the framework to lower the production cost of MNPC.

5.2 Reduction of Fluoroalkene Using Alumina Supported Rhodium Catalyst

The ability of a commercially available rhodium on alumina catalyst for the reduction of vinyl fluoride by hydrogen gas was studied. The kinetic and mechanistic information obtained from this investigation may guide the design of new applications for the treatment of waste streams containing fluorinated alkenes.

The catalytic reduction of vinyl fluoride in the aqueous phase was proposed to be mass transfer-controlled. While mass transfer calculations supports this conclusion, further confirmation of liquid-phase mass transfer being the rate-limiting step may be obtained through measurement of the activation energy of the catalytic reaction. By repeating the experiment at different reaction temperatures, the activation energy may be attained if the reaction mechanism remains unchanged, and if the activation energy is in between 8 and 12 kJ mol^{-1}, the mass transfer process may control the catalytic reaction[1].

The distinct selectivity of the two final products, ethane and fluoroethane, in the gas and liquid phase reactions suggests the important influence of adsorbed water molecules on the transition state(s) of rhodium-vinyl fluoride complex(es). To obtain a better understanding of the mechanism for product selectivity, a follow-up study is needed.

In a preliminary study, we tested the rhodium catalyst against a range of saturated halocarbons including chloroform, bromoform, bromodichloromethane,

dibromochloromethane and 2,2,3,3,4,4,4-heptafluoro-1-butanol under hydrogen. The result showed that all the trihalomethanes (THMs) was reduced, and the reaction rate increasing with increasing number of bromine substituents. However, there was no observable reduction of heptafluoro-1-butanol over a month. This indicates that the rhodium catalyst is capable of reductively cleave *sp3*-hybridized carbon-bromine and carbon-chlorine bonds, but not carbon-fluorine bond.

In recent years, fluorinated alkenes, such as 2,3,3,3-tetrafluoropropene (HFO-1234yf), have been proposed as the next generation of refrigerants to replace hydrofluorocarbons (HFCs), such as 1,1,1,2-tetrafluoroethane (HFC-134a)[2]. Unlike their predecessors HFCs and hydrochlorofluorocarbons (HCFCs), fluorinated alkenes contain *sp2*-hybridized carbon-fluorine bonds and are therefore likely to be susceptible to catalytic reduction over rhodium. To develop a feasible and robust treatment processes, information such as the reusability and turnover of the catalyst is critical. It would be essential to evaluate possible change in reaction kinetics and pathway over prolonged usage, as well as medium factors that can potentially cause deactivation of the catalyst. Successful development of a catalytic process for reductive defluorination may help to minimize the future environmental impacts of fluoroalkenes as emerging refrigerants.

5.3 Biochar as a Microbial Electron Donor and Acceptor

In this work, a wood-derived biochar was shown, for the first time, to serve as both an electron donor and acceptor for microbial transformation. The biochar, reduced either biologically or chemically, could act as an electron donor to support nitrate reduction by *Geobacter metallireducens*. When oxidized by air, the biochar served as an election acceptor for microbial acetate oxidation. These results provide an

explanation and supporting evidence for biochar-promoted nitrate reduction in a field-scale bioretention system. Because of its rechargeable nature[4], ability to support microbial oxidation-reduction reactions, and considerable electron storage capacity, biochar may be a promising material for enhancing biodegradation of contaminants in engineered systems for water treatment and site remediation.

In addition to its engineering applications, the finding also offers new insights into the microbiological role of black carbon in anoxic environments. Given its high global emission rate (~8.4 MT/y[3,4]) and ubiquity in the environment, black carbon may play an important role in a number of biogeochemical processes. First, this study reveals a previously unrecognized role of black carbon in controlling the fate of contaminants. Previous studies demonstrated that black carbon can adsorb hydrophobic organic compounds and catalyze the abiotic reduction of nitrogenous contaminants. This work further expands the role of black carbon by illustrating that it can support microbial degradation of contaminants in anoxic environments. Second, because soils contain more than twice as much carbon as the atmosphere[5], the change in soil microbial community and activity due to anthropogenic input of black carbon would affect CO_2 production and the global carbon cycle. If microorganisms like *Geobacter spp.* are widespread that can utilize the redox-active functional groups of black carbon, the high global black carbon emissions may have major implications for the carbon and nutrient cycling in aquatic and terrestrial systems. Thus, this study suggests the need for further research on the roles of anthropogenic black carbon in biogeochemistry and other areas of environmental science and engineering.

In this work, three processes were developed/investigated that may result in improved treatment methods for environmental contaminants or better understanding

of the fate mechanisms involved. While conducted using the three prevalent/emerging pollutants arsenic, fluoroalkene and nitrate, this research may be useful for the control and removal of other contaminants including oxyanions and halocarbons that threaten water quality and human and ecosystem health in many parts of the world. With our growing demand for clean water, development of more effective processes to improve water quality is critical priority in future research.

REFERENCES

(1) Viswanathan, B.; Sivasanker, S.; Ramaswamy, A. V. *Catalysis: principles and applications*. Alpha Science Int'l Ltd., 2002.

(2) Im, J.; Walshe-Langford, G. E.; Moon, J. W.; Löffler, F. E. *Environmental science & technology*, 2014, **48**, 13181-13187.

(3) Lamarque, J. F.; Bond, T. C.; Eyring, V.; Granier, C.; Heil, A.; Klimont, Z.; Lee, D.; Liousse, C.; Mieville, A.; Owen, B.; Schultz, M. G.; Shindell, D.; Smith, S. J.; Stehfest, E.; Van Aardenne, J.; Cooper, O. R.; Kainuma, M.; Mahowald, N.; McConnell, J. R.; Naik, V.; Riahi, K.; van Vuuren, D. P. *Atmospheric Chemistry and Physics*, 2010, **10**, 7017–7039.

(4) Sasser, E. *Report to Congress on Black Carbon: Department of the Interior, Environment, and Related Agencies Appropriations Act, 2010*, United States Environmental Protection Agency, 2012.

(5) United States Department of Energy. *Revealing the Role of Microbial Communities in Carbon Cycling*, 1-2, 2011.

Appendix A

ACIDIC AND BASIC PROPERTIES OF ARSENITE AND ARSENATE

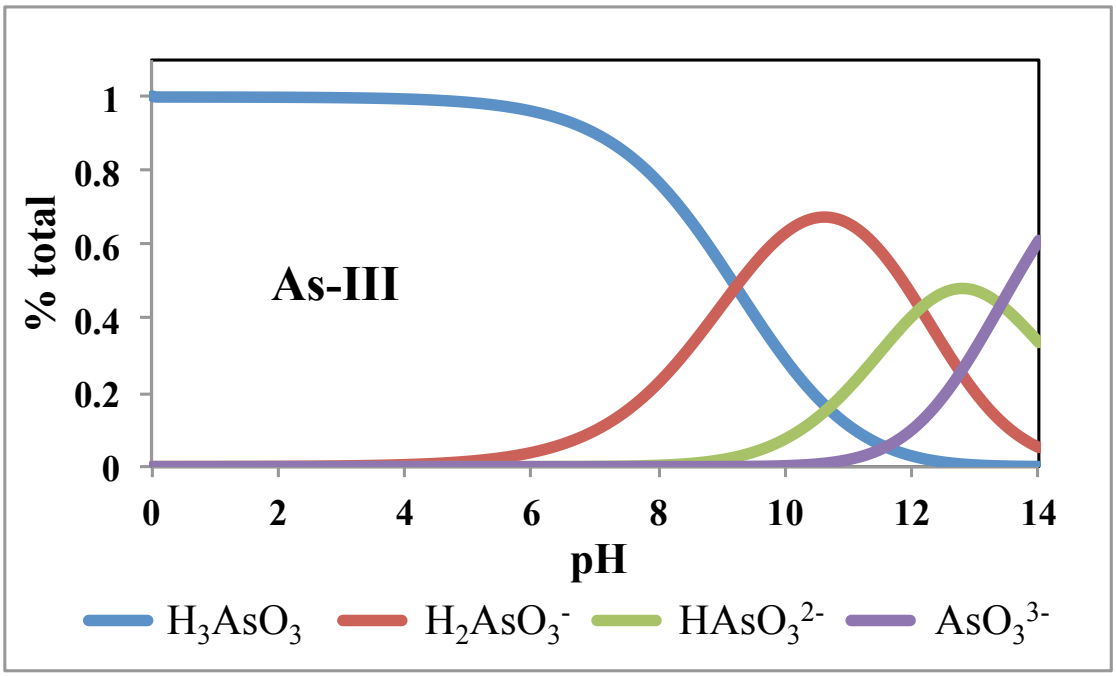

Figure A1: Change of arsenite (As(III)) under different pH. The dominant As(III) species at pH 8 is $H_3AsO_3^{(0)}$.

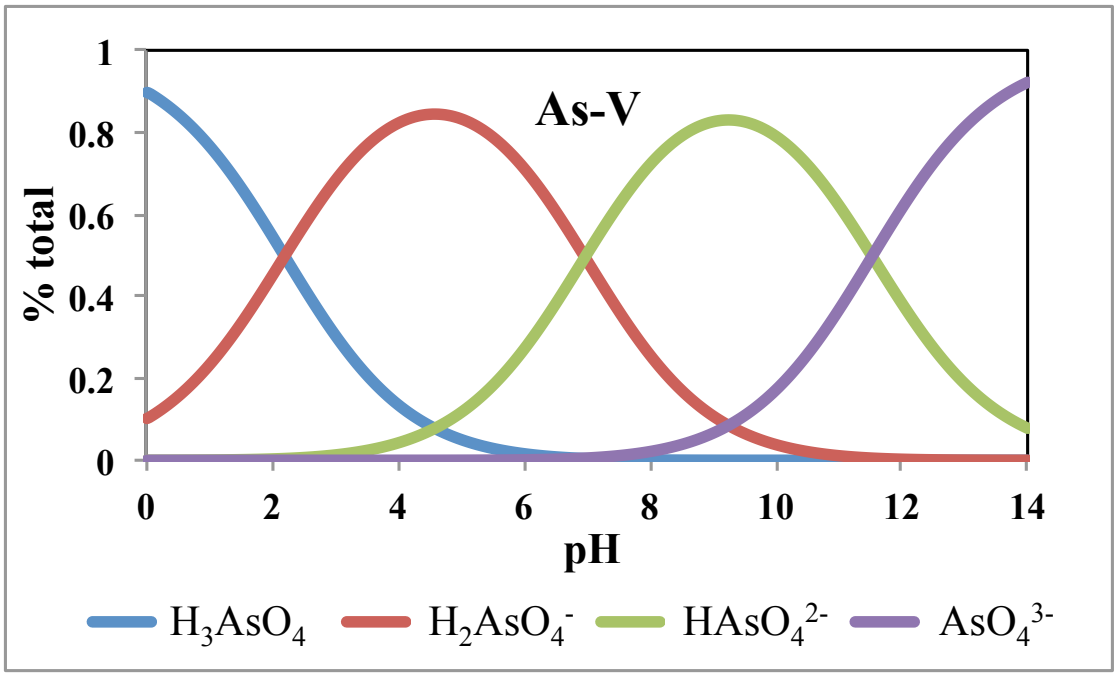

Figure A2: Change of arsenate (As(V)) under different pH. The dominant As(V) species at pH 8 is $HAsO_4^{2-}$.

The identification of dominant arsenite and arsenate species under a pH 8 buffer solution is based on the calculation of α_0, α_1, α_2 and α_3 showing in equation a1, 2, 3 and 4. The pK_{a1}, pK_{a2} and pK_{a3} values for arsenite and arsenate show in table a1.

$$\alpha_0 = \frac{H_3A}{C_{total}} = \frac{[H^+]^3}{[H^+]^3+[H^+]^2k_{a1}+[H^+]k_{a1}k_{a2}+k_{a1}k_{a2}k_{a3}} \quad \text{(a1)}$$

$$\alpha_1 = \frac{H_2A^-}{C_{total}} = \frac{[H^+]^2k_{a1}}{[H^+]^3+[H^+]^2k_{a1}+[H^+]k_{a1}k_{a2}+k_{a1}k_{a2}k_{a3}} \quad \text{(a2)}$$

$$\alpha_2 = \frac{HA^{2-}}{C_{total}} = \frac{[H^+]k_{a1}k_{a2}}{[H^+]^3+[H^+]^2k_{a1}+[H^+]k_{a1}k_{a2}+k_{a1}k_{a2}k_{a3}} \quad \text{(a3)}$$

$$\alpha_3 = \frac{A^{3-}}{C_{total}} = \frac{k_{a1}k_{a2}k_{a3}}{[H^+]^3+[H^+]^2k_{a1}+[H^+]k_{a1}k_{a2}+k_{a1}k_{a2}k_{a3}} \quad \text{(a4)}$$

Table A.1 The pK values for arsenite and arsenate

	Arsenite (As(III))	Arsenate (As(V))
pKa1	9.22	2.2
pKa2	12.13	6.97
pKa3	13.4	11.53

Appendix B

EFFECT OF CELL-ASSOCIATED BIOCHAR ON NITRATE REDUCTION

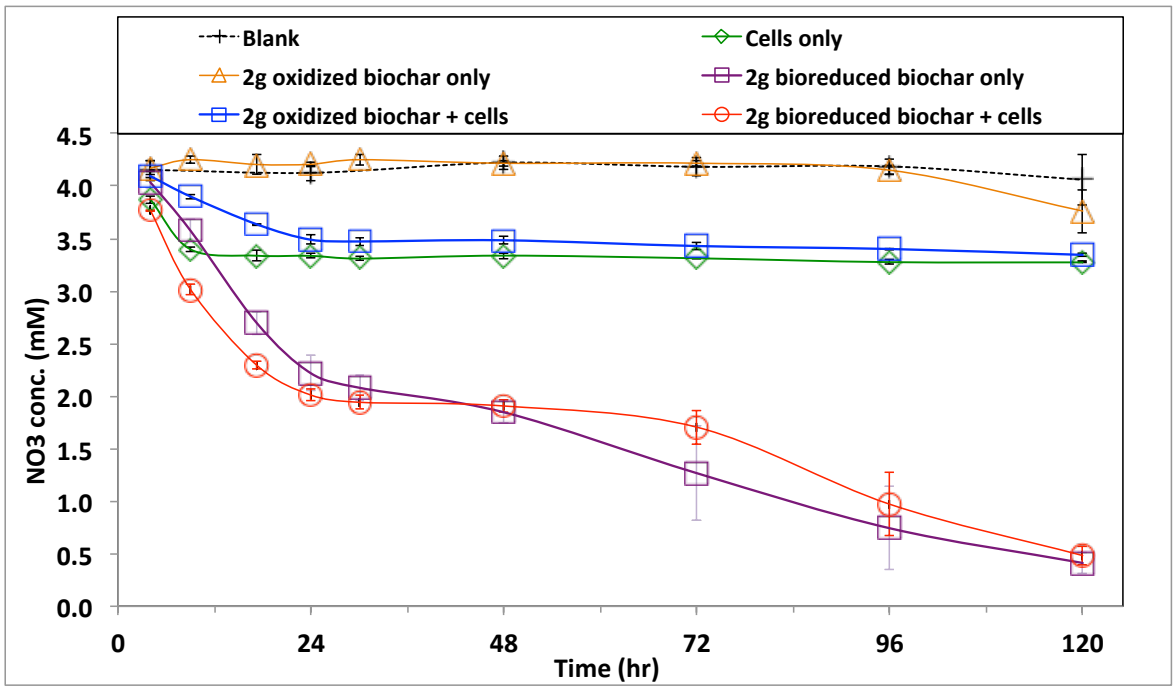

Figure B1: Nitrate reduction experiment with biologically reduced biochar, which contains blank (blank medium), cells only, 2 g of oxidized biochar with and without cells, and 2 g of biologically reduced biochar with or without cells. Initial nitrate concentration was approximately 4 mM for all reactors. Error bars represent one standard deviation from triplicate reactors. The experiment was conducted under 30˚C.

Without adding cells, the nitrate reduction of biologically reduced biochar was observed. Based on the SEM image for the washed biologically reduced biochar (Figure 4.6) and the result from chemically reduced biochar experiment (Figure 4.7), the reduction of nitrate was possibly caused by the surface associated *Geobacter metallireducens* cells.

Appendix C

COPYRIGHT PERMISSIONS

Permission for Figure 3.2, 3.3, 3.4, 3.5, 3.7, 3.8, 3.9 and 3.10.

Permissions for Figure 4.4, 4.5, 4.6, 4.7 and 4.8.

Copyright Clearance Center RightsLink®

Home | Account Info | Help | Live Chat

ACS Publications Most Trusted. Most Cited. Most Read.

Title: Wood-Derived Black Carbon (Biochar) as a Microbial Electron Donor and Acceptor

Author: Jovita M. Saquing, Yu-Han Yu, Pei C. Chiu

Publication: Environmental Science & Technology Letters

Publisher: American Chemical Society

Date: Feb 1, 2016

Logged in as: Yu-Han Yu

LOGOUT

PERMISSION/LICENSE IS GRANTED FOR YOUR ORDER AT NO CHARGE

This type of permission/license, instead of the standard Terms & Conditions, is sent to you because no fee is being charged for your order. Please note the following:

- Permission is granted for your request in both print and electronic formats, and translations.
- If figures and/or tables were requested, they may be adapted or used in part.
- Please print this page for your records and send a copy of it to your publisher/graduate school.
- Appropriate credit for the requested material should be given as follows: "Reprinted (adapted) with permission from (COMPLETE REFERENCE CITATION). Copyright (YEAR) American Chemical Society." Insert appropriate information in place of the capitalized words.
- One-time permission is granted only for the use specified in your request. No additional uses are granted (such as derivative works or other editions). For any other uses, please submit a new request.

If credit is given to another source for the material you requested, permission must be obtained from that source.

BACK CLOSE WINDOW